POLITECNICO DI MILANO

School of Industrial and Information Engineering

Master of Science in Automation and Control Engineering

Measurement Techniques for Air Gap Torque Pulsation of Synchronous Machines Fed by Adjustable Speed Drive

Supervisors:
Prof. Francesco Castelli Dezza
Ing. Maurizio Zago

Author:
Rodrigo Furriel Inocentes
Matr. 780134

Academic year: 2012/2013

To my Family and Friends

Acknowledgements

I would like to express my deepest gratitude to Engineer Maurizio Zago, Engineering Leader of the Automation & Electrical Systems - Oil, Gas & Petrochemical division of ABB S.p.A. and tutor of my thesis, for his support and for the opportunity given to me .

I wish to thank Professor Francesco Castelli Dezza, professor at School of Industrial and Information Engineering of Politecnico di Milano and the supervisor of this thesis, for the help with the theoretical and practical details of the involved methods.

I would like also to thank the team of ABB S.p.A. and CESI for the amazing opportunity of taking part of such "non-usual" experience with special challenges, equipments and solutions. Specially in the figure of Engineer Miguel Ficarra, for the support on the technical explanations of the systems and processes.

Many thanks to Professor Enrico Ragaini, professor at School of Industrial and Information Engineering of Politecnico di Milano and Cyber Security Manager - Low Voltage Products Division of ABB S.p.A., for giving me the opportunity to work with this challenging project.

The financial support of CAPES (Coordenação de Aperfeiçoamento de Pessoal de Nível Superior) through the CSF (Ciência sem fronteiras - Science without borders) program is also very gratefully acknowledged.

I would like to thank Politecnico di Milano and Escola Politécnica da Universidade de São Paulo, for making the double degree program, in which I take part, not only possible but also an example of cooperation for the growth of their students. Special thanks should be driven to the Commission of International Relations of Escola Politécnica da USP (CRINT-POLI USP) and to Professor Fernando Josepetti Fonseca for the support and the availability of always being ready to help.

Special thanks to my friends, Brazilians or not, for making this two years in Italy the best they could be and supporting the difficulties of being far from home.

Many thanks to my sister, Denise, for the support and comprehension in all this years together.

I am deeply grateful to my parents, Armando and Rosa, for their guidance, their teachings, their support on my decision of studying abroad and their daily support. To summarize, for their constant love and support, they deserve my really special thanks with all my love.

Last but not least and with all my heart, I am grateful to my dear Camilla for her love. In showing understanding, patience and encouragement she has supported me during the years and specially during this two years abroad in a way that no words are expressive enough to thank her.

Contents

List of figures

List of tables

List of symbols

Acronyms

AC	Alternate Current
ASD	Adjustable Speed Drive
ASDS	Adjustable Speed Drive Systems
DC	Direct Current
ESD	Extreme Studentized Deviate
LCI	Load (machine) Commutated Inverter
RTD	Resistance Temperature Detector
VSD	Variable Speed Drive
VSI	Voltage Source Inverter

Abstract

The use of synchronous motors associated to adjustable speed drive systems (ASDS) is a rising field in oil and gas applications, since it represents a desirable alternative in high power applications due to its higher efficiency compared to AC induction machines and DC motors. However, there are some drawbacks to the use of such combination, as the pulsating torque components resultant from current harmonics which are impressed on the motor by the converters of the drive system. In spite of their small amplitude in comparison with the driving torque, these pulsating components can excite system resonances. ASDS availability is also extremely important for the plant operation. Thus, extensive factory testing is required to reveal any possible hidden weakness of the components and system design issues. Such tests may have different set-ups and follow different standards in which the amplitude of the pulsating torque components may be required. In this context, the objective of this study was the implementation of measurement techniques of pulsating torque on a 19.3MW and a 20MW synchronous machine fed by ASDS with LCI configuration. The methods employed for the measurement of the pulsating torque (Volt-Second Ampere and Modified Input Power) were selected among those available in the literature, privileging the quality of the results as well as low costs and complexity. It was also taken into account that a significant reduction of costs and complexity is achieved by using sensors already available on the test set. The results obtained evidenced the presence of pulsating torque components related to the current harmonics. The computed values for the pulsating components were inside the expected boundaries when compared to the maximum expected values, except for the components at 120 Hz, 240 Hz and 960 Hz. However, two unexpected low frequency pulsating components were present around 20 Hz and 40 Hz. Both phenomena should have their origin studied in future developments.

Abstract Italiano

L'impiego di motori sincroni associati ad azionamenti a velocità variabile (ASDS) è di interesse crescente in applicazioni oil & gas, sopratutto per grandi potenze in relazione alla maggiore efficienza rispetto alle macchine asincrone ed ai motori in corrente continua. Tuttavia, ci sono alcuni inconvenienti nell'uso di tali sistemi, come le componenti della coppia pulsanti risultanti dalle armoniche di corrente che vengono impresse sul motore dai convertitori del sistema di azionamento. Nonostante la loro piccola ampiezza rispetto alla coppia motrice, queste componenti pulsanti possono eccitare risonanze del sistema. La disponibilità dell'azionamento è estremamente importante per il funzionamento dell'impianto. Pertanto, diversi test sono necessari per rivelare ogni possibile punto debole dei componenti e problemi di progettazione del sistema. Tali prove possono avere diversi set-up ed essere eseguite in accordo agli Standard IEC o IEEE. Nello Standard IEC 61800-4 è richiesta la determinazione dell'ampiezza delle componenti di coppia pulsanti. In questo contesto, l'obiettivo di questo studio è l'implementazione di tecniche di misura di coppia pulsante su machine sincrone di potenza 19.3MW e 20MW alimentate da ASDS con configurazione LCI. I metodi impiegati per la misura della coppia pulsante (Volt-Second Ampere e Modified Input Power) sono stati selezionati tra quelli disponibili in letteratura, privilegiando la qualità dei risultati nonché costi e complessità di esecuzione. E' stato anche tenuto conto che una significativa riduzione dei costi e della complessità è ottenuta utilizzando sensori già presenti nel test set. I risultati ottenuti dimostrano la presenza di componenti di coppia pulsanti relativi alle armoniche di corrente. I valori calcolati per le componenti pulsanti sono all'interno dei limiti previsti quando confrontati ai valori massimi previsti, salvo per le componenti a 120 Hz, 240 Hz e 960 Hz. Inoltre, due componenti pulsanti, non previste, a bassa frequenza sono presenti a circa 20 Hz e 40 Hz. Entrambi i fenomeni dovrebbero essere approfonditi ulteriormente per capirne le cause in lavori futuri.

Sommario

Introduzione

I motori sincroni sono comunemente utilizzati nelle applicazioni di grande potenza come turbocompressori, ventilatori e pompe. In queste installazioni, spesso la potenza delle machine espressa in cavalli è superiore al valore della velocità di rotazione espresso in giri al minuto.

Un motore sincrono appartiene alla classe di motori a corrente alternata (AC) ed ha come caratteristica principale il funzionamento in una velocità proporzionale alla frequenza della corrente che fluisce nella sua armatura a regime.

Questi motori continuano ad essere un'alternativa per applicazioni di grande potenza, in quanto essi hanno relativamente maggiore efficienza, circa il 97% di efficienza, rispetto alle macchine a induzione e motori DC.

Non solo la macchina in sé è importante, ma anche i sistemi di azionamento sono di fondamentale importanza, soprattutto in sistemi ad alta potenza. Un modo di azionare macchine sincrone è attraverso sistemi di azionamenti a velocità variabile (ASDS), che permettono risparmiare energia e migliorare il controllo del processo per il funzionamento più conveniente.

Un esempio di ASDS è quelle basato sulla tecnologia di ABB MEGADRIVE-LCI (Load (machine) Commutated Inverter). Questo sistema si basa su convertitori con tiristori a commutazione naturale, ed è uno dei sistemi di azionamento più efficienti del mercato, con efficienza con valori intorno al 99%.

Tuttavia, ci sono alcuni svantaggi quando si utilizzano macchine sincrone associate ad ASDS. Si potrebbe citare almeno la coppia pulsante risultante di armoniche di corrente, che sono impressi sul motore dai convertitori del sistema di azionamento. Tale coppia pulsante sebbene di ampiezza trascurabile rispetto al valore nominale della coppia può eccitare risonanze quando le loro frequenze coincidono con una frequenza naturale del sistema. Quindi la sua analisi è di fondamentale importanza e sarà al centro di questa tesi.

Particolare attenzione viene dedicata al problema del azionamento di compressori e pompe con impegno di grandi ASDS poiché questo è un campo crescente in applicazioni oil & gas, particolarmente per il trasporto di gas/olio, liquefazione del gas e iniezione di gas. In queste applicazioni la disponibilità del ASDS è di estrema importanza per il funzionamento dell'impianto che risulta nella necessità di numerosi test in fabbrica prima di consegnare al sito. Questi test hanno lo scopo di scoprire eventuali debolezze nascoste dei componenti e problemi di progettazione del sistema.

Tali prove possono avere diversi set-up e seguire gli standard diversi, in cui può essere richiesto l'ampiezza delle componenti di coppia pulsanti. In questo contesto, l'obiettivo di questo studio era l' implementazione di tecniche di misura di coppia pulsante su macchine sincrone con potenza 19.3MW e 20 MW azionate da ASDS con configurazione LCI.

Metodologia ed Esecuzione

Diversi metodi di misura della coppia pulsante sono disponibili in letteratura come quelle meccaniche:

- Misura della accelerazione angolare
- Misura della velocità di rotazione
- Metodo della coppia all'albero

o quelli elettrici, la cui l'implementazione implica l'utilizzo del modello del motore ottenuto dalla trasformazione di Park:

- Metodo delle "search coil" e sensori di corrente
- Misurazione della coppia elettromagnetica con misure della potenza assorbita
- Misurazione della coppia elettromagnetica con misure della potenza assorbita e della velocità
- Misurazione della coppia elettromagnetica con misura di tensione e di corrente ai terminali della macchina

La selezione dei metodi è stata effettuata tenendo conto della qualità dei risultati nonché costi e complessità. E' stato anche tenuto conto che una significativa riduzione dei costi e della complessità è ottenuta utilizzando sensori già presenti sul banco prova. Così i metodi scelti sono Volt-SecondAmpere (VSA) e Modified Input Power (MIP).

L'algoritmo per il calcolo della coppia è stato implementato su Matlab® secondo le seguenti equazioni:

Metodo MIP:
$$T_e \cong \frac{\mathrm{p}}{2}\frac{\mathrm{P_{in}}}{\omega}$$

Metodo VSA:
$$T_e \cong \frac{\sqrt{3}p}{6}\left\{(i_a - i_b)\int v_{ca}\ \mathrm{dt} - (i_c - i_a)\int v_{ab}\ \mathrm{dt}\right\}$$

dove p rappresenta i numeri di poli della macchina, P_{in} la potenza assorbita, ω la velocita angolare, i_j la corrente nella fase j e V_{ij} la tensione di linea tra linea i e linea j.

Il punto saliente di questa tesi è nella risoluzione dei problemi posti dal calcolo dell'integrale delle tensioni di linea presenti sul metodo VSA.

Quando si calcola l'integrale di un segnale che è composto dalla sommatoria di diverse componenti sinusoidali, non è immediato che il valore iniziale per l'integrale sia impostato al valore corretto. Diversi metodi sono stati implementati per trovare e impostare il valore iniziale per gli integrali delle tensioni di linea, ma nessuno di questi era in grado di determinare il valore preciso: il risultato del calcolo era una coppia al traferro affetta da questa imprecisione. Le soluzioni trovate sono state basate su concetti più teorici di integrale di segnali sinusoidali e sono:

- eseguire l'analisi di Fourier sulle tensioni di linea e ottenere le componenti sinusoidali del segnale con le loro ampiezze e fasi. Calcolare gli integrali di ogni componente ed infine sommarli.

- calcolo dell'integrale con il metodo trapezoidale e superare il problema della condizione iniziale attraverso una procedura di media mobile.

Risultati e Discussione

Una fase di validazione è stata realizzata facendo uso del SimPowerSystems™ toolbox di Matlab®. In questa fase i risultati ottenuti con la simulazione di modelli semplificati di motore sincrono in Simulink® sono stati confrontati con i risultati dai metodi selezionati. I risultati ottenuti con il metodo VSA sono stati più coerenti di quelli trovati con il metodo MIP. L'errore calcolato per il metodo VSA è stato limitato da un fattore pari a 16,5%, mentre il metodo MIP non ha raggiunto significativa corrispondenza tra i risultati attesi ed i risultati trovati con il metodo di calcolo. Per questo motivo, l'analisi dei dati reali con il metodo MIP non è stata presa in considerazione.

Dopo la convalida, le misure reali delle macchine in prova (19300 kW, 20000 kW a pieno carico ed a carico 75%) sono state utilizzate per calcolare le componenti della coppia pulsanti. I risultati ottenuti sono stati confrontati con i valori massimi previsti per i componenti di frequenza di coppia pulsante. In tutte le prove realizzate, la presenza dei componenti di coppia pulsanti relativi alle armoniche di corrente è stata verificata e confermata. I componenti pulsanti di tutte le frequenze attese, a parte il 120 Hz, 240 Hz e 960 Hz, sono rimasti dentro il valore massimo previsto ed i valori medi per la coppia, che sono stati anche comparati a quelli attesi, hanno presentato errore sempre minore di 2,7 %.

Conclusioni e Sviluppi futuri

Tra i due metodi di calcolo dell'integrale utilizzati per la implementazione del metodo VSA, nessuno ha mostrato risultati significativamente migliori rispetto all'altro. Il metodo di analisi di Fourier ha presentato apparentemente un migliore risultato in tutta la gamma di frequenze, ma ha anche presentato alcuni picchi spuri in frequenze non previsti. Invece, il metodo trapezoidale ha mostrato un risultato un po' inferior in tutta la gamma di frequenza, ma con la presenza di tali picchi spuri significativamente ridotta.

E' importante menzionare una differenza tra i due metodi di calcolo integrale. Per futuri sviluppi potrebbe essere interessante avere il calcolo della coppia in tempo reale (con il motore in movimento durante le prove), e per questa implementazione, il metodo trapezoidale con media mobile presenterebbe un vantaggio poiché darebbe la possibilità di calcolare la coppia per ogni nuovo piccolo set di dati mentre il metodo di Fourier richiederebbe un set di dati più grande per essere efficace.

Gli sviluppi futuri dovrebbero anche indagare le ragioni per le componenti a 120 Hz, 240 Hz e 960 Hz sui risultati con i dati di misura reali siano sopra il valore massimo previsto. Mantenendo lo stesso ragionamento, anche l'esistenza di due picchi non aspettati a bassa frequenza a 20 Hz e 40 Hz dovrebbero essere studiati

poiché la prossimità della frequenza naturale del sistema può portare conseguenze pericolose per il sistema.

Infine, dal momento che i test sviluppati durante questa tesi vengono eseguiti su sistemi in cui la disponibilità è di estrema importanza per il funzionamento degli impianti, si potrebbe valutare per successivi approfondimenti di applicare un metodo diverso di misurazione per la coppia pulsante, come il metodo delle "bobine di corrente" (search coil) o un metodo meccanico accurato. Avendo a disposizione anche questi dati, si potrebbero confrontare con i risultati del programma creato durante questa tesi e comprendere meglio i limiti della soluzione proposta.

1. Introduction

Nowadays, synchronous motors are commonly used as prime movers in "high power" applications such as large turbocompressor, fan and pump. In this installations, frequently the horsepower rating of the machine exceeds its corresponding rpm (revolution per minute) rating [1].

A synchronous motor belongs to the class of alternate current (AC) motors and has as main characteristic the operation in a speed proportional to the frequency of the current flowing in its armature under steady state condition. In the rotating magnetic field configuration, the most common one, currents flow through the armature windings and a magnetic field is created. This field rotates with a speed proportional to the frequency of the armature currents. Current also flow on the rotor (field) winding and another magnetic field is created. Both magnetic fields tend to rotate at same speed (synchronous speed) and a steady state torque results.

These motors continue to be a desirable alternative in high power applications since they have relatively higher efficiency compared to AC induction machine and DC motors. The typical value for the efficiency of the synchronous machine is around 97% [2]. But the high efficiency is not the only advantage for synchronous machines, one could add to this fact the possibility of readily control the reactive power of such kind of machine [1].

Not only the machine itself is important on a practical point of view, drive systems are also of fundamental importance when it comes to real life application, especially in high power systems. One way of driving synchronous machines is through Adjustable Speed Drive Systems (ASDS). This devices allows energy save and improve process control for more cost-effective operation [2].

An example of ASDS is the MEGADRIVE-LCI (Load (machine) Commutated Inverter) technology from ABB. It is based on converters with naturally commutated thyristors, and is one of the most efficient drive systems in the market. When associated with synchronous machine this system can bring very good efficiency results that are related with the high efficiency of synchronous machines, as already commented, and with the converter efficiency that has values around 99% [2].

However, some drawbacks appear when using synchronous machines associated with ASDS. One could mention at least the asynchronous accelerating torque during a direct on-line start and the oscillating torques at double slip frequency due to rotor asymmetry [1] without forgetting the pulsating torque resultant of current harmonics which are impressed on the motor by the converters of the drive system [3]. This pulsating torque although of amplitude frequently negligible when compared to the torque nominal value can excite resonances when their frequencies coincide with one natural frequency of the system. Then its analysis is of fundamental importance and will be the focus of this thesis.

Now that an overview was settled and before analyzing the possible methods of measuring pulsating torque some basic ideas should be illustrated. This first section will be devoted to more deeply explain the ASDS characteristics, the challenges of testing high power ASDS and the possible sources of pulsating torque.

Before going on the mentioned details some basic ideas of electromagnetism, electromechanical energy conversion and modeling of synchronous machines through the dq axis theory from Park [4] will be discussed.

1.1. Basics on electromagnetism and electromechanical energy conversion.

1.1.1. Faraday's law of electromagnetic induction

Described by Michael Faraday (1791–1867), can be presented in two different ways:

- If a moving conductor cuts lines of force (flux) of a constant magnetic field while moving, it will experience a voltage induced between its terminals.
- If a loop made of conductor material has a magnetic flux passing through it and changing with time, a voltage will be induced in the loop.

In both cases the rate of change is the critical determinant of the resulting difference of potential. Fig. 1.1 illustrates this basic relationship.

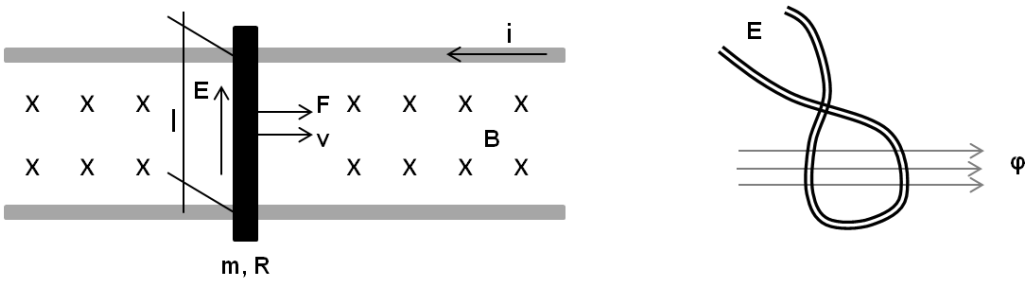

Fig. 1.1: Faraday's basic law of electromagnetic induction

Considering the illustration on the left side of Fig. 1.1, a straight conductor of length "l", mass "m" and resistance "R" is free to move on a plane perpendicular to a uniform magnetic field "B".

Then, if the conductor moves with linear speed "v", an electromotive force is induced across an element "dl" of the conductor.

$$dE = \overline{v} \times \overline{B} \cdot \overline{dl} \tag{1.1}$$

integrating over the length:

$$E = Blv \tag{1.2}$$

While on the right size of Fig. 1.1:

$$E = -\frac{d\varphi}{dt} \tag{1.3}$$

where φ is the magnetic flux crossing the loop.

1.1.2. Ampere-Biot-Savart's law of electromagnetic induced forces

Attributed to Andre Marie Ampere (1775–1836), Jean Baptiste Biot (1774–1862) and Victor Savart (1803–1862) this law establishes that if a conductor is located in a magnetic field and has a current passing through it, a force will be experience by the conductor.

Analyzing again the illustration on the left side of Fig. 1.1:

$$\overline{dF} = \bar{dl} \times \bar{B} \cdot i \tag{1.4}$$

and again integrating over the length:

$$F = Bli \tag{1.5}$$

1.1.3. Lenz's law of action and reaction

In Lenz's law (Heinrich Lenz – 1804–1865) both Faraday's law and Ampere-Biot-Savart's law come together. It states that electromagnetic-induced currents and forces will try to cancel the originating cause.

Let us consider an example:

- If a conductor is forced to move cutting lines of force of a constant magnetic field, a voltage is induced in it (Faraday's law).
- Then, if the conductor ends are connected in such a way that a current can flow, the induced current will produce a force acting on the conductor (Ampere-Biot-Savart's law).
- Finally the Lenz's law states that this force will act to oppose the movement of the conductor.

1.1.4. Electromechanical energy conversion

This simple principle states that all the electrical and mechanical energy flowing out of the system added to the energy stored in the system and to the energy dissipated as heat must be equal to all the electrical and mechanical energy flowing into the system.

1.2. Synchronous machines

Now that the basic concepts of electromagnetism and electromechanical energy conversion were briefly reviewed, the synchronous machine can be more deeply explained. However let us first make an introduction with some explanations of some basic concepts before getting to the model of such kind of machine. Fig. 1.2 shows a commercial version of a synchronous motor.

Fig. 1.2: Synchronous motor [5]

Nowadays synchronous machine are commonly found as generators in power generation systems and is not uncommon to see machines with ratings reaching up to 1500 MVA [6]. But it is important to highlight that synchronous machines can also operate as motor, and can go from the small permanent magnet synchronous motor used in analog clocks to some tens of megawatt.

This study will be carried out considering synchronous motors of about 20 MW shaft power that are the ones in which the tests will be developed. More details on the motors will be given latter.

As already mentioned a synchronous machine has as main feature the constant speed under steady state condition that is proportional to the frequency of the current in its armature. This speed can be computed as:

$$N_s = \frac{120\,f}{p} \tag{1.6}$$

where "Ns" is the synchronous speed (in rpm), "f" the frequency of the AC supply current and "p" the number of magnetic poles.

If one would like to consider the angular speed ω_s (in rad.s^{-1}), a simple transformation can be applied and:

$$\omega_s = \frac{4\pi f}{p} \tag{1.7}$$

Synchronous machines are divided into two main groups: the stationary field and the rotating magnetic field. This thesis consider for the developments the rotating magnetic field machines that are the most common and that is the group that includes the machines available for tests. Now some considerations will be made to illustrate the differences between the two groups:

1.2.1. Stationary field synchronous machine

This type of machine has salient poles (magnetized by permanent magnets or DC current) mounted on the stator. Normally a three-phase winding is mounted on the shaft and constitutes the armature that is fed through three sets of slip rings (collectors) and brushes.

This arrangement can be found in machines up to about 5 kVA in rating. For larger machines (including the ones of interest for this thesis) the typical arrangement used is the rotating magnetic field [6].

1.2.2. Rotating magnetic field synchronous machine

This type of machine has a field-winding mounted on the rotor, and the armature mounted on the stator. As already mentioned, currents flow through the armature windings and create a magnetic field. This field rotates with a speed proportional to the frequency of the currents flowing on the armature. On the field-winding there is also a current flowing and another a magnetic field is created. Both magnetic fields tend to rotate at same speed (synchronous speed).

From now on, for simplicity, the term rotating magnetic field synchronous machine will be substituted by just synchronous machine or synchronous motor. However, the configuration in discussion is only the rotating field synchronous machine and not the stationary field synchronous machine.

1.2.3. Constructive details

Insulated steel laminations are used to build the stator core. They can have different thickness and type of steel that are chosen in order to minimize eddy current, hysteresis losses and cost, while maintaining required effective core length.

For the rotor there are two types of structure: round (cylindrical) rotor and salient pole rotor as illustrated in Fig. 1.3. Generally, round rotor structure is used for high speed synchronous machines with two or four-pole (not common but possible in six-pole machines), such as steam turbine generators, while salient pole

structure is used for low speed machines with six or more poles, such as hydroelectric generators and the majority of synchronous motors [6].

An important aspect of salient-pole machines is that they usually have one or more additional windings in the rotor. The damping-windings (also known as amortisseurs) serve to damp the oscillations of the rotor around synchronous speed and can also be used to start the motor in much the same manner as do the rotor bars of a conventional squirrel cage induction motor.

1.2.3.1. Distributed three phase windings

As discussed on section 1.2.2, for the operation of rotating magnetic field machines a rotating magnetic field should result from the armature currents. But how to create a rotating field resulting from the armature currents?

Making use of a simple mathematical analysis it is possible to show that a three-phase balanced current (equal magnitudes and 120 electrical degrees apart) flowing in a balanced three-phase stator winding generates a rotating magnetic field in the machine air gap with constant magnitude.

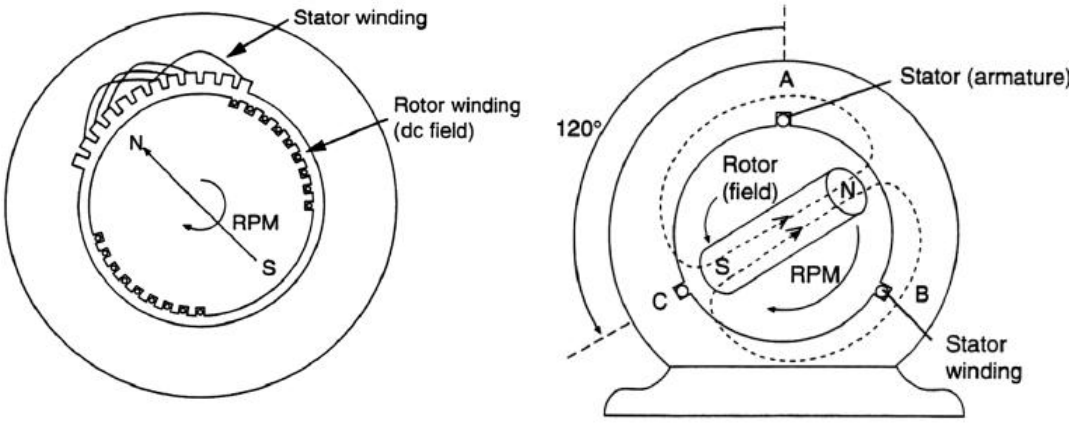

(a) Round structure

(b) Salient pole structure

Fig. 1.3: Rotor structure for a synchronous machine [6]

It is important to remark that:

$$Mechanical\ angle = \left(\frac{2}{p}\right) Electrical\ angle$$

where p is the number of poles of the machine.

The distribution of the coils in the stator is an important aspect to generate the rotating field and it is highly discussed in literature. The main idea is to have a stator that has a number of uniformly distributed slots as shown in Fig. 1.4. These slots receive coils that are connected in such a way that the current in each phase winding produces a magnetic field in the air gap as close as possible to an ideal sinusoidal distribution.

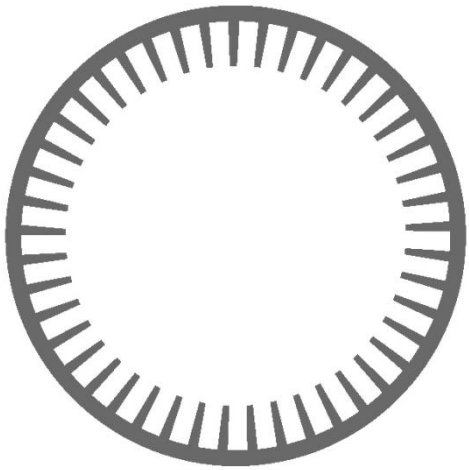

Fig. 1.4: Stator structure

As mentioned, there are different ways of configuring the stator windings in the stator slots described by the literature, but as this information is not part of the scope of this thesis one my refer to reference [6] for more information.

1.2.4. Park's transformation

Before the development of a model to study the electrical and electromechanical behavior of synchronous machines it is important to introduce the concept of Park's transformation that will be very useful on the development of such model.

In the late 20's of last century the American electrical engineer R.H. Park (1902 –1994) [4] introduced a new idea to analyze electric machines. A change of variable was formulated in which the variables (flux linkage, voltages and currents) associated with the stator windings of a synchronous machine were replaced by variables associated with fictitious windings rotating with the rotor. This transformation has as result the elimination of all time-varying inductances from the voltage equation of the synchronous machine which occur due to electric circuits in relative motion and electric circuits with varying magnetic reluctances. [7] Such transformation is known as Park's transformation or dq0 (direct-quadrature-zero) transformation.

It is important to remark that this development will be carried taking as reference the book "Analysis of Electric Machinery and Drive Systems" [7].

A transformation of the 3-phase variables of a stationary circuit elements to an arbitrary reference frame may be expressed as:

$$f_{dq0s} = \mathrm{K}_s \, f_{abcs} \tag{1.8}$$

where:

$$(f_{dq0s})^{\mathrm{T}} = [\, f_{ds} \; f_{qs} \; f_{0s}] \tag{1.9}$$

$$(f_{abcs})^{\mathrm{T}} = [f_{as} \; f_{bs} \; f_{cs}] \tag{1.10}$$

$$\mathrm{K}_s = \frac{2}{3}\begin{bmatrix} \cos\theta & \cos\left(\theta - \frac{2\pi}{3}\right) & \cos\left(\theta + \frac{2\pi}{3}\right) \\ \sin\theta & \sin\left(\theta - \frac{2\pi}{3}\right) & \sin\left(\theta + \frac{2\pi}{3}\right) \\ \frac{1}{2} & \frac{1}{2} & \frac{1}{2} \end{bmatrix} \tag{1.11}$$

$$\omega = \frac{\mathrm{d}\theta}{\mathrm{dt}} \tag{1.12}$$

Note that f can represent either voltage, current, flux linkage, or electric charge.

The s subscript indicates that the variable, parameter or transformation is associated with the stationary circuit.

The transformation is illustrated in Fig. 1.5.

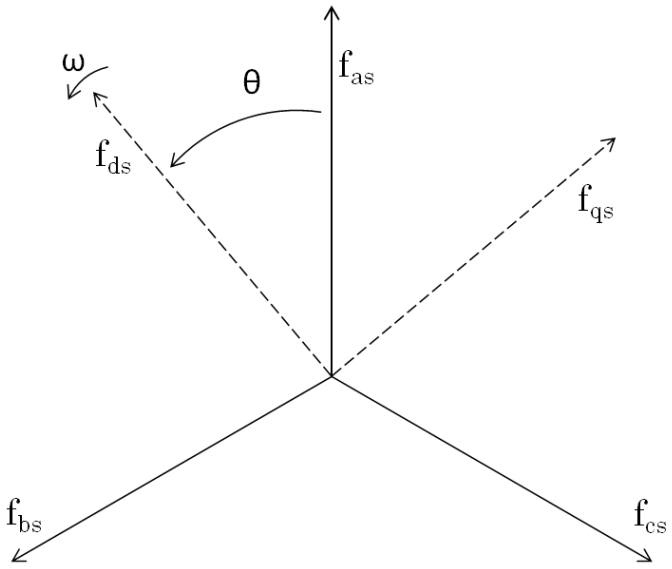

Fig. 1.5: Park's transformation

It can be shown that for the inverse transformation we have:

$$(K_s)^{-1} = \begin{bmatrix} \cos\theta & \sin\theta & 1 \\ \cos\left(\theta - \frac{2\pi}{3}\right) & \sin\left(\theta - \frac{2\pi}{3}\right) & 1 \\ \cos\left(\theta + \frac{2\pi}{3}\right) & \sin\left(\theta + \frac{2\pi}{3}\right) & 1 \end{bmatrix} \tag{1.13}$$

where ω represents the angular velocity and θ the angular position of the arbitrary reference frame. And from (1.12):

$$\theta = \int \omega \, dt \tag{1.14}$$

or in definite integral:

$$\theta = \int_0^t \omega(\xi) \, d\xi + \theta(0) \tag{1.15}$$

The original Park's transformation as presented above, although revolutionary, is not power invariant and slight modifications were presented to add this property to the transformation. The transformation as shown below takes as reference the book "Power System Control and Stability" [8] and is power invariant.

Consider now a transformation matrix T_s such that:

$$f_{dq0s} = T_s \, f_{abcs} \tag{1.16}$$

where Ts is given by:

$$T_s = \sqrt{\frac{2}{3}} \begin{bmatrix} \cos\theta & \cos\left(\theta - \frac{2\pi}{3}\right) & \cos\left(\theta + \frac{2\pi}{3}\right) \\ \sin\theta & \sin\left(\theta - \frac{2\pi}{3}\right) & \sin\left(\theta + \frac{2\pi}{3}\right) \\ \frac{\sqrt{2}}{2} & \frac{\sqrt{2}}{2} & \frac{\sqrt{2}}{2} \end{bmatrix} \tag{1.17}$$

and the inverse transformation:

$$(T_s)^{-1} = \sqrt{\frac{2}{3}} \begin{bmatrix} \cos\theta & \sin\theta & \frac{\sqrt{2}}{2} \\ \cos\left(\theta - \frac{2\pi}{3}\right) & \sin\left(\theta - \frac{2\pi}{3}\right) & \frac{\sqrt{2}}{2} \\ \cos\left(\theta + \frac{2\pi}{3}\right) & \sin\left(\theta + \frac{2\pi}{3}\right) & \frac{\sqrt{2}}{2} \end{bmatrix} \tag{1.18}$$

Note that $(T_s)^{-1} = (T_s)^T$ or, in other words, T_s is orthogonal which means that the transformation is power invariant and that we should use the same power equation on a_s-b_s-c_s and d_s-q_s-0_s [8]. Then:

$$P = v_{as}\, i_{as} + v_{bs}\, i_{bs} + v_{cs}\, i_{cs} = (v_{abcs})^{T}\, i_{abcs}$$

$$= \left((T_s)^{-1}\, v_{dq0s}\right)^{T} \left((T_s)^{-1}\, i_{dq0s}\right)$$

$$= \left(v_{dq0s}\right)^{T} \left((T_s)^{-1}\right)^{T} (T_s)^{-1}\, i_{dq0s}$$

$$= \left(v_{dq0s}\right)^{T} T_s\, (T_s)^{-1}\, i_{dq0s} = \left(v_{dq0s}\right)^{T}\, i_{dq0s}$$

$$= v_{ds}\, i_{ds} + v_{qs}\, i_{qs} + v_{0s}\, i_{0s} \qquad (1.19)$$

The transformation of stationary circuit variables into the arbitrary reference frame are shown in Appendix A. This transformations are useful, but not essential, to understand the motor modeling.

1.2.5. Synchronous motor model

This section is dedicated to the development of a model that allows the study of the electrical and electromechanical behavior of a synchronous motor. The model that we are looking for is the one considering the 3-phase salient-pole synchronous machines, illustrated in Fig. 1.6, that in most cases can be used to describe any synchronous machine with slight modifications. This model will be developed taking as reference the books "Analysis of Electric Machinery and Drive Systems" [7] and "Power System Control and Stability" [8].

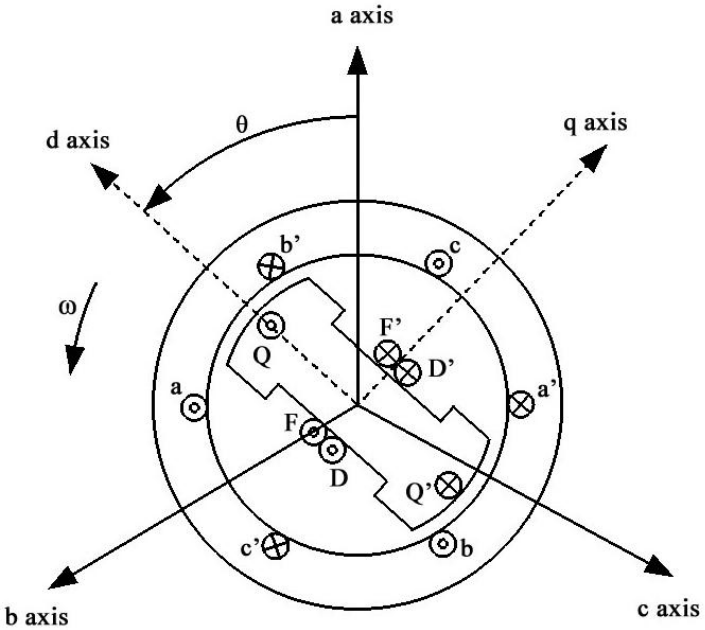

Fig. 1.6: Synchronous machine model

1.2.5.1. Flux linkage equations

In Fig. 1.6 six mutually coupled coils are present. These coils can be split into two groups: stator coils and rotor coils. The first group is composed of the three phase stator windings a-a', b-b' and c-c', by your time, the second group is composed of the field winding, F-F', and two damper windings D-D' and Q-Q'. Then the flux linkages can be described by the following matrix (here a simplification on the notation is made, lowercase subscripts are related to stator quantities while uppercase subscripts are related to rotor quantities):

$$\begin{matrix}\text{stator}\\ \\ \\ \text{rotor}\\ \\ \\ \end{matrix}\left\{\begin{bmatrix}\lambda_a\\ \lambda_b\\ \lambda_c\\ \lambda_F\\ \lambda_D\\ \lambda_Q\end{bmatrix}\right. = \left[\begin{array}{ccc:ccc} L_{aa} & L_{ab} & L_{ac} & L_{aF} & L_{aD} & L_{aQ}\\ L_{ba} & L_{bb} & L_{bc} & L_{bF} & L_{bD} & L_{bQ}\\ L_{ca} & L_{cb} & L_{cc} & L_{cF} & L_{cD} & L_{cQ}\\ \hdashline L_{Fa} & L_{Fb} & L_{Fc} & L_{FF} & L_{FD} & L_{FQ}\\ L_{Da} & L_{Db} & L_{Dc} & L_{DF} & L_{DD} & L_{DQ}\\ L_{Qa} & L_{Qb} & L_{Qc} & L_{QF} & L_{QD} & L_{QQ}\end{array}\right] \cdot \begin{bmatrix} i_a\\ i_b\\ i_c\\ i_F\\ i_D\\ i_Q\end{bmatrix} \tag{1.20}$$

where L_{ij} = self-inductance for i = j;
= mutual inductance for i ≠ j.

for example L_{aa} is the self-inductance of the a coil of the stator, L_{ab} is the mutual inductance between the coils a and b of the stator and L_{aF} is the mutual inductance between the a coil of the stator and the F coil on the rotor.

It is important to note that, in any case, $L_{ij} = L_{ji}$. Another important fact, shown by Prentice [9], is that most of the inductances in this model will vary with the rotor position and thus with time.

Now let us develop the equations for these inductances:

Stator:

self-inductances ($L_s > L_m$)

$$L_{aa} = L_s + L_m \cos 2\theta \tag{1.21}$$

$$L_{bb} = L_s + L_m \cos 2\left(\theta - \frac{2\pi}{3}\right) \tag{1.22}$$

$$L_{cc} = L_s + L_m \cos 2\left(\theta + \frac{2\pi}{3}\right) \tag{1.23}$$

mutual inductances ($|M_s| > L_m$)

$$L_{ab} = L_{ba} = -M_s - L_m \cos 2\left(\theta + \frac{\pi}{6}\right) \tag{1.24}$$

$$L_{bc} = L_{cb} = -M_s - L_m \cos 2\left(\theta - \frac{\pi}{2}\right) \tag{1.25}$$

$$L_{ca} = L_{ac} = -M_s - L_m \cos 2\left(\theta + \frac{5\pi}{6}\right) \tag{1.26}$$

Note that L_s, M_s and L_m are constant and that signs of mutual inductance terms depend on assumed current directions and coil orientations.

Rotor:

self-inductances

$$\text{field winding: } L_{FF} = L_F \tag{1.27}$$

$$\text{D-damper winding: } L_{DD} = L_D \tag{1.28}$$

$$\text{Q-damper winding: } L_{QQ} = L_Q \tag{1.29}$$

mutual inductances

$$\text{field / D-winding: } L_{FD} = L_{DF} = M_R \tag{1.30}$$

$$\text{field / Q-winding: } L_{FQ} = L_{QF} = 0 \tag{1.31}$$

$$\text{D-winding / Q-winding: } L_{DQ} = L_{QD} = 0 \tag{1.32}$$

Note that saturation and slot effect are neglected, then all rotor self-inductances are constant.

Note also that the field winding is align with the D-winding what makes the mutual inductance between them invariant with respect to θ. On the other hand, the components on the pairs field/Q-winding and D-winding/Q-winding are displaced with 90° of electrical angle between them, thus the mutual inductance is zero.

Stator-to-rotor mutual inductances:

armature / field

$$L_{aF} = L_{Fa} = M_F \cos\theta \tag{1.33}$$

$$L_{bF} = L_{Fb} = M_F \cos\left(\theta - \frac{2\pi}{3}\right) \tag{1.34}$$

$$L_{cF} = L_{Fc} = M_F \cos\left(\theta + \frac{2\pi}{3}\right) \tag{1.35}$$

armature / D-winding

$$L_{aD} = L_{Da} = M_D \cos\theta \tag{1.36}$$

$$L_{bD} = L_{Db} = M_D \cos\left(\theta - \frac{2\pi}{3}\right) \tag{1.37}$$

$$L_{cD} = L_{Dc} = M_D \cos\left(\theta + \frac{2\pi}{3}\right) \tag{1.38}$$

armature / Q-winding
$$\begin{cases} L_{aQ} = L_{Qa} = M_Q \cos\theta & (1.39) \\ L_{bQ} = L_{Qb} = M_Q \cos\left(\theta - \frac{2\pi}{3}\right) & (1.40) \\ L_{cQ} = L_{Qc} = M_Q \cos\left(\theta + \frac{2\pi}{3}\right) & (1.41) \end{cases}$$

It is easy to see that most of the inductances presented up to now are dependent on the rotor position, in other words, dependent on time what would make the next computations quite complex (computations will require the time derivative of the inductances). Thus the idea is to simplify (1.20) referring all quantities to a rotor frame of reference through a Park's transformation applied to the a-b-c partition. Then, pre-multiplying (1.20) by:

$$\begin{bmatrix} T_s & 0 \\ 0 & I_3 \end{bmatrix}$$

where T_s is given by (1.17) and I_3 is a 3x3 identity matrix. Thus:

$$\begin{bmatrix} T_s & 0 \\ 0 & I_3 \end{bmatrix}\begin{bmatrix} \lambda_{abc} \\ \lambda_{FDQ} \end{bmatrix} = \begin{bmatrix} T_s & 0 \\ 0 & I_3 \end{bmatrix}\begin{bmatrix} L_{ss} & L_{sR} \\ L_{Rs} & L_{RR} \end{bmatrix}\begin{bmatrix} T_s^{-1} & 0 \\ 0 & I_3 \end{bmatrix}\begin{bmatrix} T_s & 0 \\ 0 & I_3 \end{bmatrix}\begin{bmatrix} i_{abc} \\ i_{FDQ} \end{bmatrix} \quad (1.42)$$

where:
L_{ss} = stator-stator inductances
$L_{sR} = L_{Rs}$ = stator-rotor inductances
L_{RR} = rotor-rotor inductances

That results in:

$$\begin{bmatrix} \lambda_d \\ \lambda_q \\ \lambda_0 \\ \lambda_F \\ \lambda_D \\ \lambda_Q \end{bmatrix} = \begin{bmatrix} L_d & 0 & 0 & k M_F & k M_D & 0 \\ 0 & L_q & 0 & 0 & 0 & k M_Q \\ 0 & 0 & L_0 & 0 & 0 & 0 \\ k M_F & 0 & 0 & L_F & M_R & 0 \\ k M_D & 0 & 0 & M_R & L_D & 0 \\ 0 & k M_Q & 0 & 0 & 0 & L_Q \end{bmatrix} \cdot \begin{bmatrix} i_d \\ i_q \\ i_0 \\ i_F \\ i_D \\ i_Q \end{bmatrix} \quad (1.43)$$

where $k = \sqrt{\frac{3}{2}}$ and the constant inductances are:

$$L_d = L_s + M_s + \frac{3}{2}L_m \quad (1.44)$$

$$L_q = L_s + M_s - \frac{3}{2}L_m \quad (1.45)$$

$$L_0 = L_s - 2M_s \quad (1.46)$$

In (1.44) L_d is the direct axis self-inductance and can be understood as a self-inductance of a fictitious coil align with the direct axis which is representing the a-b-c stator coils of the stator. The same is valid for L_q in (1.45) and L_0 in (1.46).

In (1.43) λ_d is the flux linkage in a circuit equivalent to the original one but moving with the rotor and centered on the d axis. Similarly, λ_q, is centered on the q axis. Flux linkage λ_0 is completely uncoupled from the other circuits.

1.2.5.2. Voltage equations

The voltage equations for the windings presented in Fig. 1.6 can be written as:

$$\begin{bmatrix} v_a \\ v_b \\ v_c \\ v_F \\ v_D \\ v_Q \end{bmatrix} = \begin{bmatrix} r_a & 0 & 0 & 0 & 0 & 0 \\ 0 & r_b & 0 & 0 & 0 & 0 \\ 0 & 0 & r_c & 0 & 0 & 0 \\ 0 & 0 & 0 & r_F & 0 & 0 \\ 0 & 0 & 0 & 0 & r_D & 0 \\ 0 & 0 & 0 & 0 & 0 & r_Q \end{bmatrix} \cdot \begin{bmatrix} i_a \\ i_b \\ i_c \\ i_F \\ i_D \\ i_Q \end{bmatrix} + \begin{bmatrix} \dot{\lambda}_a \\ \dot{\lambda}_b \\ \dot{\lambda}_c \\ \dot{\lambda}_F \\ \dot{\lambda}_D \\ \dot{\lambda}_Q \end{bmatrix} + \begin{bmatrix} v_n \\ 0 \end{bmatrix} \tag{1.47}$$

where usually $v_D = v_Q = 0$ and v_n is the voltage on the center of the star connection (voltage drop on the neutral connection), that is given by:

$$\begin{aligned} v_n &= r_n \begin{bmatrix} 1 & 1 & 1 \\ 1 & 1 & 1 \\ 1 & 1 & 1 \end{bmatrix} \begin{bmatrix} i_a \\ i_b \\ i_c \end{bmatrix} + L_n \begin{bmatrix} 1 & 1 & 1 \\ 1 & 1 & 1 \\ 1 & 1 & 1 \end{bmatrix} \begin{bmatrix} \dot{i}_a \\ \dot{i}_b \\ \dot{i}_c \end{bmatrix} \\ &= R_n i_{abc} + L_n \dot{i}_{abc} \end{aligned} \tag{1.48}$$

Usually $r_a = r_b = r_c = r$, and a simplification on the notation can be made. Defining:

$$R_{abc} = r\, I_3 \tag{1.49}$$

where I_3 is the 3x3 identity matrix. Thus:

$$\begin{bmatrix} v_{abc} \\ v_{FDQ} \end{bmatrix} = \begin{bmatrix} R_{abc} & 0 \\ 0 & R_{FDQ} \end{bmatrix} \cdot \begin{bmatrix} i_{abc} \\ i_{FDQ} \end{bmatrix} + \begin{bmatrix} \dot{\lambda}_{abc} \\ \dot{\lambda}_{FDQ} \end{bmatrix} + \begin{bmatrix} v_n \\ 0 \end{bmatrix} \tag{1.50}$$

where:

$$(v_{FDQ})^T = \begin{bmatrix} v_F & v_D & v_Q \end{bmatrix} = \begin{bmatrix} v_F & 0 & 0 \end{bmatrix} \tag{1.51}$$

$$(i_{FDQ})^T = \begin{bmatrix} i_F & i_D & i_Q \end{bmatrix} \tag{1.52}$$

$$(\lambda_{FDQ})^T = \begin{bmatrix} \lambda_F & \lambda_D & \lambda_Q \end{bmatrix} \tag{1.53}$$

As in the flux linkage equations, this computation may be complex since it involves the time derivative of terms that are time dependent (in $\dot{\lambda}$). This complexity can be eliminated by applying the Park's transformation on the stator partition. In other words, pre-multiplying both sides of (1.50) by :

$$\begin{bmatrix} T_s & 0 \\ 0 & I_3 \end{bmatrix}$$

where T_s is given by (1.17) and I_3 is a 3x3 identity matrix.

Analyzing term by term, the left-hand side is given by:

$$\begin{bmatrix} T_s & 0 \\ 0 & I_3 \end{bmatrix} \begin{bmatrix} v_{abc} \\ v_{FDQ} \end{bmatrix} = \begin{bmatrix} v_{dq0} \\ v_{FDQ} \end{bmatrix} \tag{1.54}$$

The first term of the right-hand side can be developed according to Appendix A what gives:

$$\begin{bmatrix} T_s & 0 \\ 0 & I_3 \end{bmatrix} \begin{bmatrix} R_{abc} & 0 \\ 0 & R_{FDQ} \end{bmatrix} \cdot \begin{bmatrix} i_{abc} \\ i_{FDQ} \end{bmatrix} = \begin{bmatrix} R_{abc} & 0 \\ 0 & R_{FDQ} \end{bmatrix} \cdot \begin{bmatrix} i_{dq0} \\ i_{FDQ} \end{bmatrix} \tag{1.55}$$

for the second term, again considering the developments maid in Appendix A:

$$\begin{bmatrix} T_s & 0 \\ 0 & I_3 \end{bmatrix} \begin{bmatrix} \dot{\lambda}_{abc} \\ \dot{\lambda}_{FDQ} \end{bmatrix} = \begin{bmatrix} T_s \dot{\lambda}_{abc} \\ \dot{\lambda}_{FDQ} \end{bmatrix} \tag{1.56}$$

where:

$$T_s \dot{\lambda}_{abc} = \dot{\lambda}_{dq0} + \begin{bmatrix} -\omega\lambda_q \\ \omega\lambda_d \\ 0 \end{bmatrix}$$

and ω is the angular speed.

For the last term:

$$\begin{bmatrix} T_s & 0 \\ 0 & I_3 \end{bmatrix} \begin{bmatrix} v_n \\ 0 \end{bmatrix} = \begin{bmatrix} n_{dq0} \\ 0 \end{bmatrix} \tag{1.57}$$

where n_{dq0} is the voltage drop from the neutral to ground in the dq0 coordinate system, and is given by:

$$\begin{aligned} n_{dq0} &= T_s v_n = T_s R_n T_s^{-1} i_{dq0} + T_s L_n T_s^{-1} \dot{i}_{dq0} \\ &= \begin{bmatrix} 0 \\ 0 \\ 3r_n i_0 \end{bmatrix} + \begin{bmatrix} 0 \\ 0 \\ 3L_n \dot{i}_0 \end{bmatrix} \end{aligned} \tag{1.58}$$

Then, this voltage drop occurs just in the zero sequence.

Summarizing, equation (1.50) can be rewritten as:

$$\begin{bmatrix} v_{dq\,0} \\ v_{FDQ} \end{bmatrix} = \begin{bmatrix} R_{abc} & 0 \\ 0 & R_{FDQ} \end{bmatrix} \cdot \begin{bmatrix} i_{dq\,0} \\ i_{FDQ} \end{bmatrix} + \begin{bmatrix} \dot{\lambda}_{dq\,0} \\ \dot{\lambda}_{FDQ} \end{bmatrix} + \begin{bmatrix} \dot{T}_s T_s^{-1} \lambda_{dq\,0} \\ 0 \end{bmatrix} + \begin{bmatrix} n_{dq\,0} \\ 0 \end{bmatrix} \quad (1.59)$$

Considering balanced conditions, the zero-sequence voltage is always equal to zero and a simplification on the notation can be made. Let:

$$R = \begin{bmatrix} r & 0 \\ 0 & r \end{bmatrix};\ R_R = \begin{bmatrix} r_F & 0 & 0 \\ 0 & r_D & 0 \\ 0 & 0 & r_Q \end{bmatrix};\ S = \begin{bmatrix} -\omega\lambda_q \\ \omega\lambda_d \end{bmatrix} \quad (1.60)$$

thus:

$$\begin{bmatrix} v_{dq} \\ v_{FDQ} \end{bmatrix} = \begin{bmatrix} R & 0 \\ 0 & R_R \end{bmatrix} \cdot \begin{bmatrix} i_{dq} \\ i_{FDQ} \end{bmatrix} + \begin{bmatrix} \dot{\lambda}_{dq} \\ \dot{\lambda}_{FDQ} \end{bmatrix} + \begin{bmatrix} S \\ 0 \end{bmatrix} \quad (1.61)$$

1.2.5.3. Torque equation

The total three-phase power input into a synchronous machine is given by:

$$P_{in} = v_a\, i_a + v_b\, i_b + v_c\, i_c \quad (1.62)$$

That from (1.19) can be rewritten as:

$$P_{in} = v_d\, i_d + v_q\, i_q + v_0\, i_0 \quad (1.63)$$

Considering balanced system but not necessarily steady-state conditions. Then, $v_0 = i_0 = 0$ and:

$$P_{in} = v_d\, i_d + v_q\, i_q \quad (1.64)$$

Substituting v_d and v_q with (1.61):

$$P_{in} = \left(i_d\, \dot{\lambda_d} + i_q\, \dot{\lambda_q}\right) + \left(i_q\, \lambda_d - i_d\, \lambda_q\right)\omega + r\left(i_d{}^2 + i_q{}^2\right) \quad (1.65)$$

Concordia [10] observes that the three terms are identifiable as the rate of change of stator magnetic field energy, the power transferred across the air gap, and the stator ohmic losses respectively. The machine torque is obtained from the second term divided by the angular speed of the machine:

$$T_e = \frac{p}{2}\left(i_q\, \lambda_d - i_d\, \lambda_q\right) \quad (1.66)$$

where p is the number of poles of the machine. The term $\frac{p}{2}$ appears from the relation between the mechanical angle and the electrical angle.

1.3. Adjustable speed drive systems (ASDS)

Now that the model for a synchronous motor was described, it is time to address some ideas on the problem of controlling and driving such machine. One way of realizing this task is through the usage of adjustable speed drive systems (ASDS) or variable speed drives systems (VSDS), that are the components that will be discussed in the following sections.

These components have as main characteristic the control of the speed of machinery and many industrial processes require their use, such as assembly lines, compressors and pumps. Having this in mind, especial attention is being devoted to the problem of driving compressors and pumps by means of large ASDS since this is an increasing field in oil and gas applications, specially for gas/oil transportation, gas liquefaction and gas injection/lift [3]. This growth in the usage of ASDS can be mainly associated to the increase of efficiency of the system when comparing situations with and without use of ASDS. This fact can be easily illustrated with an general example:

Let us think about the possibilities of changing the air flow in a process. This change can be done at least in two different ways:

- the first and more traditional way requires the use of a fixed speed motor connected to a fan that generates a air flow invariably higher than the one that is required and dampers can be used to reduce this airflow.
- the second approach could make use of ASDS to directly control the speed of the motor driving the fan and generating just the required airflow.

Now it is easy to understand that when using an ASDS the efficiency of the system can be considerably higher since it avoids the loss of energy associated to the generation of an airflow bigger than the necessary one and then reducing it by mean of mechanical constraints. This idea can be easily generalized for fans, pumps, compressors associated with dampers, control valves and so on.

Now that an overview was done in ASDS, let us get into some details of ASDS and the importance of testing them. Before that a remark should be done, ASDS and VSDS may be purely mechanical, electromechanical, hydraulic, or electronic and the ones discussed in this thesis are the purely electronic ones.

1.3.1. Typical configuration of an ASDS

An adjustable speed drive system is typically composed of: input converter transformer, frequency converter, motor, system control and protection and in addition any needed harmonic filter and cooling system. There are two different topologies of ASDS available on the market: Voltage Source Inverter (VSI) and Load Commutated Inverter (LCI) [3].

In the voltage source inverter the front end is composed by a three-phase diode-bridge rectifier that converts the AC voltage supply into a DC voltage. After this stage, a dc-link constituted of a shunt capacitor is connected to the DC side of the rectifier reducing the ripple on the DC voltage. Then, an inverter is used to reconvert the DC voltage into a three-phase AC voltage with variable frequency and sometimes variable magnitude. Finally, this generated AC voltage is used as input to the motor. The Fig. 1.7 illustrates the typical schemes for a VSI ASDS.

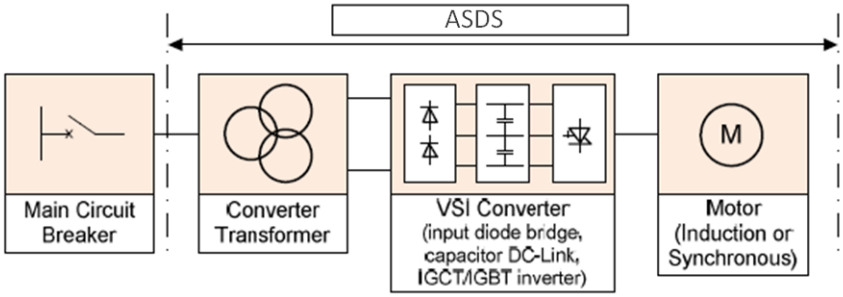

Fig. 1.7: Typical VSI ASDS scheme [3]

In the load commutated inverter the main idea on the transformations still the same of the VSI but different stages are used. In the front end a thyristor bridge rectifier is utilized, as dc-link a DC-reactor is introduced and the last stage is composed by a thyristor inverter. Fig. 1.8 illustrates the typical schemes for a LCI ASDS. For more information about the LCI converters one may refer to chapter 9 of reference [2].

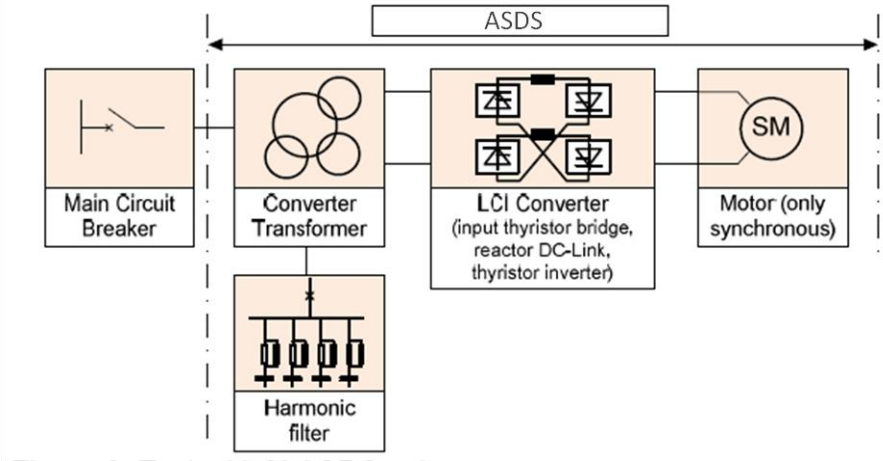

Fig. 1.8: Typical LCI ASDS scheme [3]

On the market it is possible to find some configurations of LCI drives and one of them is the MEGADRIVE-LCI Medium Voltage AC Drive from ABB. It is available in the power range from 1000 kW to 100000 kW and is also suitable for

high-speed applications with turbo machines up to approximately 7000 rpm. It can be water-cooled or air-cooled depending on the power capability of the system [2].

The MEGADRIVE-LCI is composed of:

- power part and DC-reactor
- converter control unit
- other components depending on the application

For example, considering the drive configuration that has as aim the continuous operation of the motor in variable speed, a third component of the LCI is the excitation unit. On the other hand, when the application is the Soft Starter that has as aim the starting of the motor from zero speed to nominal speed and synchronization of the motor with the line, a third and a fourth component are included and they are a bypass disconnector for output transformer and a synchronizer [2].

Focusing on the system tested during this thesis, the MEGADRIVE-LCI utilized consists of a water-cooled version with 12/12-pulse one-channel connection and type code W1212-483N465. When necessary more information will be given during this text and for further information one may refer to reference [2].

1.3.2. Testing large ASDS

After presenting the basic aspects of ASDS the key point for this thesis arrives, more specifically the testing of large ASDS for oil and gas applications that, as already mentioned, is an increasing field for the ASDS. It is important to highlight that in these applications the ASDS availability is of extreme importance for the plant operation which results on the necessity of extensive factory testing before delivering at site. These tests aim to uncover any possible hidden weakness of the components and system design issues [3].

During the testing stage the following aspects are checked:

- Verify that the system design and integration have been properly done;
- Ensure that the required performances are met;
- Check that the protection devices and setting work effectively;
- Test ASDS rated power and any overloads the system is designed for;
- Run the temperature rise test with the actual distorted currents;
- Evaluate system efficiency

These checks are made according to international standards and/or oil and gas company specifications. The international standards of most interest for this field are IEC61800-4 [11], IEEE1566 [12]. In Appendix B a table is presented with the main aspects of each standard.

Each test procedure has its own peculiarity but the point to be stressed here is that for the IEC standard the measurement of torque pulsation is required. This

thesis will discuss methods for such measurement and comment results of the application of such measurement technique in large ASDS under test. But first some aspects of the test set-up and the origin of the torque pulsation will be introduced.

1.3.2.1. Test set-up

The first issue to be addressed when testing ASDS with power in the megawatt range is that the availability of a suitable load machine cannot be taken for granted. For this reason and depending on the ASDS topology, different set-ups can be applied to run the test at required load.

The first set-up can be used in situations in which two or more LCI ASDS are part of the project. In this case the back to back test is the typical set-up. Considering that LCI ASDS are intrinsically regenerative, the back to back test has as idea the line-up of the two systems one against the other with one operating as motor and the other as generator [3]. Fig. 1.9 illustrates the typical back to back set-up.

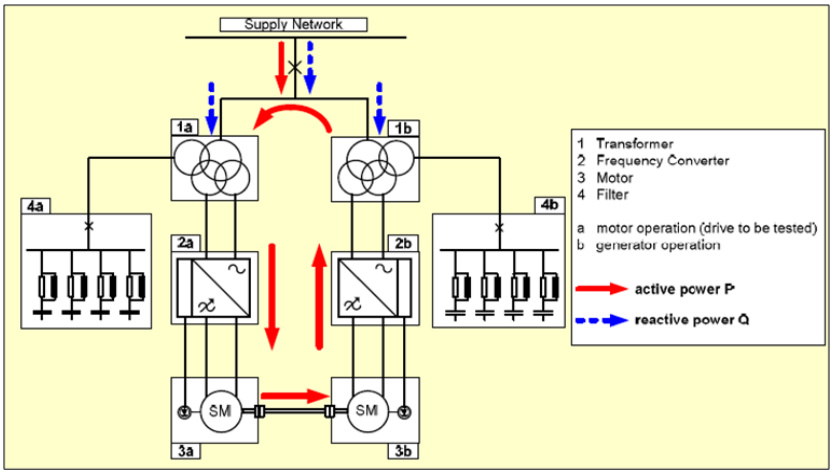

Fig. 1.9: Back to back typical set-up [3]

However, when VSI ASDS are used, since their input diode bridge are not regenerative, or when only one ASDS is part of the project, a different approach need to be followed. Considering the large power involved, the test bed concept based on the energy recirculation is the best strategy to be adopted. This idea consists on having a regenerative braking machine that is able to compensated the reactive power absorbed by the load machine. In this way, only the losses of the two systems are supplied by the test bed feeding network [3]. This type of test can be referred as full load test and is illustrated by Fig. 1.10. This configuration will be the one used during the tests realized in this thesis and some other details will be given further ahead when discussing the test facilities.

Another important aspect is that some challenges are imposed by such test configuration, but as they are not part of the main scope of this thesis they will not be discussed. For more details one may refer to reference [3] in which they are fully presented and possible solutions are discussed.

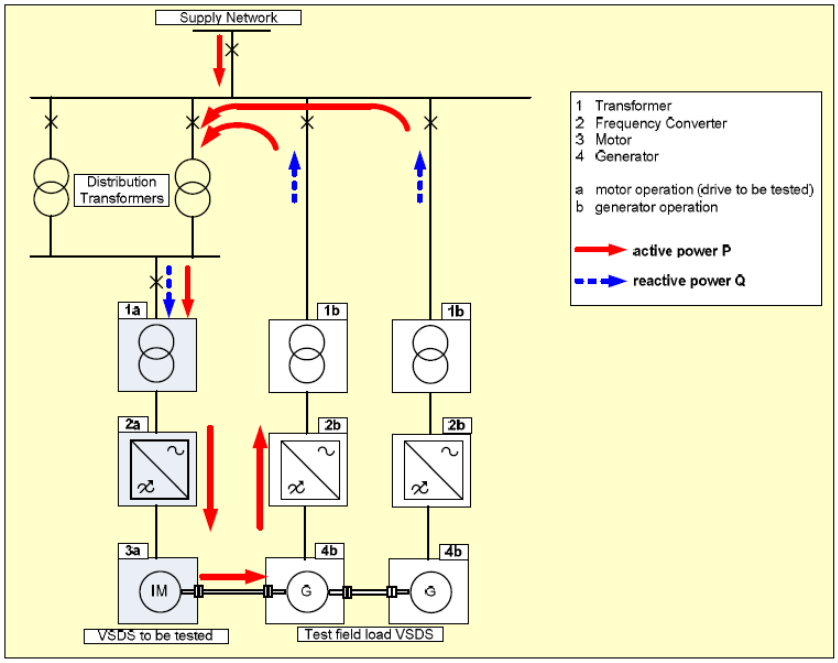

Fig. 1.10: Full load test typical set-up [3]

1.3.2.2. Air gap torque pulsation in ASDS tests

As mentioned on the beginning of this section, the air gap torque pulsation measurement is one of the tests requested by the IEC61800-4. So let us explain the importance and the possible origin of such torque pulsation.

As any mechanical system, a synchronous motor and the load connected to it can be represented by a equivalent system of masses and springs, with natural frequencies associated to the spring constant and masses [1]. Some systems are intrinsically sufficient damped or sufficient stiff that resonances are not of concern. On the other hand, some systems are inherently flexible and resonances may arise by the excitation caused by the pulsating torque [13]. It is important to highlight that this resonance may occur even if the magnitude of the pulsating torque can normally be neglected in respect of its nominal value [3].

Concerning the test of large ASDS care should be taken on the design of the coupling between the machine under test and the braking machine in order to withstand short circuit torques and avoid possible resonances due to the pulsating torque in the air gap [3].

Fig. 1.11 shows an illustrative example of the coupling between motor and braking machine (evidenced in red), an analysis of the tension over the shaft line and an analysis of critical frequencies of the illustrated system.

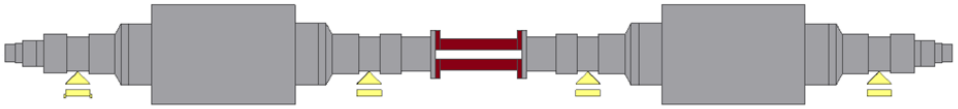

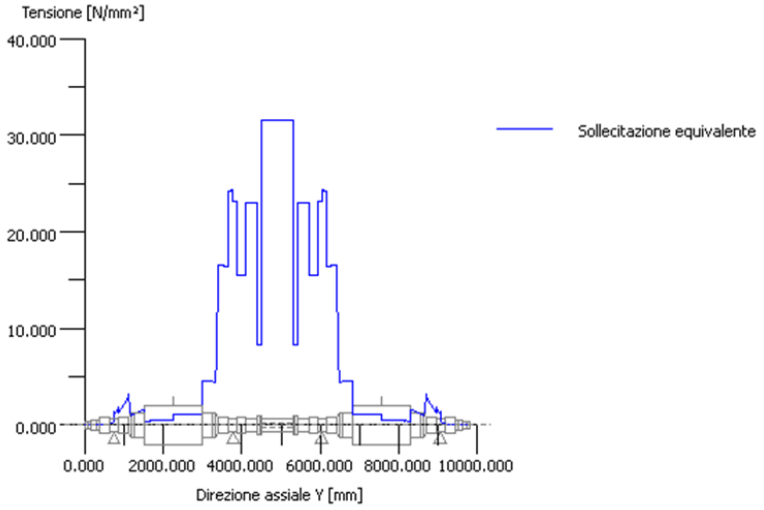

Frequenze naturale/N. di giri critici

1.	Frequenza naturale:	0.00 Hz,	N. di giri critico:	0.01 1/min	Rotazione corpo rigido Y 'Albero 1'
2.	Frequenza naturale:	39.32 Hz,	N. di giri critico:	2359.29 1/min	Torsione 'Albero 1'
3.	Frequenza naturale:	98.83 Hz,	N. di giri critico:	5929.61 1/min	Assiale 'Albero 1'
4.	Frequenza naturale:	124.09 Hz,	N. di giri critico:	7445.53 1/min	Flessione XY 'Albero 1'
5.	Frequenza naturale:	124.09 Hz,	N. di giri critico:	7445.53 1/min	Flessione YZ 'Albero 1'
6.	Frequenza naturale:	131.42 Hz,	N. di giri critico:	7884.96 1/min	Flessione XY 'Albero 1'
7.	Frequenza naturale:	131.42 Hz,	N. di giri critico:	7884.96 1/min	Flessione YZ 'Albero 1'
8.	Frequenza naturale:	227.57 Hz,	N. di giri critico:	13654.12 1/min	Flessione YZ 'Albero 1'
9.	Frequenza naturale:	227.57 Hz,	N. di giri critico:	13654.12 1/min	Flessione XY 'Albero 1'
10.	Frequenza naturale:	316.08 Hz,	N. di giri critico:	18964.82 1/min	Assiale 'Albero 1'

Fig. 1.11: Illustrative example of coupling between motor and braking machine

The torque pulsation can mainly derive from two different components: the asynchronous start of the motor and the current harmonics impressed on the motor by the converter.

1.3.2.3. Starting torque pulsations

According to literature [1] and IEEE standards [13], all salient pole synchronous machines develop the following components of electromagnetic torque during the starting phase:

- A time-average or unidirectional component. This component is useful to accelerate the machine and results from the interaction between the forward rotating component of the rotor currents and the symmetrical alternating component of the air gap flux linkage.
- An initial transient (decaying) component which results from the initial asymmetrical component of the inrush current interacting with the symmetrical component of the air gap flux linkages.
- A steady state component at twice slip frequency (difference between the synchronous speed and the rotor speed multiplied by the number of pole pairs) which results from the asymmetry of the rotor electrical and magnetic circuits.

Pulsating electromagnetic torques caused by rotor asymmetry are considered to be the most important detrimental pulsating component. For this reason the three causes of the rotor asymmetry are presented below. It is important to remark that this geometry repeats once per pole pitch.

- Magnetic permeance variations which are the result of the salient pole being relatively easily magnetized at the center of the interpolar space.
- Main field windings which encircle only the direct axis and not the quadrature axis.
- Variable bar span of the damper winding (amortisseus).

An additional component of continuous torque pulsation at slip frequency is added when the main field winding is excited by direct current, this addition happens due to the fact that the electromagnetic geometry repeats once for every two poles. In most cases the field winding is shorted either across the terminals or through a field discharge resistor. If the acceleration phase (before synchronizing speed is reached) occurs with the field excitation being applied, an additional large component of pulsating torque appears with a frequency one-half of the slip frequency. On the other hand, if the field excitation is not applied the frequency of the pulsating torque varies almost linearly from twice the line frequency at standstill to zero at synchronous speed.

Although of big importance the pulsating torque arising from the asynchronous start will not be the focus of this thesis, since the machines tested during this thesis are composed by a round rotor and not a salient pole machine, in which this source of torque pulsation is of more interest.

1.3.2.4. Current harmonics torque pulsations

When dealing with LCI drive, like all other drive systems utilizing static converter equipment, current harmonics are generated and forced upon the supply network and the synchronous machine. At this point it is important to highlight that not only the supply network is affected by the corresponding current harmonics but also the machine will be affected [2].

The origin of such current harmonics relies on the fact that the current in the DC link will not be completely smooth, even if there is a dc-reactor. The voltage harmonics of constant frequency in the line converter DC voltage and those of variable frequency in the machine converter DC voltage, produce non-characteristic ripples in the DC current. This results in additional non-integer harmonics (the exact definition for non-integer harmonics is given on the following) in the line currents, in the machine currents and in the electrical torque on the machine [2].

Considering the motor side, the pulsating torque frequencies of uniform LCI configuration are well-known. Assuming a constant network frequency f_N (or slightly shifting within the industrial and international standards), and a drive output frequency f_M. Assuming a p-pulse configuration ($p = 6$ for 6-pulse, $p = 12$ for 12-pulse and $p = 24$ for 24-pulse LCI system). The pulsating torque are located at the following frequencies [3][14]:

- integer pulsating torques with frequencies: $n \cdot f_M$ $(n = p \cdot l)$
- non-integer pulsating torques with frequencies: $k \cdot f_N$ $(k = p \cdot l)$
- non-integer pulsating torques depending both on the network frequency and the motor frequency according to: $|n \cdot f_M \pm k \cdot f_N|$ $(n = p \cdot l;\ k = p \cdot l)$
- where $l = 0, 1, 2, 3$ ...

One way of reducing the harmonic currents on the machine side (and also on the line side) is to split the converter into two converters operating 30° phase displaced with respect to each other. Such a 12-pulse converter will eliminate the 5^{th} and 7^{th} harmonics, which normally are the largest, under all operating conditions. To reduce even more the harmonics on the line side the converter can be split into four converters operating 15° phase displaced with respect to each other. This operation (24-pulse converter) will eliminate not only the 5^{th} & 7^{th} harmonics but also the 11^{th} & 13^{th} and 17^{th} & 19^{th} harmonics [2].

The idea of making LCI configurations more complex is understandable when considering that on the motor side, the current harmonic reduction is directly reducing the air gap torque pulsation. In these complex configurations the number of pulses, p, in the grid side can be different from the number of pulses, q, on the motor side. Then [14]:

- integer pulsating torques with frequencies: $n \cdot f_M$ $(n = q \cdot l)$
- non-integer pulsating torques with frequencies: $k \cdot f_N$ $(k = p \cdot l)$
- non-integer pulsating torques depending both on the network frequency and the motor frequency according to: $|n \cdot f_M \pm k \cdot f_N|$ $(n = q \cdot l;\ k = p \cdot l)$
- where $l = 0, 1, 2, 3$ ...

Fig. 1.12 illustrates the pulsating torque frequency for a LCI 12/12 pulse (the one in use during the tests developed during this thesis).

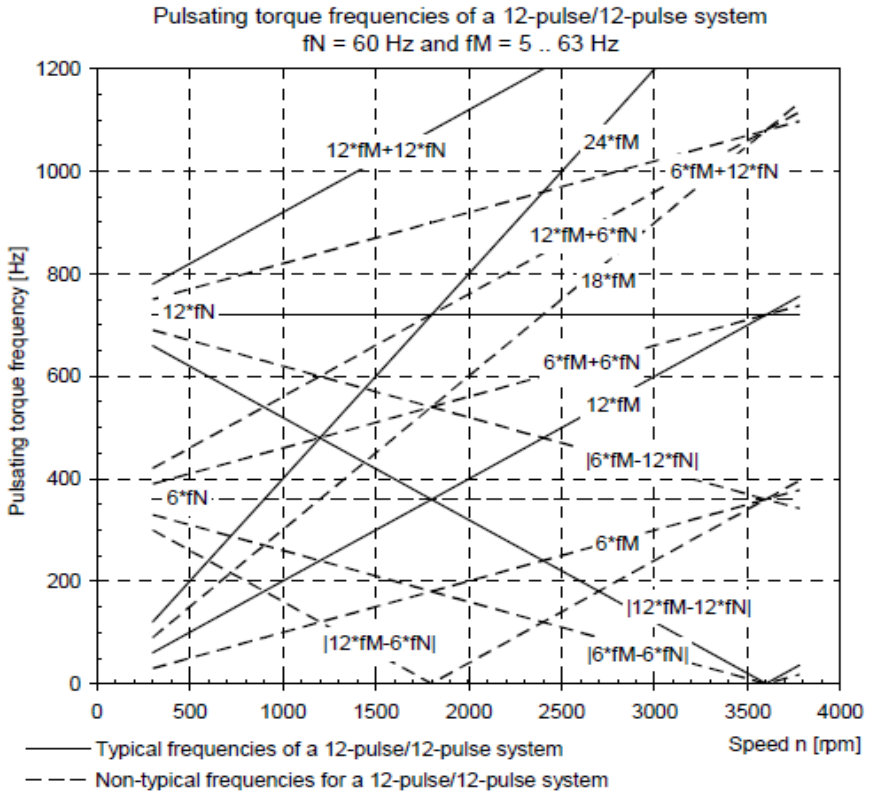

Fig. 1.12: Pulsating torque frequencies [3]

1.4. ABB

Now that all the theoretical concepts were covered, let us introduce some key facts of ABB and its Oil, Gas & Petrochemical division in Italy. This section will be also devoted to the presentation of the testing facilities used during this thesis.

1.4.1. ABB key facts

ABB is a global leader in power and automation technologies.

- Headquarter in Zurich
- 145,000 employees in about 100 countries
- In 1988 ASEA (Allmänna Svenska Elektriska Aktiebolaget) and BBC (Brown, Boveri & Cie) merge and ABB was formed.
- $39 billion in revenue (2012)

Power and productivity for a better world™

1.4.2. ABB S.p.A. (Italy): Key facts

- Headquarter in Milan
- Over 5,500 employees (2010)
- € 2,463 million in revenue (2010)

Among the several divisions of ABB present in Italy there is the Process and Automation division in which the Automation & Electrical Systems for Oil, Gas & Petrochemical takes place.

1.4.3. ABB at CESI

1.4.3.1. CESI S.p.A. (Italy): Key facts

National Research Center for Electrical Application.

- Headquarter in Milano
- Laboratories in Milano, Piacenza, Segrate, Mannheim and Berlin
- Main activities:
    - Test on electromechanical and electronic components
    - Studies, consulting and supplies for electric power systems (generation, transmission, distribution and control)
    - System and product certification services

1.4.3.2. Full load and back to back test facilities

ABB worked in close cooperation with CESI to develop the test facilities, which helps ABB to meet the increasing demand from OEMs (Original Equipment Manufacturers) and end-users.

These facilities enable ABB to deliver tested equipment meeting the stringent requirements of the oil and gas and other industries, in which full load testing of electrical equipment is required.

The test facility is composed of two test bay disposed in a area of 4,000 sqm. In Fig. 1.13 an illustration of the test area can be seen.

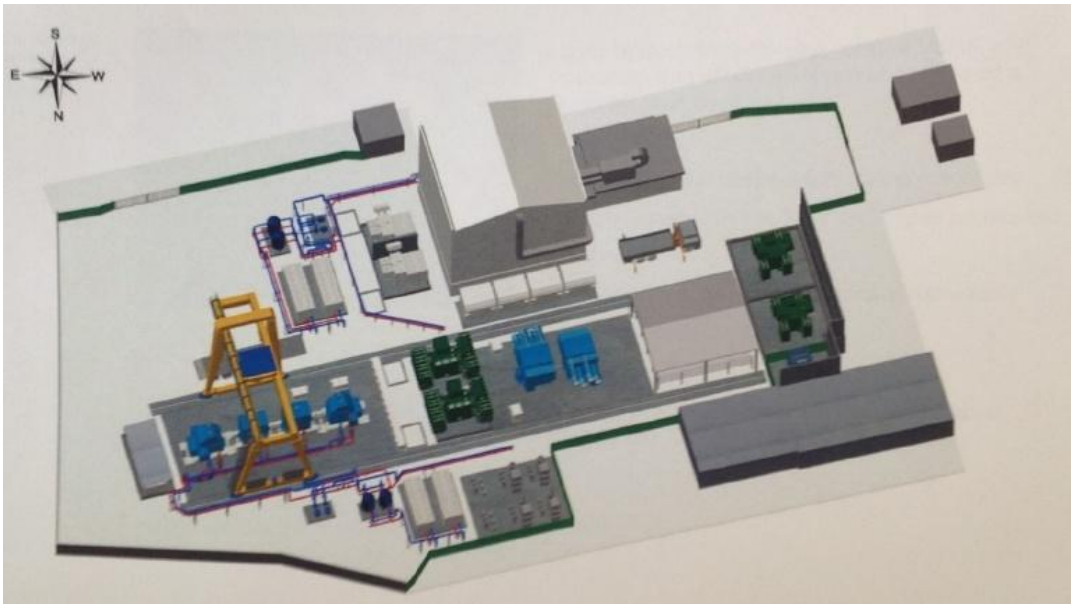

Fig. 1.13: CESI test area

Characteristics of the back to back test bay:

- back to back tests up to 45MW shaft power or more on a case by case basis
- 1,900 sqm area
- 240 sqm inertial platform for rotating machinery
- supply voltages 24kV, 33kV and higher on request
- testing:
  - Performance measurements at full load
  - Vibrations
  - Noise

Characteristics of the full load test bay (the one used on tests realized during this thesis) that can be seen in Fig. 1.14:

- full load tests up to 30MW shaft power
- 2,100 sqm area
- 240 sqm inertial platform for rotating machinery
- supply voltages 6.6kV, 11kV, 24kV, 33kV and higher on request
- two regenerative load ASDS up to 15MW each, 30MW in tandem configuration
- testing:
  - Performance measurements at full load
  - Vibrations
  - Noise

Fig. 1.14: Full load test bay

1.5. Objectives

This thesis has as objective the implementation of measurement techniques of pulsating torque on a 19.3MW and a 20MW round rotor synchronous machine fed by ASDS with LCI configuration. Such machines and driving systems were produced by ABB and passed through test procedures on CESI .

An important aspect to be considered during the thesis development is the selection of the available methods for pulsating torque measurement, since it must take into consideration the cost and complexity of the possible solution. Then, the main target to be pursued is to have methods in which the measurements use, as much as possible, already available sensors (current and voltage).

The methods presented in literature will be discussed on the following section and the ones fulfilling the requirements for this work will be implemented and will have the results commented on the following chapters.

2. Methods

After introducing the main aspects to be considered during this thesis, this section will be devoted to explain and compare the methods present in the literature for the measurement of the torque pulsation on synchronous machines. Even though the methods utilized for measurement of pulsating torque on synchronous machines are more described as the measurements of starting torque pulsations of salient pole machines [1][13], the main ideas of such methods can be extended to any instantaneous torque measurement.

On the measurement of pulsating torque, the electrical system has a strong influence on the level of pulsation and simple mathematical models are not able to describe it accurately. Therefore, methods that involve the usage of mechanical or electrical measurements are the preferred test methods. These methods can be divided into two groups: mechanical methods and electrical methods, depending on the measurements to be taken in order to compute the pulsating torque [13].

The following topics will be devoted to briefly present some more details on the methods available in literature. For more details, one may refer to references [1] and [13].

2.1. Mechanical methods for electromagnetic air gap torque measurement

The most "natural" and traditional idea for torque measurement is the use of strain gauges coupling the load and the motor shaft. But the use of these equipments, in association with an electric conditioning equipment, yields accurate results just for constant or slowly varying torque. Then, the reliability for transient torque measurements cannot be guaranteed, because of limits of their dynamic behavior and the inertia of the machine rotor, which influences the results [15]. Not forgetting to mention that the equipment needed in this method and even the set-up of such measurement equipment can be very expensive. Thus, other mechanical methods based on other measurements are presented:

2.1.1. Measurement of angular acceleration

This method utilizes the relation between angular acceleration and electromagnetic torque given by the equation (2.1):

$$T_e = \frac{2J}{p}\frac{d^2\theta}{dt^2} + T_{w+f} \qquad (2.1)$$

where:

J is the mass moment of inertia of the rotor

p is the number of poles

T_{w+f} is the torque drop due to windage and friction

$\frac{d^2\theta}{dt^2}$ is the angular acceleration of the rotor, in electrical radians per second square

t is the time

all the measurements in SI units.

In most cases the effect of the windage and the friction can be neglected. This fact is not true for machines with unusually large bearing or fan.

The measurement of acceleration can be obtained by piezoelectric accelerometers or other angular accelerometers, such as those that are closed loop. For each specific case, some limitations arises from the characteristics of the accelerometers chosen (for more details, please refer to [13]).

2.1.2. Measurement of rotational speed

The measurement of the rotational speed can also be used to compute the pulsating torque. Theoretically, the angular velocity of the shaft can be differentiated to provide shaft angular acceleration, and then utilized on equation (2.1). In practice, very high resolution is required to examine transient torques and, even though success has been achieved in measuring instantaneous angular acceleration by the differentiation of the angular speed, this method is not recommended over the accelerometer method [13].

2.1.3. Torque shaft method

A special shaft (torque shaft) must be attached between the motor and the load for measure the torque transmitted between them on an instantaneous basis. This system is rather delicate, but when used properly, gives results over a bandwidth much wider than the torque pulsation frequencies of interest [13]. The instantaneous electromagnetic torque can be related to measured strain according to equation (2.2).

$$T_{strain} = \left[T_e - T_{w+f} - \frac{2J}{p}\frac{d^2\theta}{dt^2}\right] - \left[\frac{2J_{load}}{p}\frac{d^2\theta_{load}}{dt^2} + T_{load}\left(\theta_{load}, \frac{d\theta_{load}}{dt}\right)\right] \quad (2.2)$$

Where:

J is the mass moment of inertia of the rotor

p is the number of poles

T_{w+f} is the torque drop due to windage and friction

T_e is the air gap torque

$\frac{d\theta}{dt}$ is the angular velocity of the rotor, in electrical radians per second square

t is the time

load as a subscript denotes the components of the inertia, torque and electrical angular rotation on the load side of the torque shaft

all the measurements in SI units.

One more time the windage and the friction can be neglected in most cases. This fact is not true for machines with unusually large bearing or fan.

In general, the load varies as a function of the angular position and also as function of the angular velocity. If the load characteristics are completely known as a function of these parameters, the air gap torque can be computed using this method. However, practically, only in exceptional cases this calculation can be completed accurately [13].

2.2. Electrical methods for electromagnetic air gap torque measurement

In this section, the torque equation presented in section 1.2.5.3 will be the main artifact to be used. So it is convenient to have it in mind:

$$T_e = \frac{p}{2}\left(i_q \lambda_d - i_d \lambda_q\right) \tag{2.3}$$

2.2.1. Search coil and current sensors method

This method consists on a "direct" measurement of the air gap flux and the stator current which are the components of the electromagnetic torque, as presented in equation (2.3).

The measurement of the flux can be made by the use of Hall probes or search coils inserted in the air gap of the machine. When using Hall probes several practical limitations arises, between them it is important to mention:

- possibility of damage on the probes during installation.
- possibility of damage on the probes during measurement due to the fact that they are placed directly on the armature winding, which in general is one of the hottest portions of the machine.

These limitations make the use of Hall probes not convenient for the measurement of electromagnetic torque.

On the other hand, the use of search coils together with current sensors represents the most accurate method for electromagnetic measurement and consists

on measuring the voltage induced in these coils and integrating them to produce the measure of the air gap flux linkage [1].

Kamerbeek [16] has shown that if hysteresis is neglected and if the magnetic field can be considered as a state function, the electromagnetic torque acting on the shaft can be expressed as the integral described by equation (2.4).

$$T_e = \int_A R\, B_r\, H_\phi \, dA \tag{2.4}$$

Where:

A is the area of the cylindrical surface described by the air gap

B_r is the radial component of air gap magnetic flux density

H_ϕ is the tangential component of magnetic field intensity

R is the radius from the shaft center line to the surface of the stator core facing the air gap

all the measurements in SI units.

Equation (2.4) also assumes that the flux penetrating the ends of the machines is zero [1].

Considering that no eddy currents or permanent magnetization exists in the stator iron and that saliency exists only on the rotor, Holt [17] has shown that:

$$T_e = \frac{\sqrt{3}\, p}{2}\, K_w \left[i_c \int_0^t v_{mb}\, dt - i_b \int_0^t v_{mc}\, dt \right] \tag{2.5}$$

where:

K_w is the fundamental number of effective turns of the armature winding divided by the fundamental number of turns of the search coil winding

p is the number of poles

v_{mb} , v_{mc} are the induced voltage in a pair of search coils located concentric with the magnetic axis of the b and c phases of the machine windings, respectively. For more details, please refer to [13]

i_b , i_c are the currents in phase b and c, respectively

all the measurements in SI units.

The good performance of this method makes it attractive, but the extra cost arising from the installation of the flux coils and the possible breakage of the coil wires, during operation, do to vibrations are a considerable drawback [1].

2.2.2. Measurement of electromagnetic torque using input power sensing

This method makes use of the concept of "synchronous watts", introduced by Mayer and Owen [18], which provides another mean of computing the electromagnetic torque:

$$T_e \cong \frac{p}{2}\frac{P_{ag}}{\omega} \tag{2.6}$$

where P_{ag} is the power transferred across the air gap from stator to rotor.

In terms of terminal quantities:

$$T_e \cong \frac{p}{2}\frac{(P_{in} - P_{loss} - P_{leak})}{\omega} \tag{2.7}$$

where:

P_{in} is the power flow into the stator terminals

P_{loss} is the instantaneous copper losses

P_{leak} is the instantaneous time rate of change of magnetic field energy stored in the stator leakage magnetic field

p is the number of poles

ω is the angular frequency of the applied voltage

When the stator magnetic stored energy is assumed to not vary rapidly, equation (2.7) can be rewritten:

$$T_e \cong \frac{p}{2}\frac{(P_{in} - P_{loss})}{\omega} \tag{2.8}$$

In Ojo et al. [1], this method is named as the modified input power method (MIP) .

For large machines operating in quasi steady-state condition, the quantities P_{loss} and P_{leak} can be, generally, neglected [1]. Thus:

$$T_e \cong \frac{p}{2}\frac{P_{in}}{\omega} \tag{2.9}$$

This approach is somewhat less accurate than the volt-ampere method (that will be presented on item 2.2.4), but for large machines both methods yield almost the same solution.

2.2.3. Measurement of electromagnetic torque using electrical power input and speed sensing

The input power can be obtained by the equations (1.64) and (1.65) introduced in section 1.2.5.3:

$$P_{in} = \mathrm{v}_d\, \mathrm{i}_d + \mathrm{v}_q\, \mathrm{i}_q \tag{2.10}$$

Substituting v_d and v_q with (1.61):

$$P_{in} = \left(\mathrm{i}_d\, \dot{\lambda}_d + \mathrm{i}_q\, \dot{\lambda}_q\right) + \left(\mathrm{i}_q\, \lambda_d - \mathrm{i}_d\, \lambda_q\right)\omega + \mathrm{r}\left(\mathrm{i}_d{}^2 + \mathrm{i}_q{}^2\right) \tag{2.11}$$

Remember that equation (2.11) can be expressed as:

$$P_{in} = P_{mag} + P_{mec\,h} + P_{loss} \tag{2.12}$$

Where the term P_{loss} is the instantaneous stator cooper lose, P_{mag} is the instantaneous time rate of change of magnetic field energy stored in the magnetic field and $P_{mec\,h}$ is the shaft output power. These terms can be expressed as:

$$P_{mag} = \left(\mathrm{i}_d\, \dot{\lambda}_d + \mathrm{i}_q\, \dot{\lambda}_q\right) \tag{2.13}$$

$$P_{mec\,h} = \left(\mathrm{i}_q\, \lambda_d - \mathrm{i}_d\, \lambda_q\right)\omega \tag{2.14}$$

$$P_{loss} = \mathrm{r}\left(\mathrm{i}_d{}^2 + \mathrm{i}_q{}^2\right) \tag{2.15}$$

Analyzing equations (2.3) and (2.12), one can conclude:

$$T_e = \left(\frac{P_{in} - P_{mag} - P_{loss}}{\omega_r}\right)\frac{\mathrm{p}}{2} \tag{2.16}$$

where:

ω_r is the actual mechanical angular speed of the rotor

p is the number of poles

When operating in quasi-steady state condition, the time rate of change of magnetic field energy stored in the magnetic field, P_{mag}, is nearly zero. And, if the stator cooper loses are negligible, P_{loss}, this method for the torque measurement can be sufficiently accurate [1].

2.2.4. Measurement of electromagnetic torque using terminal voltage and current sensing

Before presenting the method, it is important to mention the structure of a "VI observer" that will be used in the following steps. This observer allows the

computation of the flux linkage on the dq axis based on the dq voltages and currents, and states:

$$\lambda_{d,q} = \int (v_{d,q} - r\, i_{d,q})\mathrm{dt} \tag{2.17}$$

Special attention must be driven to the flux computation in order to suppress any offset in the numerical integrations without influencing the current and flux aperiodic components [19].

Now, starting from equation (2.3) and (2.17), if eddy currents, armature tooth saturation, skin effect stator resistance and magnetic hysteresis are neglect, the electromagnetic torque of a synchronous machine can be expressed as a function of the terminal currents and voltages, as [1]:

$$T_e = \frac{\sqrt{3}\, p}{6}\Big\{(i_a - i_b) \int [v_{ca} - r_s(i_c - i_a)]\mathrm{dt} - (i_c - i_a) \int [v_{ab} - r_s(i_a - i_b)]\mathrm{dt}\Big\} \tag{2.18}$$

where:

i_a , i_b , i_c	Are the currents in phase a, b and c, respectively
v_{ab}	is the voltage of line a with respect to line b
v_{ca}	is the voltage of line c with respect to line a
p	is the number of poles

all the measurements in SI units.

In reference [1] this method is named: modified volt-second ampere (MVSA) method. An important aspect of the MVSA method is that, since the stator resistance changes with temperature and is only approximately, the results must be interpreted with care [1].

In machines above 764 kW (1000 hp), the effect of stator resistance can be neglected [13], thus:

$$T_e \cong \frac{\sqrt{3}\, p}{6}\Big\{(i_a - i_b) \int v_{ca}\ \mathrm{dt} - (i_c - i_a) \int v_{ab}\ \mathrm{dt}\Big\} \tag{2.19}$$

This method is named, in reference [1], as volt-second ampere (VSA) method and allows the computation of the electromagnetic torque using only two line-to-line voltages and two current measurements [13].

The same idea presented in this method is also used on the "digital transient torque measurement", technique presented on reference [19] and explored on reference [15].

2.3. Comparison between methods

Ojo et al. [1] compared the results of the methods for a 25 hp salient pole Synchronous motor, while Gillard [20] compared the methods for a 14000 hp synchronous motor, and the main results of these comparisons will be briefly shown in this section. For detailed explanation one may refer to references [1] and [20]. Both comparisons were made for the analysis of pulsating torque during the starting of the synchronous machine, but, as already mentioned, the idea can be generalized for any instantaneous torque measurement.

For the 25 hp synchronous motor the results found by Ojo et al.[1] are:

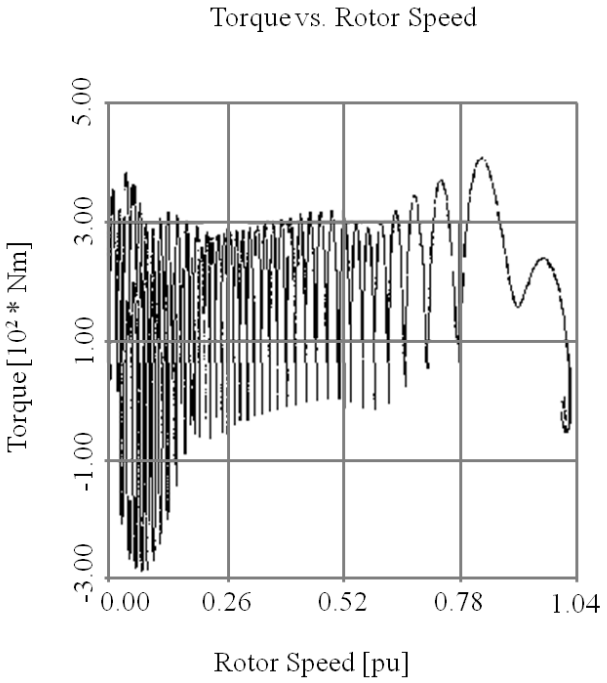

Fig. 2.1: Simulation results of the electromagnetic torque (modified from [1])

Fig. 2.1 shows the starting instantaneous torque computed using the full order simulation model [1]. For this simulation, the formulas for voltage and flux linkage introduced on section 1.2.5.1 and section 1.2.5.2 were used to build the equivalent circuit of the motor, which is utilized as simulation model.

Fig. 2.2 illustrates the result of the electromagnetic torque measurement obtained with the use of an Hoodwin Instruments accelerometer. As already mentioned about the mechanical methods, while the average value for the torque is reasonably accurate, the pulsation on the torque is severely attenuated [1].

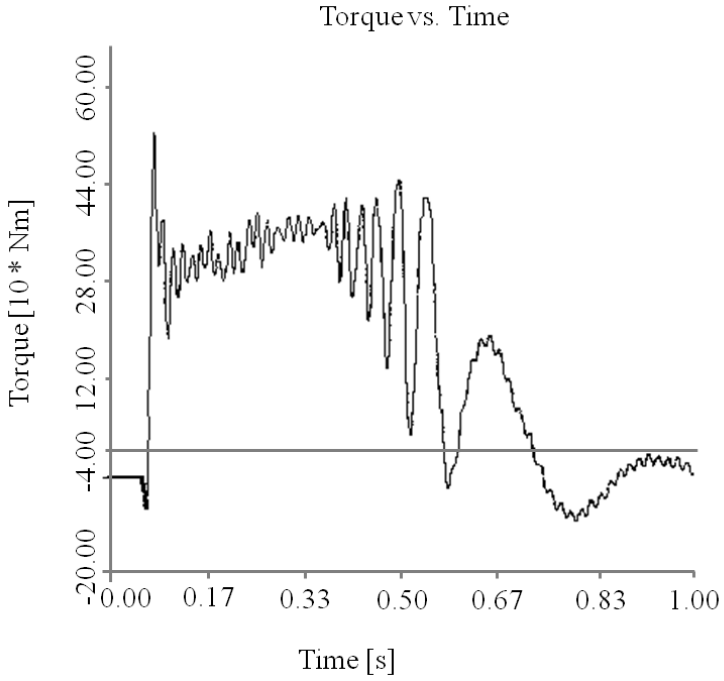

Fig. 2.2: Electromagnetic torque vs. time for full voltage start with shorted field using accelerometer method (modified from [1])

Fig. 2.3 illustrates the results of the electromagnetic torque measurement obtained using the direct search coil method. The results have good correlation with the simulation results (Fig. 2.1). The main difference is the small 120 Hz ripple that appears when the rotor is approaching synchronous speed, but it occurred due to measurement error [1].

Fig. 2.4 shows the results when using the MIP method. They are reasonably good, except in the regions in which the magnetic stored energy change rapidly (low speed and around half speed) [1].

Fig. 2.5 shows the measurement results using the MVSA method. Note that there is a notable similarity between this result and the one making use of the search coil technique (Fig2.3). Again a 120 Hz torque ripple, when rotor is approaching synchronous speed, appears due to measurement error [1].

Fig. 2.6 illustrates the results using the VSA method. This time a significant difference from Fig. 2.5 can be seen. At low speed the pulsating torque components are significantly increased, showing that, unless when dealing with a very large machine, neglecting the effects of the stator resistances can cause significant errors on the torque measurements [1].

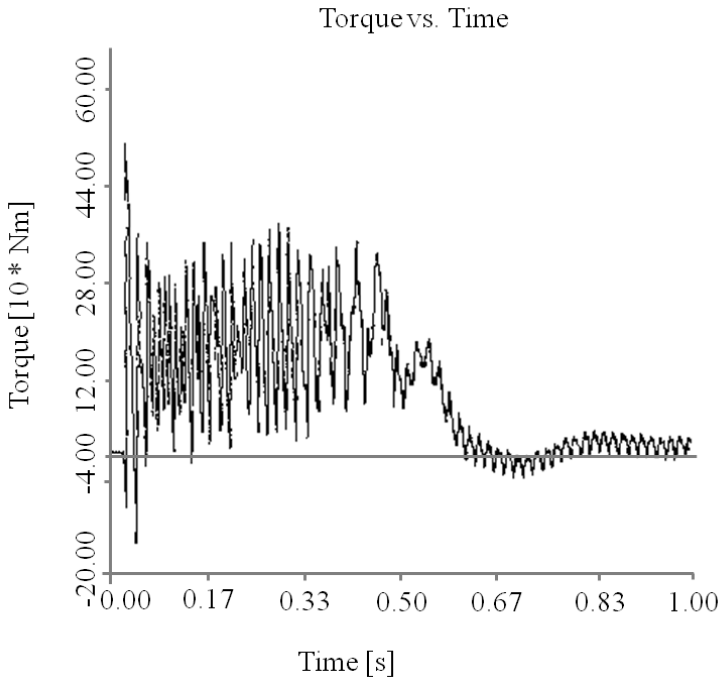

Fig. 2.3: Electromagnetic torque vs. time for full voltage start with shorted field using stator current and flux coil measurement (modified from [1])

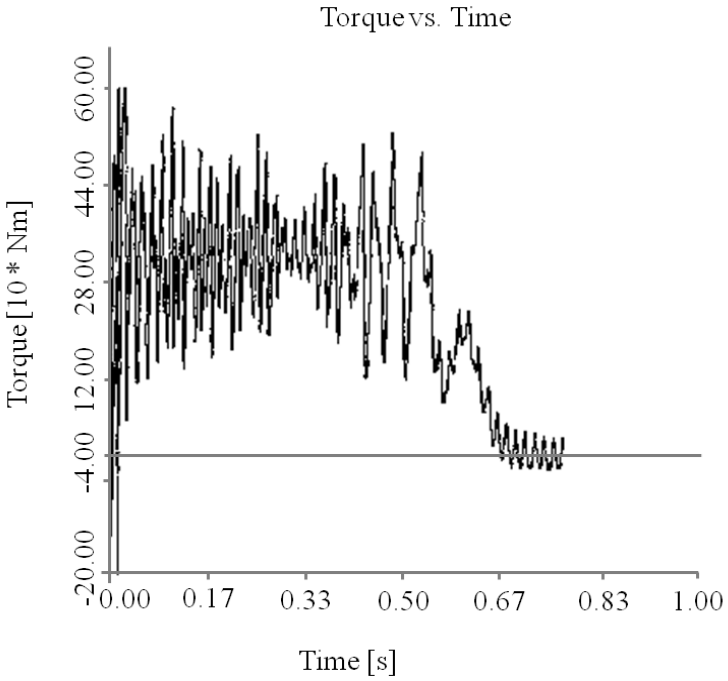

Fig. 2.4: Electromagnetic torque vs. time for full voltage start with shorted field using MIP method (modified from [1])

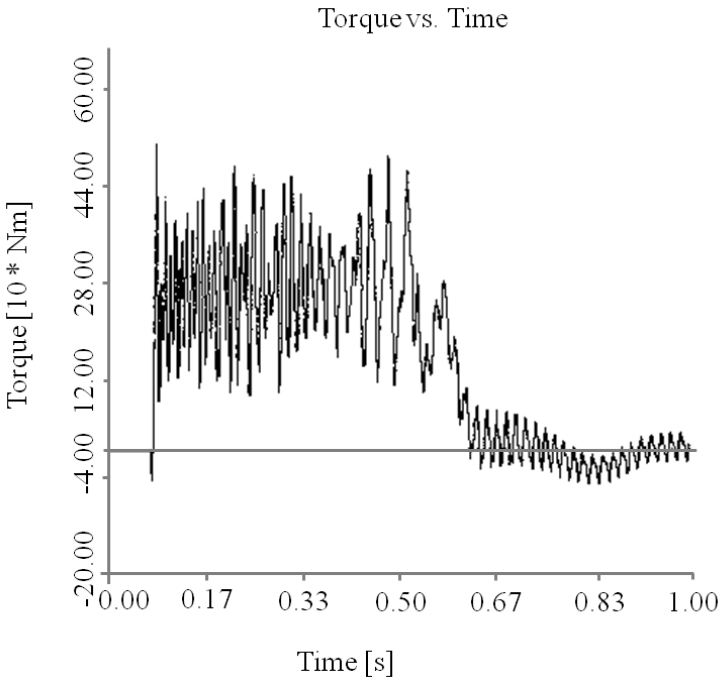

Fig. 2.5: Electromagnetic torque vs. time for full voltage start with shorted field using MVSA method (modified from [1])

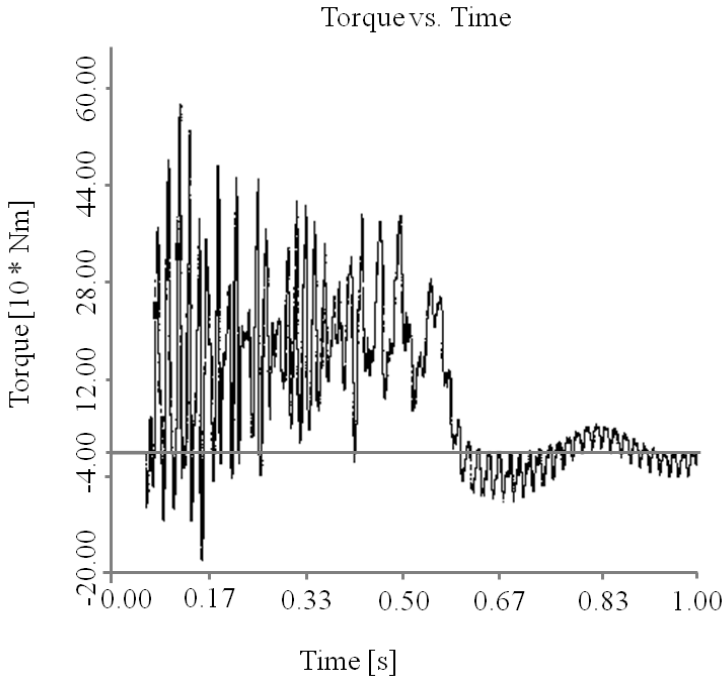

Fig. 2.6: Electromagnetic torque vs. time for full voltage start with shorted field using VSA method (modified from [1])

For the 14 000 hp synchronous motor the results found by Gillard [20] are:

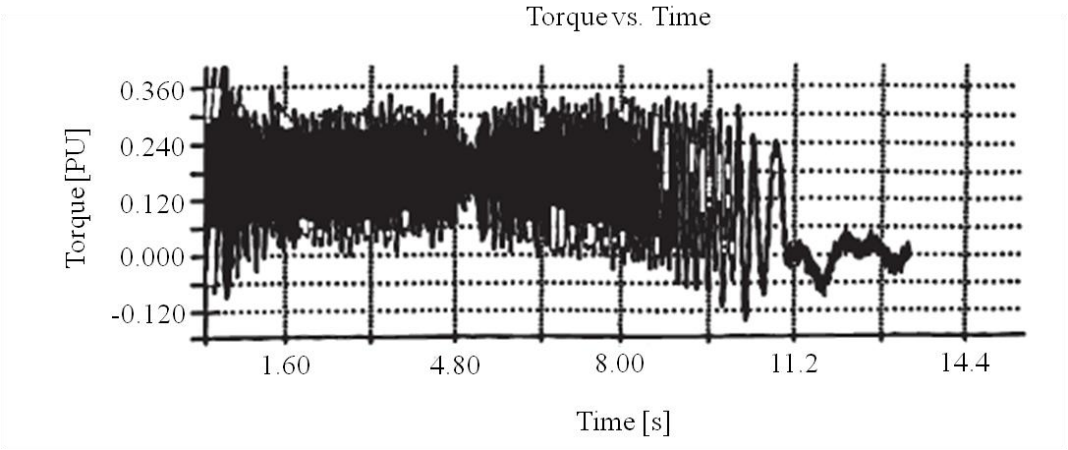

Fig. 2.7: Electromagnetic torque vs. time with VSA method (modified from [20])

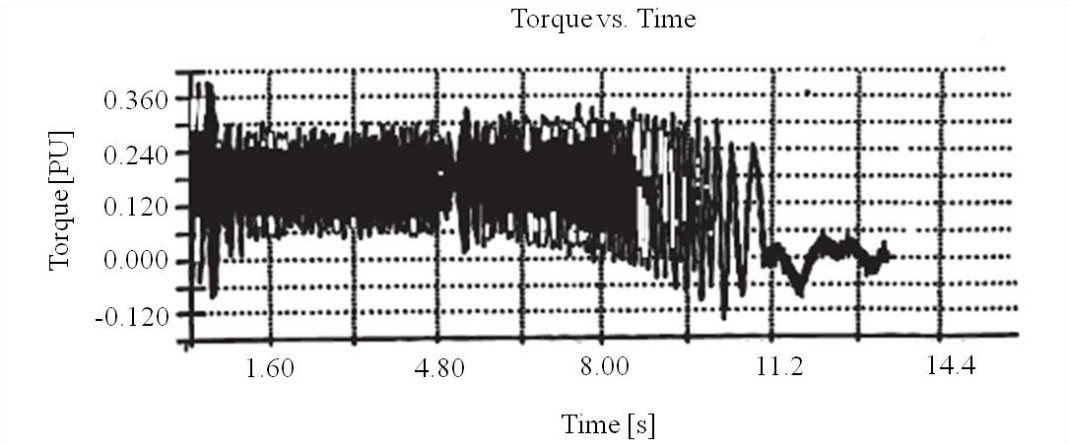

Fig. 2.8: Electromagnetic torque vs. time with input power method (modified from [20])

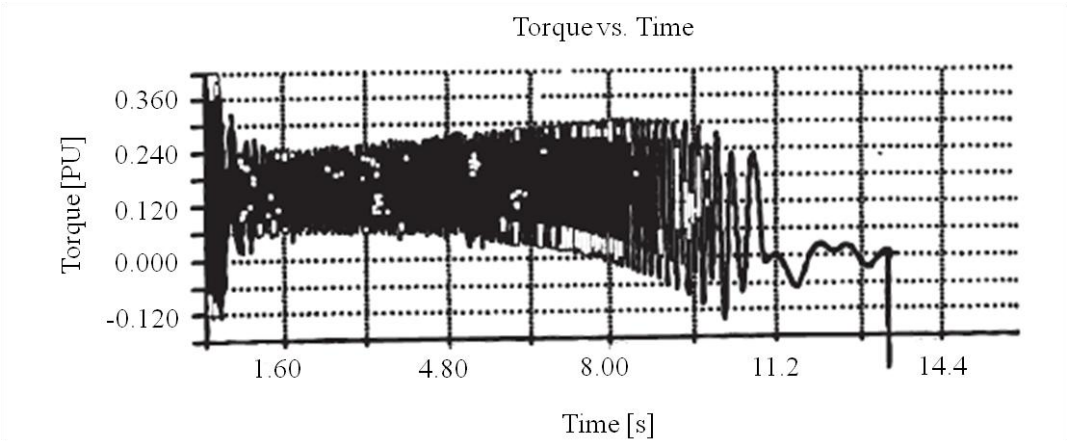

Fig. 2.9: Electromagnetic torque vs. time with accelerometer method (modified from [20])

As mentioned in section 2.2.2, the use of VSA and input power method yield results almost identical when dealing with large machines. In Fig. 2.7 and Fig. 2.8 that present the results of the VSA and the input power method, respectively, this similarity of the results can be observed [13].

In Fig. 2.9 that illustrates the use of the accelerometer method , the behavior is similar to the one found in Fig. 2.2. The average value for the torque is reasonably accurate but the pulsation on the torque is attenuated.

2.4. Methods selection

The selection of the methods used for the measurement of the pulsating torque in this thesis followed two main steps. The first was the selection between the mechanical and electrical methods, the second was the definition of the specific method between the category chosen.

The first step was defined taking in consideration the fact that the mechanical methods present high cost of the equipments, high installation cost and long set up time. Not only the cost was taken in consideration, but also the fact that, in some applications, the result of mechanical methods can be not totally correct when considering not only the average torque but also the pulsation torque (as explained on section 2.1 and shown on section 2.3).

After all these considerations, the category of the method chosen was the electrical one and its drawbacks will be presented in more details when analyzing each electrical method for the selection of the second step.

For the second step, the first electrical method discarded was the search coil method. Although of high accuracy, this method presents high cost of installation and maintenance, as shown on section 2.2.1.

The second electrical method considered was the power input and speed sensing. This method, in some conditions, can be much less accurate then the VSA, MVSA and synchronous watt techniques [13] and also will not be used.

The two remaining electrical methods seems to fit on the objectives of this thesis and will be considered in parallel for the measurement of the pulsating torque in synchronous machines driven by ASDS.

Since the machines considered are large machines (20 MW of shaft power), the input power method (synchronous watt technique) will be considered in the form of the equation (2.9) while the terminal voltage and current sensing method will be used in the form of the equation (2.19) (VSA method). This selection was made taking in consideration the properties of each method described on section 2.2.2 and 2.2.4, respectively.

It is important to highlight that for the VSA method, special attention must be driven to the computation of the integral present on the equation in order to suppress any offset present on the data without influencing aperiodic components, as already mentioned on section 2.2.4.

Another important characteristic of both methods is that, in general, no extra equipment or installation is required, since the electrical connections for voltage and currents measurements for power analysis are already made [15].

3. Tests and Implementation

3.1. Test set-up

The first aspect to me mentioned on the implementation of the pulsating torque measurement technique is the test set-up utilized during the motor tests developed by ABB at CESI. As shown on section 1.3.2.1, there are two possible configurations for such kind of test, the back to back configuration and the full load configuration. For the tests developed during this thesis, as each project involves only one LCI system, thus there is not a second LCI system to be used as load, the configuration selected was the full load option.

The measurements made during the tests are shown on Fig. 3.1 and the whole test configuration is shown on Fig. 3.2, in which the measurements of special importance for this thesis are also evidenced:

- Measurements M 6.0 and M 6.1 are composed by three-phase voltage measurement and three-phase current measurement each one, with frequency of 50Hz. These measurements were utilized just as an extra analysis when the check of the current harmonics on the line side of the converter was of interest.
- Measurements M 7.0 and M 7.1 are composed also by three-phase voltage measurement and three-phase current measurement with 60Hz frequency, for each measurement set. These measurements were the ones actually used on the pulsating torque computation.

The test set-up shown on Fig. 3.2 illustrates the system under test connected to two braking regenerative machine composed of an VSI converter each, containing active rectifiers which make them also capable of generating reactive power [3]. As explained on section 1.3.2.1, this configuration is based on the test bed concept and has as main advantage the fact that only the losses of the two systems must be supplied by the network, since the reactive power absorbed by the load machine is compensated by the braking machines [3].

The main parameters of the motors and braking machines for the test set-up are shown on Table 3.1. It is important to note on the table and also on Fig. 3.2 that, for the development of the tests, a gearbox with reduction of 2:1 was introduced between the motor under test and the braking machines. This fact is explained by the different speed developed by the machines that must be matched to ensure a proper working condition to the system.

Motor data		
	Test 1	Test 2
Shaft power	19300 kW	20000 kW
Speed	3600 rpm	3600 rpm
Rated voltage	2 x 3930 V*	2 x 3930 V*
Rated current	1553 A	1608 A
Winding connection	Star	Star
Number of poles	2	2
Rotor data	Horizontal, round	Horizontal, round
Driving system	LCI.DR W1212-483N465	LCI.DR W1212-483N465
Braking machines (for each machine)		
Shaft power	15000 kW	
Speed	1800 rpm	
Rated voltage	3150 V	
Driving system	ACS6000	
Gearbox	2:1	

Table 3.1: Main data for test set-up

* The motors are supplied with two three-phase system that are 30° phase displaced to reduce the harmonic currents on the machine side (and also on the line side), as explained on section 1.3.2.4.

The currents and voltages acquired during the tests were measured by Rogowski coils and resistive-capacitive potential divider, respectively, and the signals were sampled by a data acquisition system from National Instruments that operates with 15kHz of sampling frequency. More details about the measurement equipment can be found on Appendix C.

An aspect to be highlight at this point is that no anti-aliasing filter was present on the sampling process, what can introduce problems related to aliasing on the sampled data. The possible consequences of the absence of such filter on the measurements will be briefly discussed on the next topic.

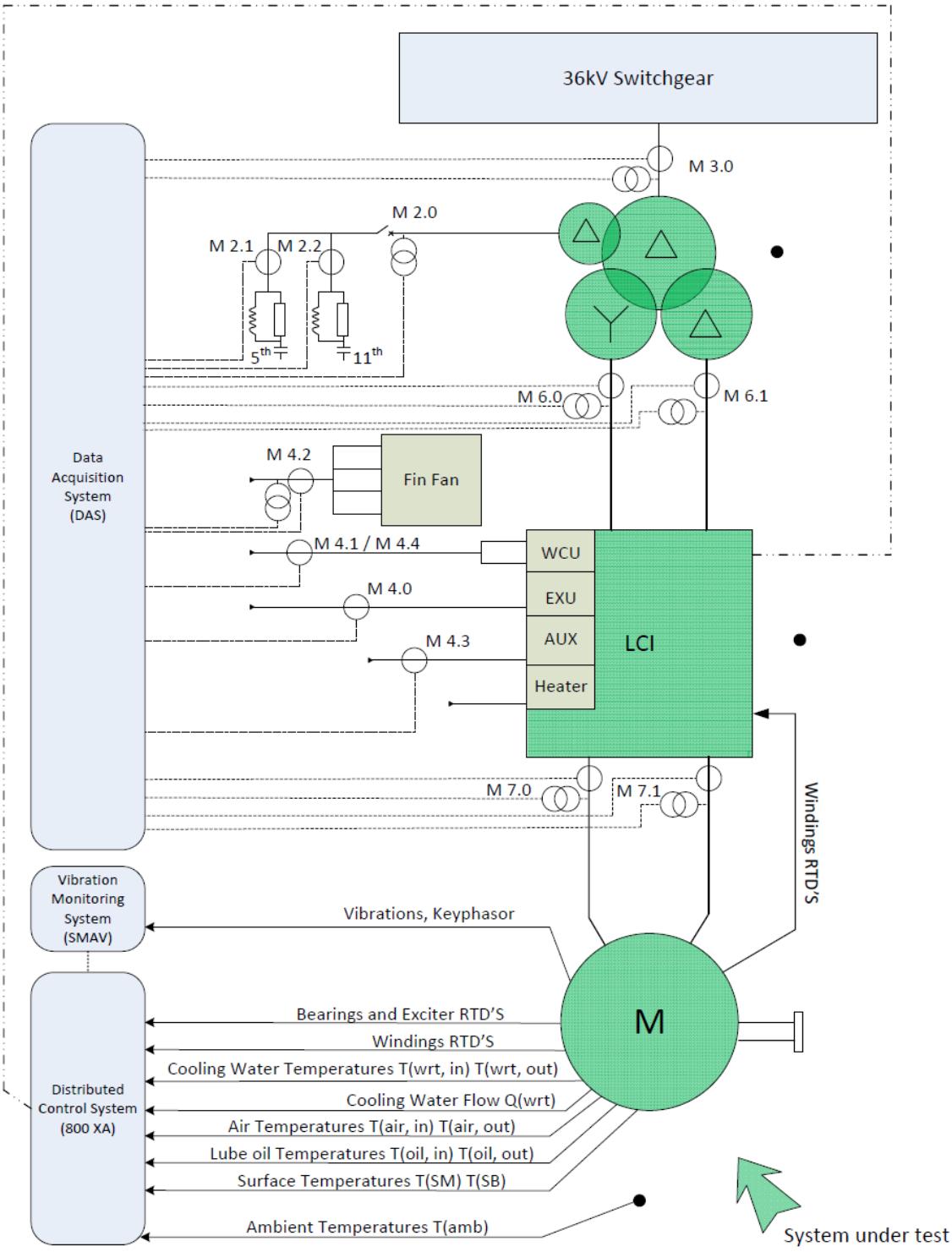

Fig. 3.1: Full load test: measurements

The nominal values for the measurements of interest are shown on Table 3.2.

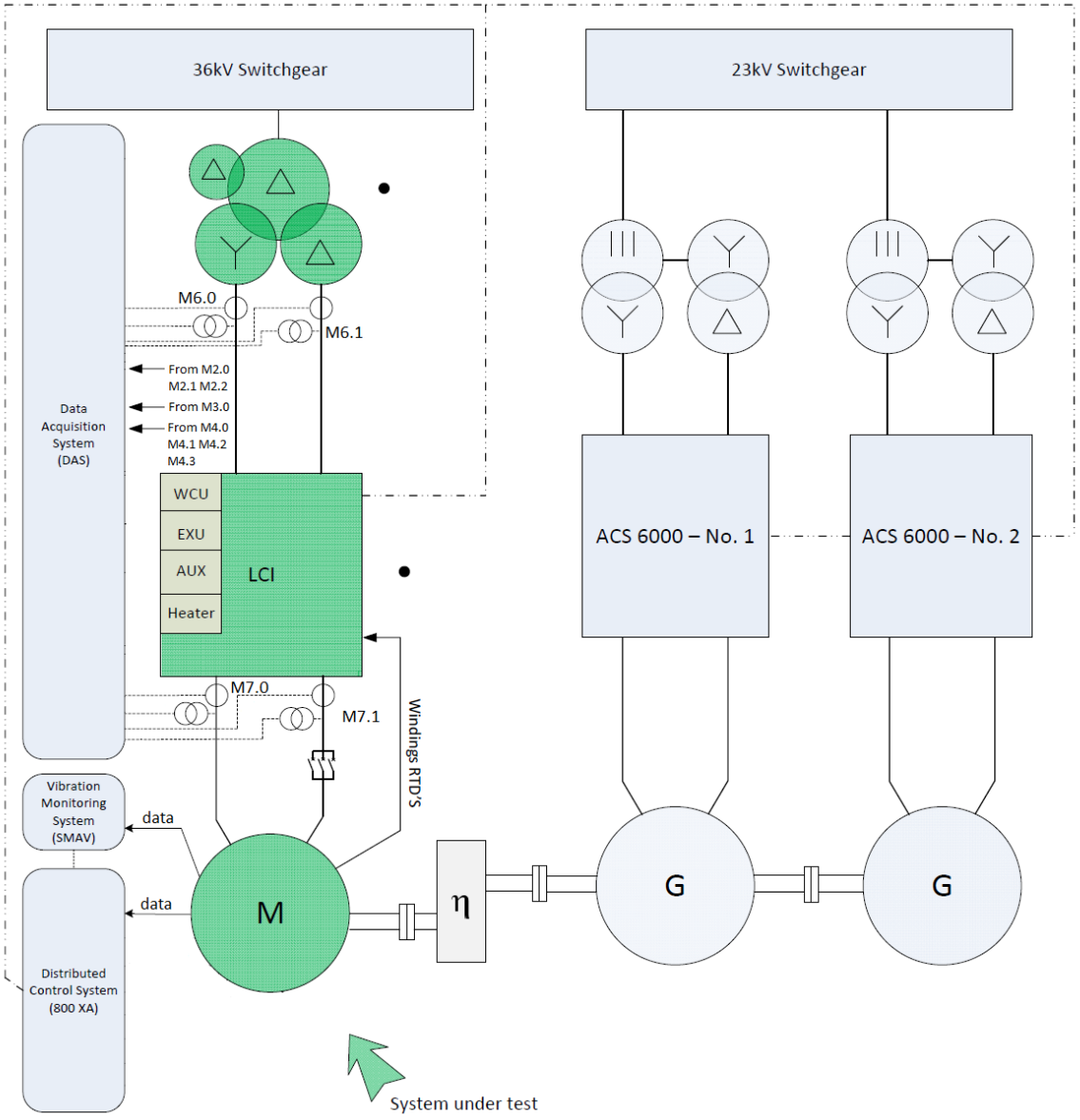

Fig. 3.2: Full load test: configuration

		Motor 1	Motor 2
M 3.0	Voltage	33 kV	33 kV
	Current	461 A	461 A
	Frequency	50 Hz	50 Hz
M 6.0	Voltage	4730 V	4730 V
	Current	1608 A	1608 A
	Frequency	50 Hz	50 Hz
M 6.1	Voltage	4730 V	4730 V
	Current	1608 A	1608 A
	Frequency	50 Hz	50 Hz
M 7.0	Voltage	3930 V	3930 V
	Current	1553 A	1608 A
	Frequency	60 Hz (variable)	60 Hz (variable)
M 7.1	Voltage	3930 V	3930 V
	Current	1553 A	1608 A
	Frequency	60 Hz (variable)	60 Hz (variable)

Table 3.2: Measurement data

Photos of the testing system can be seen on Appendix D.

3.1.1. Aliasing and anti-aliasing filter

Aliasing is the phenomenon that happens when a signal is sampled with a frequency that is not high enough, resulting in a reconstructed signal different from the desired one [21].

In order to have the reconstructed signal and the original signal with the same information, the Fundamental Sampling Theorem gives the conditions to be met. This theorem is attributed to C.E. Shannon, and states *"If a function x(t) contains no frequency higher than BW hertz, it is completely determined by giving its ordinates at a series of points spaced 1/(2BW) seconds apart"* (original statement of the Sampling Theorem, as appears in the 1949 Shannon's paper) [21].

This effect and its impact on the spectrum analysis is presented on an example on Fig. 3.3. The top figure shows a generic analog signal and its spectrum; the center one shows the signal reconstruction when the sampling frequency is lower than the minimum allowed, causing aliasing; the bottom figure shows a situation in which the frequency is higher than the minimum required and the signal is reconstructed in the correct form, no aliasing [21].

Even if it is guaranteed that no components of the signal will be higher than $f_s/2$, unfortunately, other components such as noise and unwanted harmonics can be added to the signal and the aliasing phenomenon can happen again if an anti-aliasing filter is not present [21].

Thus the anti-aliasing filter has as purpose to avoid that signal components and/or noises at frequency higher than $f_s/2$ are sampled and then wrongly reconstructed and understood as part of the original signal. It is important to highlight that if no filter was used before sampling, nothing else can be done to avoid the wrong reconstruction of the signal.

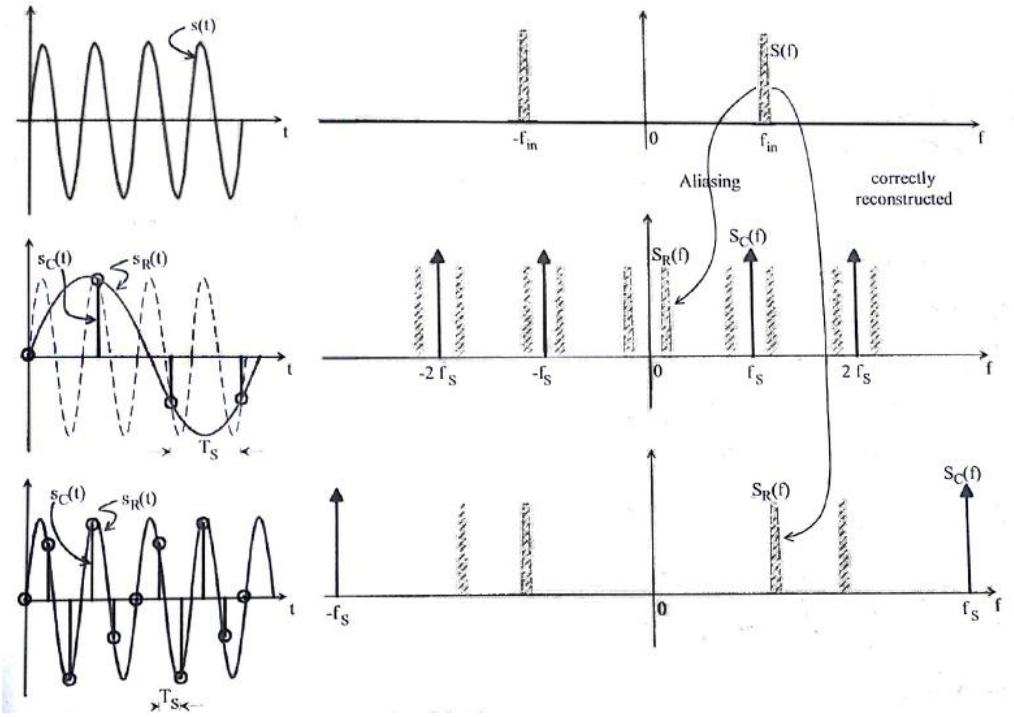

Fig. 3.3: Analog time-continuous signal (at the top), sampled with $f_s<2*f_{max,}$ with aliasing (in the center), and correctly sampled with $f_s>2*f_{max}$ (at the bottom) [21]

Fig. 3.4 shows the effect of a signal with an disturbance at 130kHz sampled at 88kHz with no anti-aliasing filter.

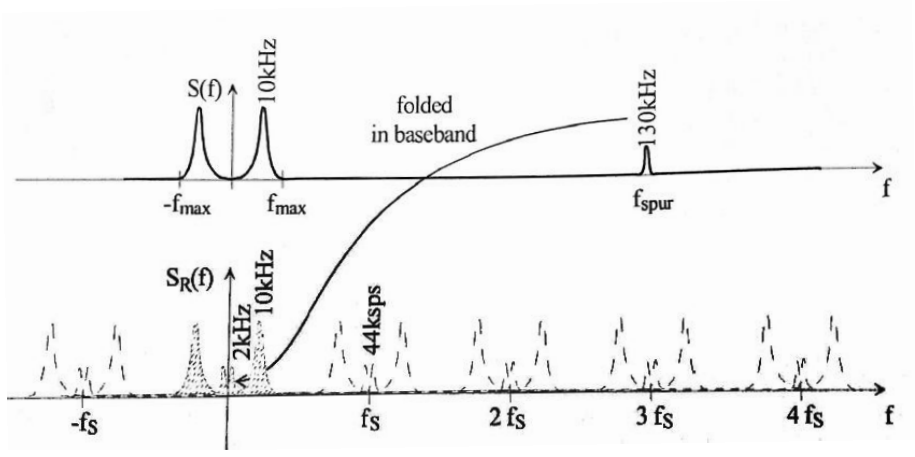

Fig. 3.4: Effect of f_{spur} higher than $f_s/2$ [21]

3.1.2. LCI configuration

As mentioned on section 1.3.1, the systems under test are from the family MEGADRIVE-LCI from ABB, and consists of a water-cooled version with 12/12-pulse one-channel connection and type code W1212-483N465.

The 12/12 pulse configuration thyristor bridge used on the mentioned LCI can be seen on Fig. 3.5.

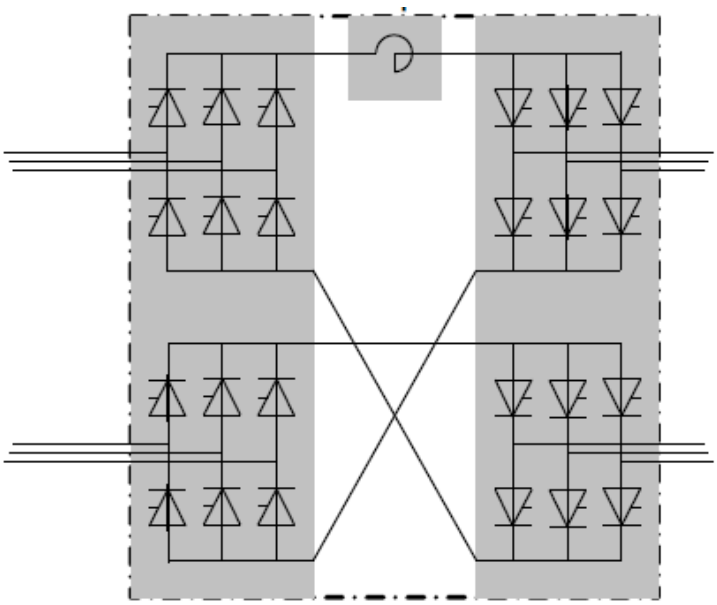

Fig. 3.5: One-channel 12/12-pulse series connection thyristor bridge [2]

This configuration has the benefit of reducing the 5^{th} and the 7^{th} current harmonics, which are normally the largest, impressed by the LCI on the line and on the machine side [2].

3.2. Algorithm implementation

The methods selected on section 2.4 (modified input power method (MIP) and volt-second ampere method (VSA)) represented by the equations 2.9 and 2.19 presented on section 2.2.2. and 2.2.4 were implemented on an algorithm with help of the commercial software Matlab®. The implementation followed the order shown on Fig. 3.6 and each step will be discussed in details on the following items.

3.2.1. Data acquisition

The measurements made at CESI were available on an *.tmds file from LabVIEW®. This file is usually transformed on an Excel (*.xls) file with use of

TDM import, an add-on tool provided by National Instruments. Having the excel file on hand, the data went through a simple conversion to acquire real physical meaning and it was read to be used.

To simplify and increase performance of the data acquisition by Matlab®, the data concerning the measurements M 7.0 and M 7.1 were transferred into an *.txt file, reducing significantly the file size from around 60 Mbytes to 2 Mbytes, making the acquisition process significantly faster.

Then, the data was transferred to Matlab® making use of the well known functions "fopen" and "fscanf".

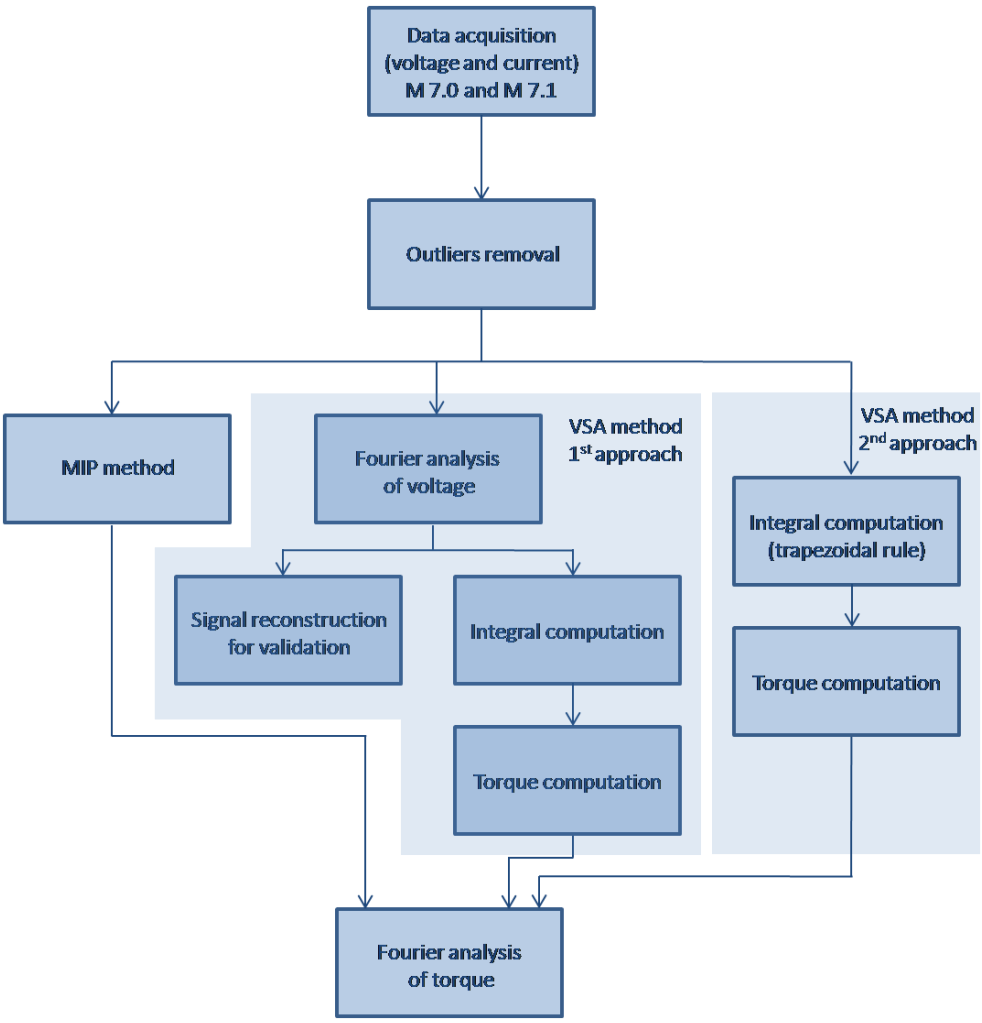

Fig. 3.6: Algorithm implementation

3.2.2. Outliers removal

Different authors have proposed many definitions for an outlier that are seemingly no universally accepted. For example the definition given by Grubbs (Grubbs, 1969) and quoted in Barnett & Lewis (Barnett and Lewis, 1994):

"An outlying observation, or outlier, is one that appears to deviate markedly from other members of the sample in which it occurs."

A further outlier definition from Barnett & Lewis (Barnett and Lewis,1994) is:

"An observation (or subset of observations) which appears to be inconsistent with the remainder of that set of data." [22]

Other definitions were given by John (John, 1995) and Aggarwal (Aggarwal and Yu, 2001) and can be found on reference [22]. For this thesis, the definition of outliers is in line with the definitions quoted on the previous paragraphs.

The causes of the appearance of outliers can be various. For example, the physical apparatus for taking measurements may have suffered a transient malfunction, or there may have been an error in data transmission or transcription [22].

As the definition, there is no rigid mathematical definition of what constitutes an outlier, but there are several approaches that were suggested on literature. One can refer to reference [22] to have an overview on the proposed solutions.

For this thesis the method selected was the Rosner's test, also known as Rosner's many-outlier test, that is a generalization of the Extreme Studentized Deviate (ESD) originally suggested by Grubbs (1969) [23], and can be used to detect one or more outliers in an univariate data set that follows an approximately normal distribution.

The basis of the test is to set a upper bound for the number of outliers on the data set and the ESD test essentially performs k separate tests: a test for one outlier, a test for two outliers, and so on up to k outlier [24].

The test is implemented as follow, this development takes as reference [24]:

- With a data set of n samples, compute:

$$R_i = \frac{max_i|x_i - \bar{x_i}|}{s} \tag{3.1}$$

  where:
  $\bar{x_i}$ denotes the sample mean
  s denotes the sample standard deviation

- Remove the observation that maximizes $|x_i - \bar{x_i}|$ and re-compute equation (3.1) with n-1 observation.
- Repeat the process until k observations have been removed. (resulting in k test statistics R_1, R_2, ..., R_k)

- Correspondently to the k test statistics, compute k critical values given by equation (3.2).

$$\lambda_i = \frac{(n-i)t_{p,n-i-1}}{\sqrt{(n-i-1+t_{p,n-i-1}^2)(n-i+1)}} \tag{3.2}$$

Where:
i = 1, 2, ... k
$t_{p,\,v}$ is the 100p percentage point from the t distribution with v degrees of freedom.
and p is given by equation (3.3).

$$p = 1 - \frac{\alpha}{2(n-i-1)} \tag{3.3}$$

Where:
α is the significance level.

- The number of outliers is determined by finding the largest i such that $R_i > \lambda_i$.

3.2.3. VSA method

The VSA method was implemented as stated on section 2.2.4 by equation (2.19) that is now recalled for clarity.

$$T_e \cong \frac{\sqrt{3}\,p}{6}\left\{(i_a - i_b)\int v_{ca}\,\mathrm{dt} - (i_c - i_a)\int v_{ab}\,\mathrm{dt}\right\} \tag{3.4}$$

The algorithm for the torque computation was implemented on Matlab® and despite the apparently simple implementation, the problems imposed by the computation of the integral of the line-to-line voltages was the point to be stressed on this implementation.

The computations start with the transformation of line-to-neutral voltages measured on CESI, acquired from the input file and that passed through an outlier removal process, on line-to-line voltages.

The line-to-line voltages are then utilized for the integral computation that will be described on the following item. However, before considering the integral computation implemented on this thesis, a point to be highlighted are the difficulties faced that were the key point for the solution proposed.

When computing the integral of a signal that is composed by the summation of several sinusoidal components, it is not immediate that the initial value for the integral will be set to the proper value. Several methods were implemented to find

and set the initial value for the integrals of the line-to-line voltages, but none of them were able to set the precise value, resulting on a torque component extremely affected by this imprecision. The solutions found were based on more theoretical concepts of integral of sinusoidal signals and will be presented on the following section.

3.2.3.1. 1st approach for integral computation

The first solution proposed was the one of performing a Fourier analysis (making use of the "fft" function of Matlab®) on the line-to-line voltages and obtaining the sinusoidal components of the signal with their amplitudes and their phases. Having this on hand, the signals were reconstructed for validation and also the integral was computed by the simple mathematical relation:

$$\int A\sin(\omega t + p)\ \mathrm{dt} = -\frac{A}{\omega}\cos(\omega t + p) + c \qquad (3.5)$$

This operation simplifies the integral computation when considering the initial condition but increases the implementation complexity. Not only, but also gives better results on the torque computation that can be related to the good quality of the signal reconstruction.

An important fact to be mentioned is that when dealing with Fourier analysis it is advisable to use a windowing procedure to reduce the impact of the finiteness of the sampled signal when considering the signal periodic on the FFT algorithm. The window used was the Hanning window.

The main drawback of such method is that due to the windowing process the set of data is reduced since the borders of the signal cannot be considered anymore, resulting in a reconstructed signal and a integrated signal containing less data points than the initial data set.

Some more details on the windowing process will be given on the following section.

3.2.3.2. Windowing for spectrum computation

The computation of the FFT transform assumes that the finite data set is one period of a periodic signal. For the FFT, both the time domain and the frequency domain are circular topologies, so the start point and the endpoint of the time waveform are interpreted as if they were connected together. Therefore, the finiteness of the sampled signal may result in a truncated waveform that when replicated to compute the FFT may generate "wrong connection", as the one seen on Fig, 3.7.

When dealing with sampled signals that are a summation of sinusoidal signals is difficult to ensure that no "wrong connection" will occur. Then it is

difficult to prevent the distortion on the spectrum analysis, as the one shown on Fig. 3.8.

The solution is to consider a windowing processes that consists on weighting the borders samples of the signal with smaller weights than the ones on the center of the signal. Hamming, Hanning, Blackman and triangular are examples of windows that can be applied.

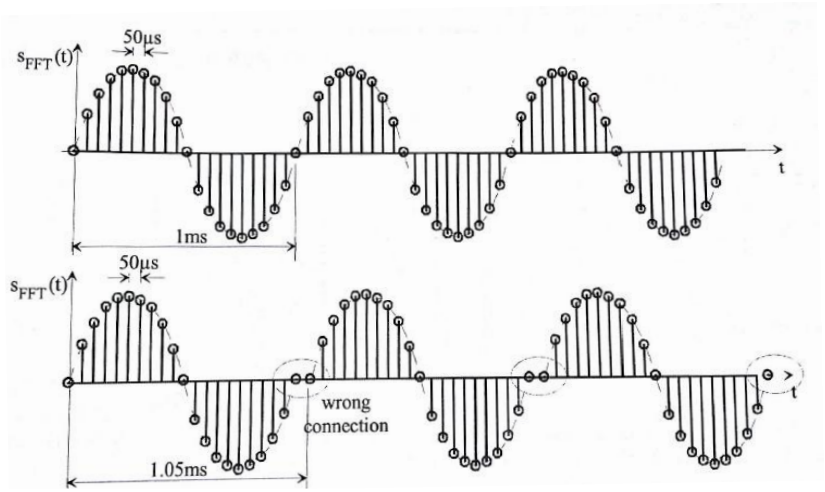

Fig. 3.7: Example of wrong connection on FFT [21]

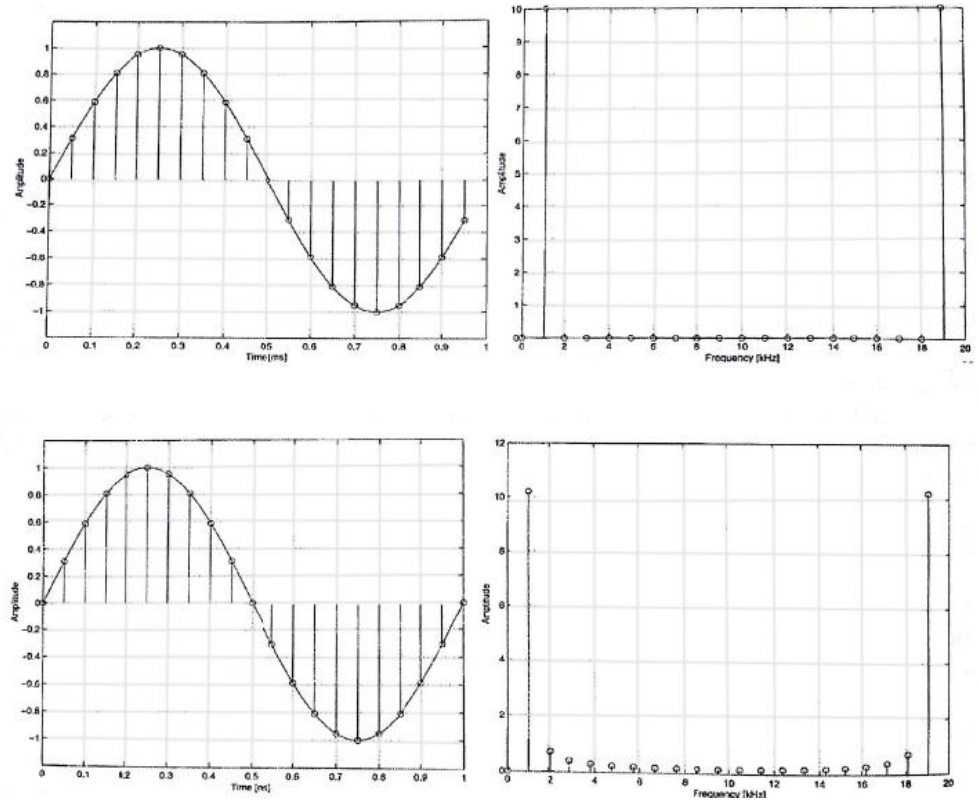

Fig. 3.8: Deformation of the FFT due to wrong connection [21]

3.2.3.3. 2nd approach for integral computation

The second approach proposed consists on the computation of the integral by the well-known trapezoidal method (making use of the "cumtrapz" function of Matlab®).

To set the initial condition for the integral, a theoretical result was applied. It is known that, in our case, as the line-to-line voltages have average value approximately zero, the line-to-line voltage integral should also have mean approximately equal to zero. Thus, two methods were proposed to set the integral mean to zero.

The first one was to simply compute the mean of the integral signal and remove from every point of the signal the computed mean. By your time, the second method consists on computing a moving average of the integral signal and removing from each point the respective computed average value.

Comparing the results found for both methods, the better performance was obtained with the one making use of the moving average technique and its results will be shown on the results discussion.

3.2.4. MIP method

The MIP method was implemented as stated on section 2.2.2 by equation (2.9) that is now recalled for clarity.

$$T_e \cong \frac{p}{2}\frac{P_{in}}{\omega} \tag{3.6}$$

To implement this method, the input power was estimated making use of the currents and line-to-ground voltages obtained after an outlier removal process on the measurements given by CESI.

It is important to mention that, as on the VSA method, the cooper losses are neglected. However, this is not the only approximation made, the instantaneous time rate of change of magnetic field energy stored in the stator leakage magnetic field was also neglected, as suggested by literature, and the effect of this approximation will be better discusses on the results.

3.2.5. Fourier analysis of the torque

After having the torque computed by both methods, the Fourier analysis was once more utilized to evidence the frequencies present on it. To implement this analysis the function "fft" from Matlab® was used, remembering always to use the windowing process in order to diminish the effects of "wrong connections" as discussed on section 3.2.3.2. Again the window selected was the Hanning window.

In sequence, a simple peak detection algorithm was implemented in order to generate tables containing the values for the amplitude of each present frequency.

3.2.6. Graphical interface

In order to simplify the interaction between users and program, a graphical interface was created with help of the "GUI" tool of Matlab®. This interface is composed by four principal areas:

- data input area (blue area on Fig. 3.9): is the area in which the initial data is inserted to the computation . The data required are:
  - *.txt file containing voltage data
  - *.txt file containing current data
  - motor speed (rpm)
  - number of poles
  - line frequency: 50 or 60 Hz
  - sampling frequency (kHz)
- output selection area (orange area on Fig. 3.9): is the area in which the user selects which results to have as output. The options are:
  - Plot voltages and currents with outliers
  - Plot voltages and currents without outliers
  - Plot voltage data and reconstructed signal after the FFT analysis for the VSA method. (used for validation)
  - Plot FFT analysis of the data voltage and the reconstructed signal. (used for validation)
  - Plot torque computed by MIP method and VSA method.
  - Plot FFT analysis of computed torque by MIP and VSA methods.
  - Save excel table with the peaks present on the FFT analysis of the torque.
- buttons and status panel area (red area on Fig. 3.9): is the area in which the user can start and check the status of the computation and can also start the current analysis program. The components are:
  - run button: when pressed, starts the torque computation.
  - current analysis button: initially disabled, becomes enable when the torque computation is finished and, when pressed, starts the current harmonics analysis that will be better explained on section 3.2.7.
  - status panel: shows the status of the computation and possible errors on the data input.
- results area (green area on Fig. 3.9): is the area in which the main results are shown to the user. It is composed by:
  - two plotting areas. The first on the left is designated to the plot of the computed torque by the VSA method vs time and the one on the right is designated to the plot of the Fourier analysis of the computed torque. (The reason why just the VSA method is shown on the main window of the graphical interface will be explained in details on the results comments)
  - a table in which the amplitude of the frequency components that are expected from theory are shown.

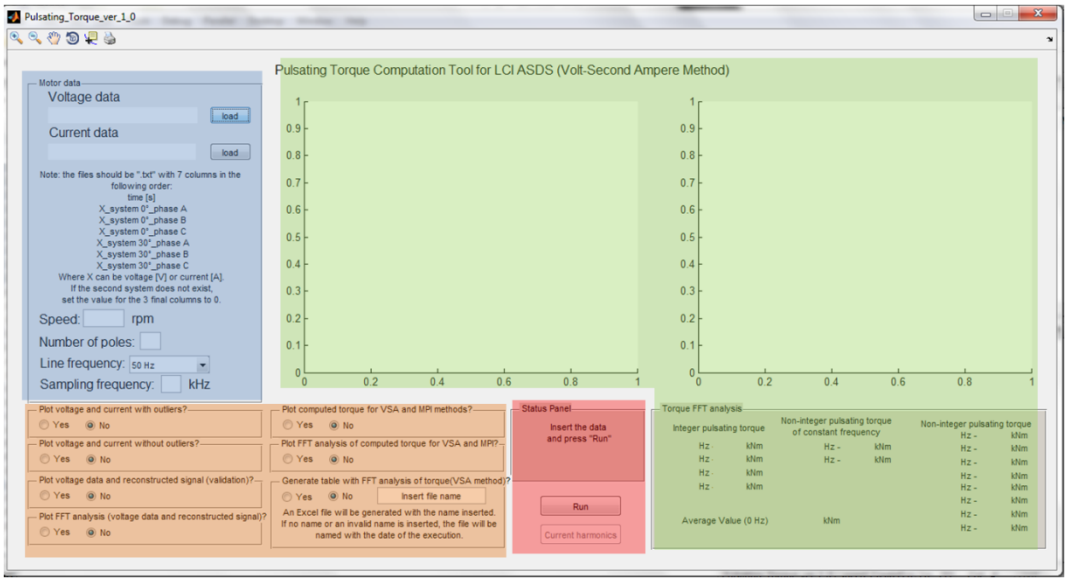

Fig. 3.9: Graphical interface areas

Fig. 3.10 shows an example of the graphical interface with results of the torque computation.

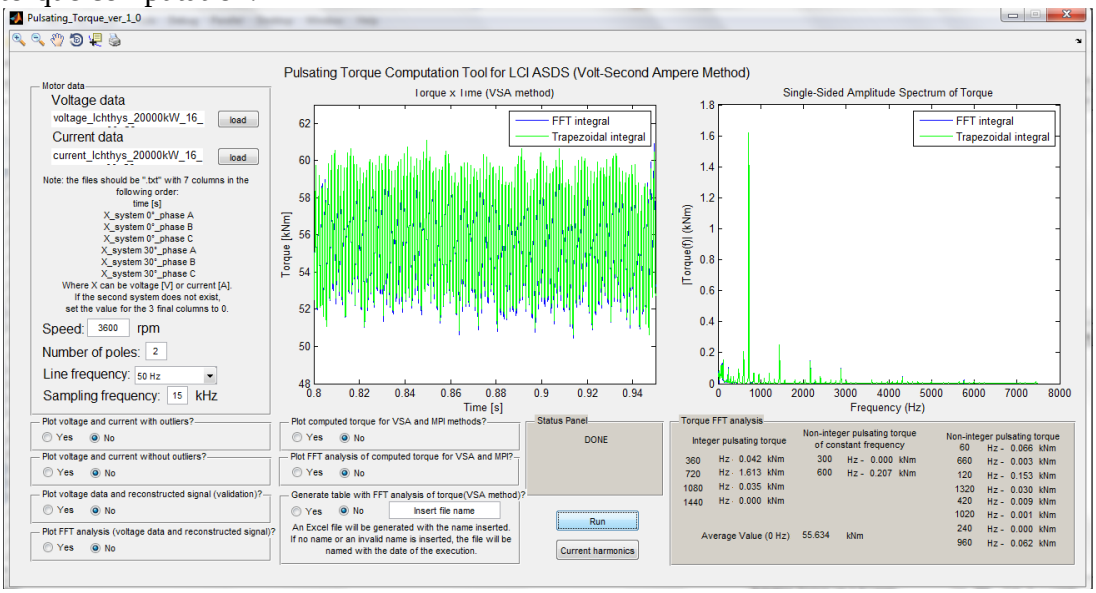

Fig. 3.10: Graphical interface with results

3.2.7. Current harmonics analysis

As mentioned on section 1.3.2.4, torque pulsations on synchronous machines fed by LCI systems are strongly related to the harmonics impressed by the LCI on the motor and line side currents. Knowing that, the implementation exhibits as an "extra" a current harmonics analysis through Fourier analysis.

When the button "Current harmonics" is pressed on the torque analysis window, a "pop-up" is opened giving the option to the user to select the line side current measurements, as shown on Fig. 3.11. The user can also proceed without selecting this data and performing the harmonics analysis just on the motor side currents.

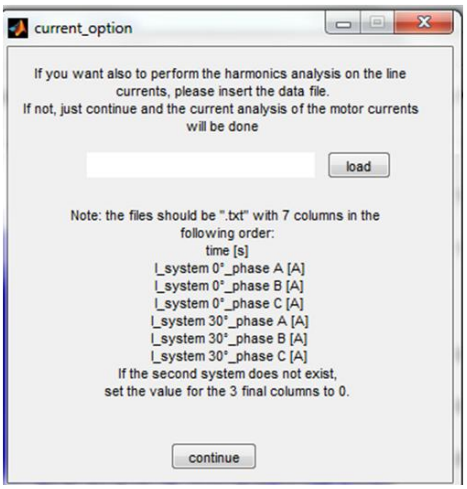

Fig. 3.11: Option for evaluation of current harmonics on the line side

In this thesis, the measurements for the line side currents are those indicated as M 6.0 and M 6.1 on Fig. 3.1.

When the button continue is pressed the following situations can happen:

- If the user has selected the input data for the line side currents, two windows will be opened. The motor side current harmonics analysis window and the line side current harmonics analysis window.
- On the other hand, if the user has not selected the input data for the line currents, just the motor side current harmonics analysis window will be opened.

3.2.7.1. Motor side current harmonics analysis window

The motor side current harmonics analysis window can be divided in two regions, as can be seen on Fig 3.12. The first one, on the top, is the region concerning the 0 degree system, and the second one, on the bottom, is concerning the 30 degree system.

Each region is composed by three plotting areas where the spectrum analysis are plotted for the currents on the motor side, before and after the outlier removal process. A table is also present to display the percentage of the frequencies found on the analysis with respect to the fundamental one.

Finally, two options are given two the user on this window. The first one is to save the values present on the tables to an Excel file and the second one is to enlarge the plots in individual windows.

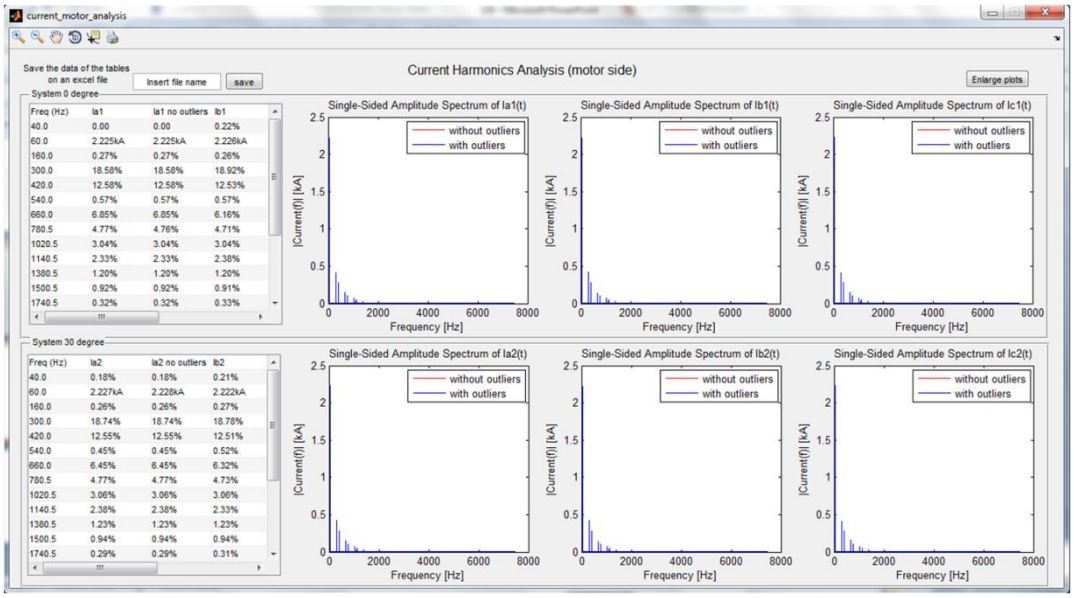

Fig. 3.12: Current harmonics analysis on the motor side

3.2.7.2. Line side current harmonics analysis window

The line side current harmonics analysis window, that can be seen on Fig. 3.13, presents the same features as the motor side one. The only difference is that no outlier removal process is performed, and then the harmonics analysis is computed just on the original signal.

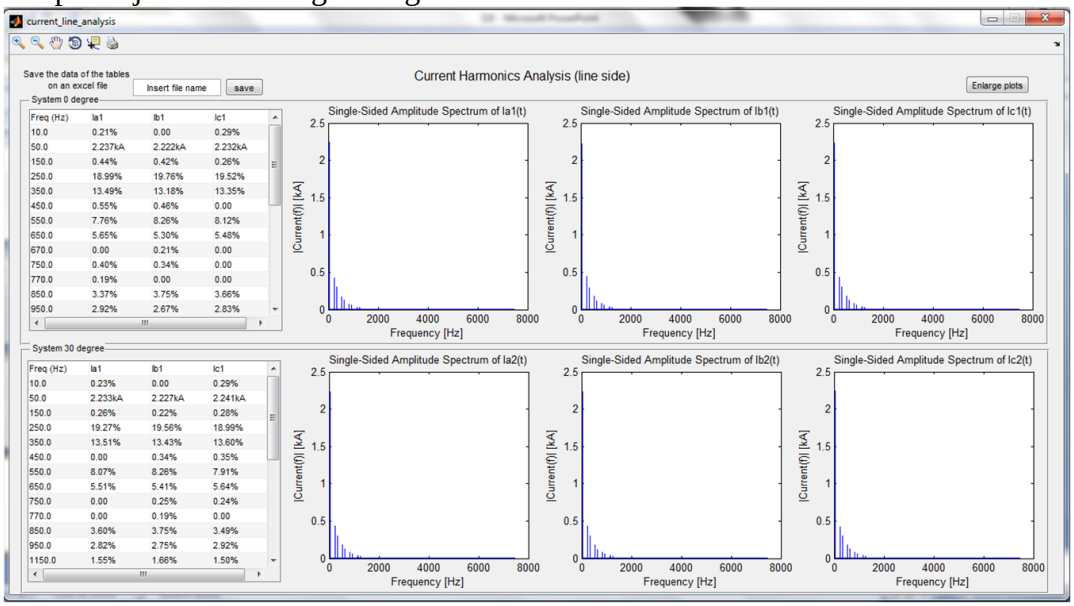

Fig. 3.13: Current harmonics analysis on the line side

3.2.8. Results validation

For the validation of the results, a Simulink® model was implemented making use of the SimPowerSystems™ toolbox for Matlab®.

The first validation was made with a preset model of a 111.9 kW, 762 V, 4 poles synchronous machine available on the mentioned toolbox. This decision was taken to remove the possibility of inconsistencies on the machine modeling that could make difficult to understand if the possible mistakes on the validation were related to the machine modeling or the torque computation by the selected methods.

It is important to mention that the procedure of using a different machine should not change the result of the validation since the methods selected (VSA and MIP) should work independently of the machine characteristics.

To implement such test, the voltages measured on the real machine were resized to fit the machine model requirements and the currents and torque were "measured" from the simulation, as shown on Fig. 3.14.

Finally, with the voltages and currents measured on the simulation, the torque was also computed through the selected methods (VSA and MIP) and compared with the one found through the simulation. This results will be discussed on section 4.1.

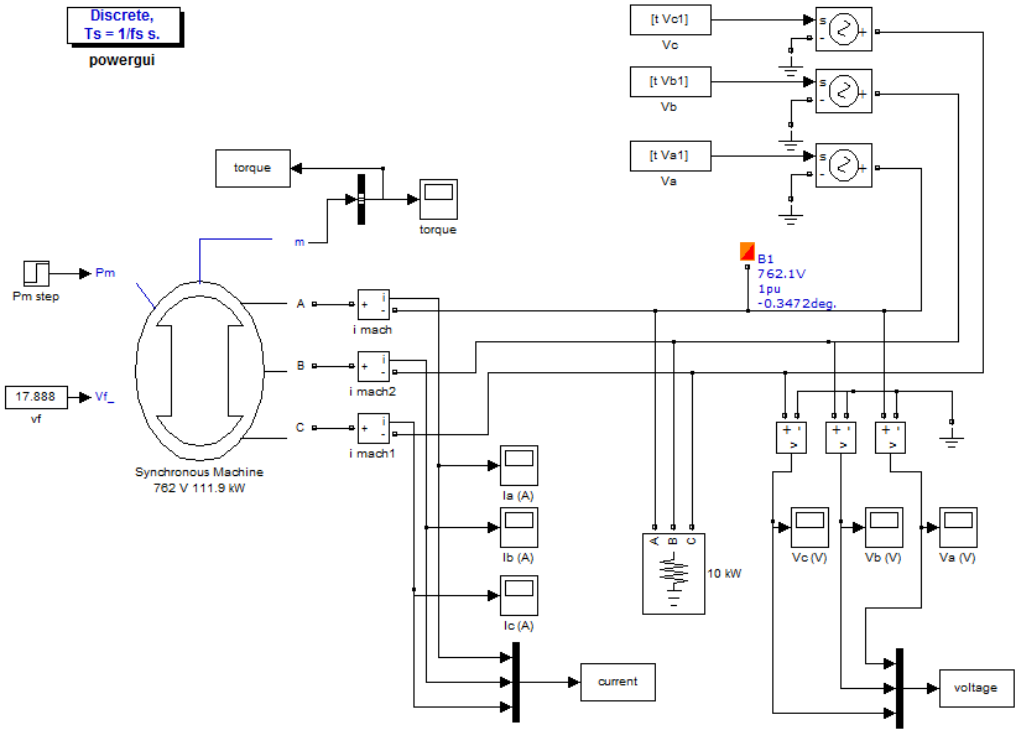

Fig. 3.14: Simulink® model for validation

A second step on the validation was made and a motor model of one of the tested motors (19300 kW, 2 x 3930 V, 2 poles) was implemented in Simulink®, in an away very similar to the one shown on Fig. 3.14. However, for simplicity, the two supply systems of the real motor were simplified with just one supply system on the simulated model.

The procedure of simplifying the supply system may change the result obtained for the torque on the simulation when comparing with the result found with real data. But the result found for the torque computed with the selected methods (VSA and MIP) using voltages and currents "measured" from the simulation should be very similar to the one obtained as the result of the simulation itself. Thus, once more, this procedure should not change the result of the validation. The results for this simulation are also presented on section 4.1.

4. Results and discussion

4.1. Method and implementation validation

As explained on section 3.2.8 the first validation was realized making use of a preset model of a synchronous machine on the SimPowerSystems™ toolbox of Simulink™. The results of such validation can be seen on Fig. 4.1, Fig. 4.2, Fig. 4.3 and Fig. 4.4.

Remarks:

- Fig. 4.2 presents the same results as the ones shown on Fig. 4.1 but with different time scales, making easier to evidence the behavior of the results found.
- In this section, the values for the torque are presented as negative, following the convention of the SimPowerSystems™ simulation, in which is stated that the torque for the simulated synchronous machine is negative when dealing with a motor and positive when dealing with a generator.

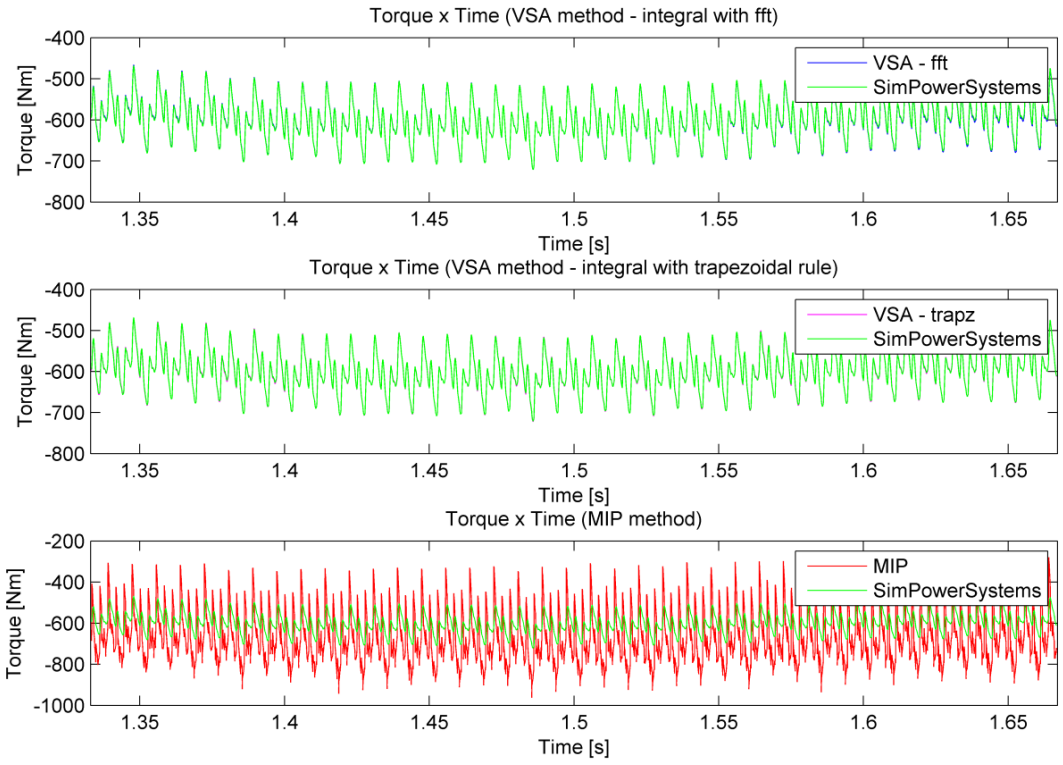

Fig. 4.1: Comparison torque x time for VSA method, MIP method and simulation with SimPowerSystems preset motor model (111.9 kW)

On Fig. 4.1 and Fig. 4.2, starting from the top plot one can notice good match between the VSA method computed with help of FFT and the simulation results for the torque. On the middle plot it is also notable the good correlation between the VSA method computed by the trapezoidal rule and the simulation results. On the other hand, on the bottom plot, it is easy to notice the bad match between the MIP method and the simulation results.

Such difference on the computed values by the MIP method may be explained by looking on the simplifications maid when applying such method. In special the simplification of assuming that the variation of stator magnetic stored energy can be neglect.

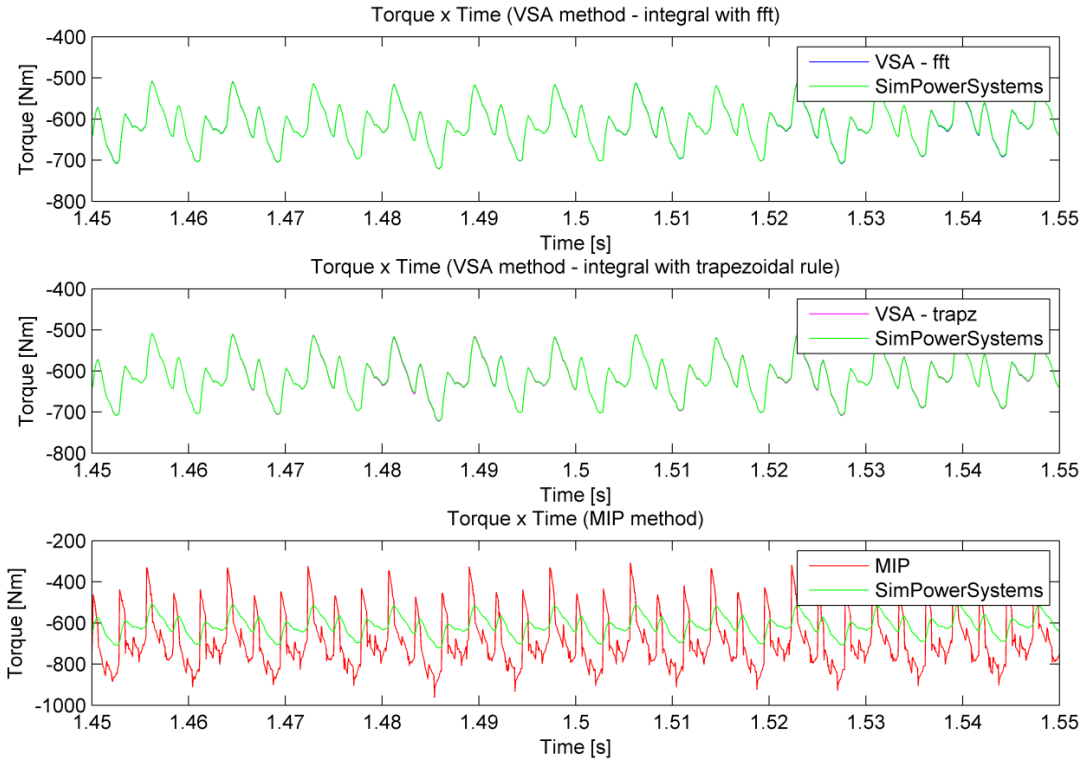

Fig. 4.2: Comparison torque x time for VSA method, MIP method and simulation with SimPowerSystems preset motor model (111.9 kW) - details in evidence

Fig. 4.3 shows the spectral analysis of the torque results. For better visualization the constant component of the torque was omitted from the plot. However, this constant component can be found on Table 4.1 and all the frequency components can be found on Table E.1 (Appendix E).

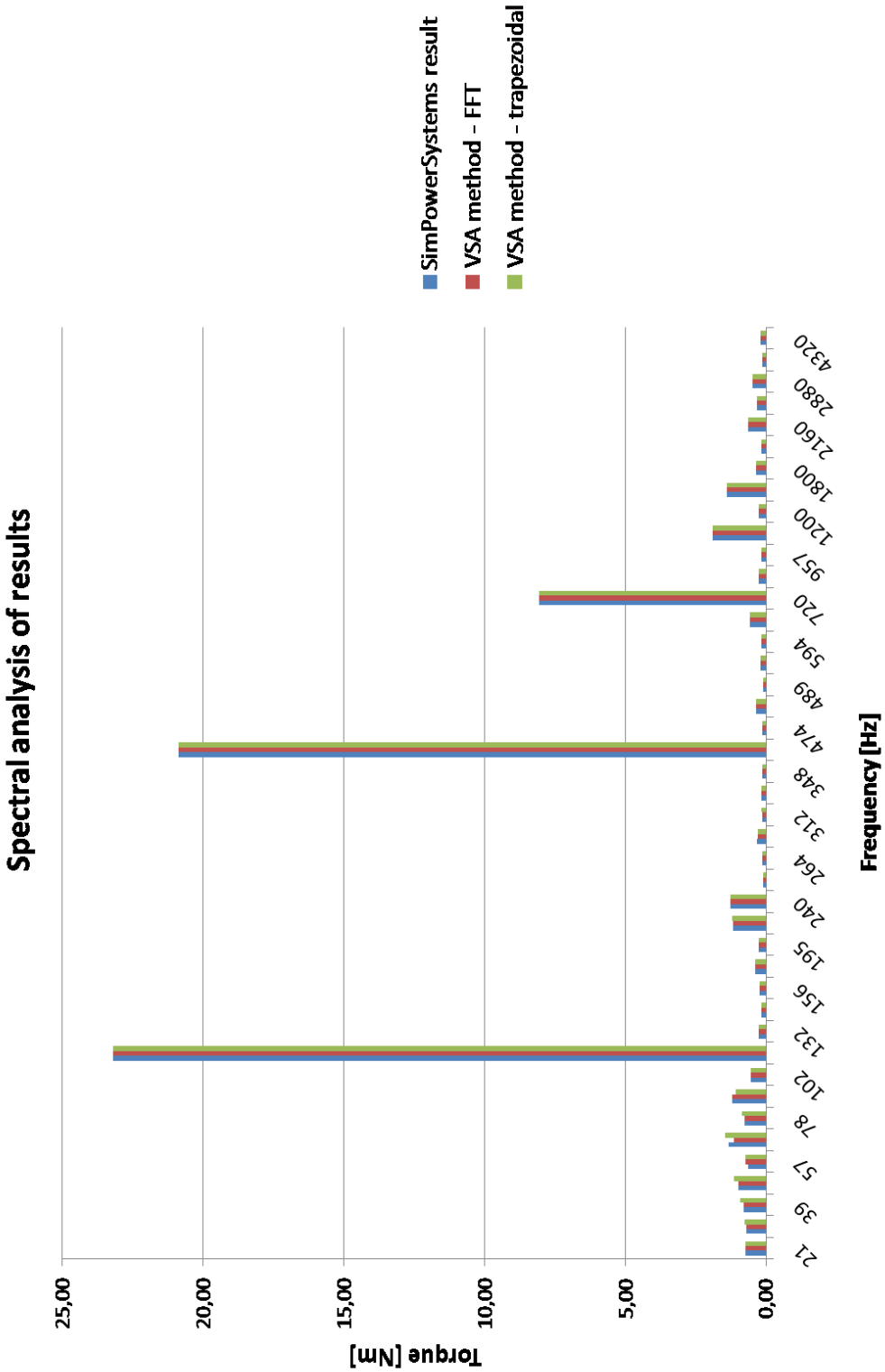

Fig. 4.3: Spectral analysis of results for preset model

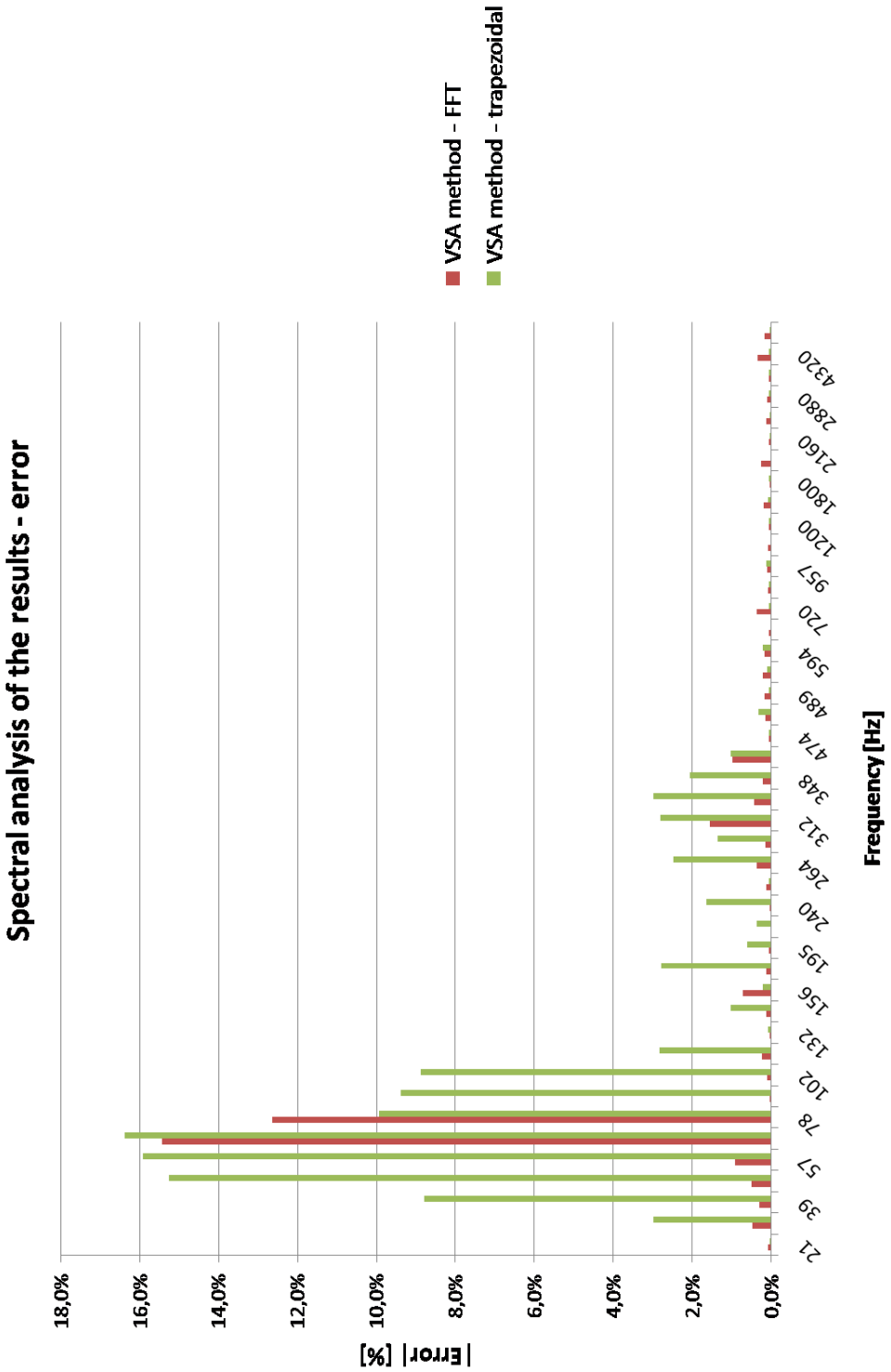

Fig. 4.4: Spectral analysis of results for preset model - error

On Fig. 4.4 the error between the values computed with VSA method and the values obtained by the simulation are shown. In this figure, one can notice the apparent better performance of the VSA method computed through the FFT procedure for integral computation. However, both methods present error always smaller than 16.5% and the critical region for the error is located near 60 Hz (the fundamental frequency of the voltage to be integrated).

SimPowerSystems result	VSA method results			
	VSA method - FFT		VSA method - trapezoidal	
Torque [kNm]	Torque [kNm]	|Error| [%]	Torque [kNm]	|Error| [%]
6.00E-01	6.01E-01	0.1%	6.01E-01	0.0%

Table 4.1: Constant components of computed torques and corresponding errors - preset model

Continuing the process of validation, as explained on section 3.2.8, a simplified model of one of the machines under test was implemented and the results are shown on Fig. 4.5, Fig. 4.6, Fig. 4.7 and Fig. 4.8.

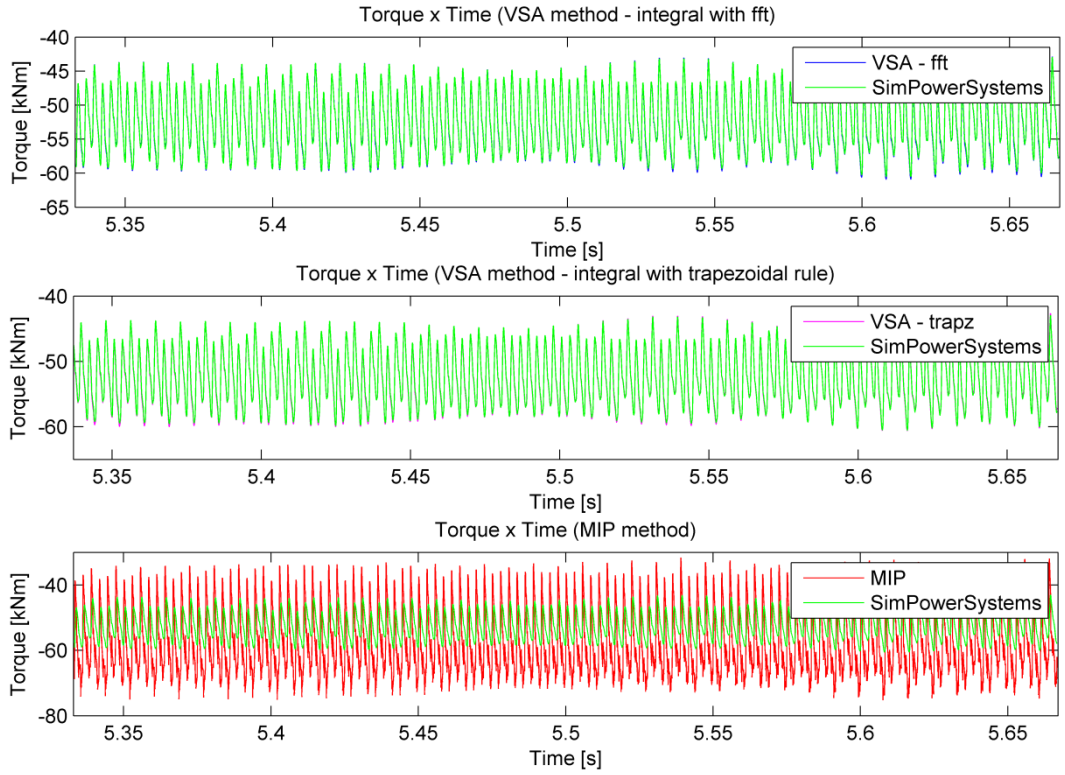

Fig. 4.5: Comparison torque x time for VSA method, MIP method and simulation with simplified motor model (19300 kW - single alimentation system)

Fig. 4.5 and Fig 4.6 show one more time the good match between the VSA method computed by both integral calculation procedures and the simulation results for the torque, on the top and middle plot. By your time, the MIP method on the bottom plot shows again a worst performance, as already discussed. This worst performance found on the validation process of the MIP method is the reason why it will be abandoned for the subsequent analysis.

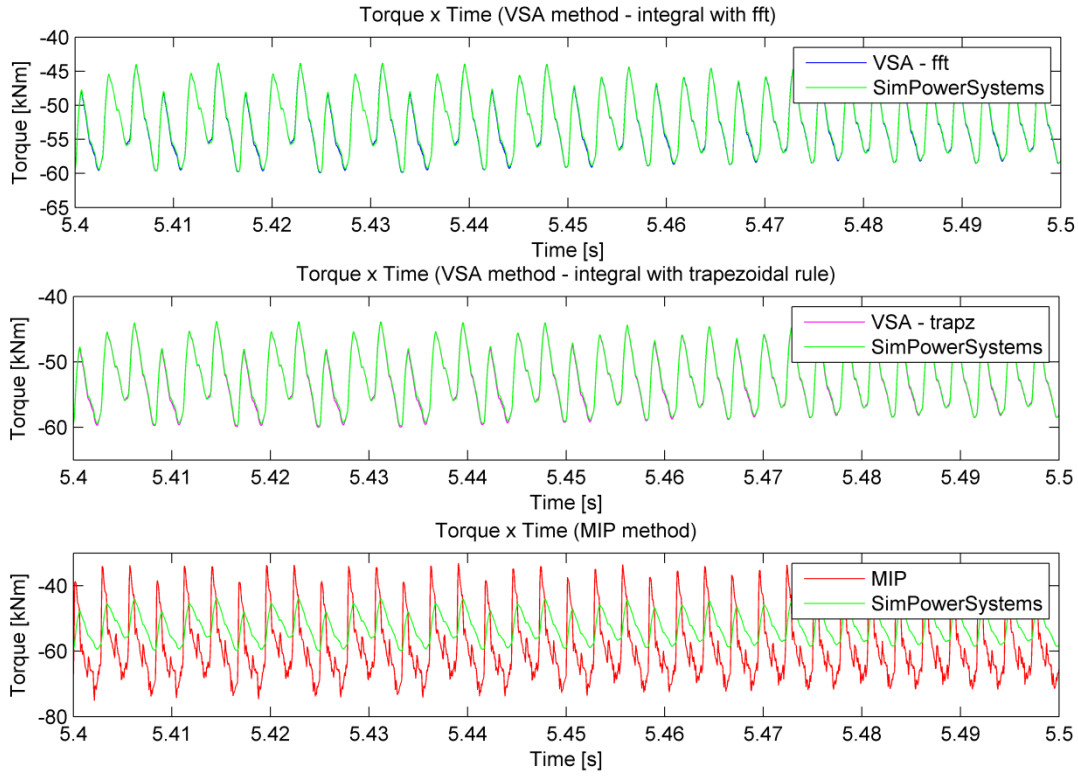

Fig. 4.6: Comparison torque x time for VSA method, MIP method and simulation with simplified motor model (19300 kW - single alimentation system) - details in evidence

Fig. 4.7 shows the spectral analysis of the torque results for the simplified motor model (19300 kW - single alimentation system). For better visualization the constant component of the torque and also the components with frequency higher than 4080 Hz were omitted from the plot. However, the constant component can be found on Table 4.2 and all the frequency components can be found on Table E.2 (Appendix E).

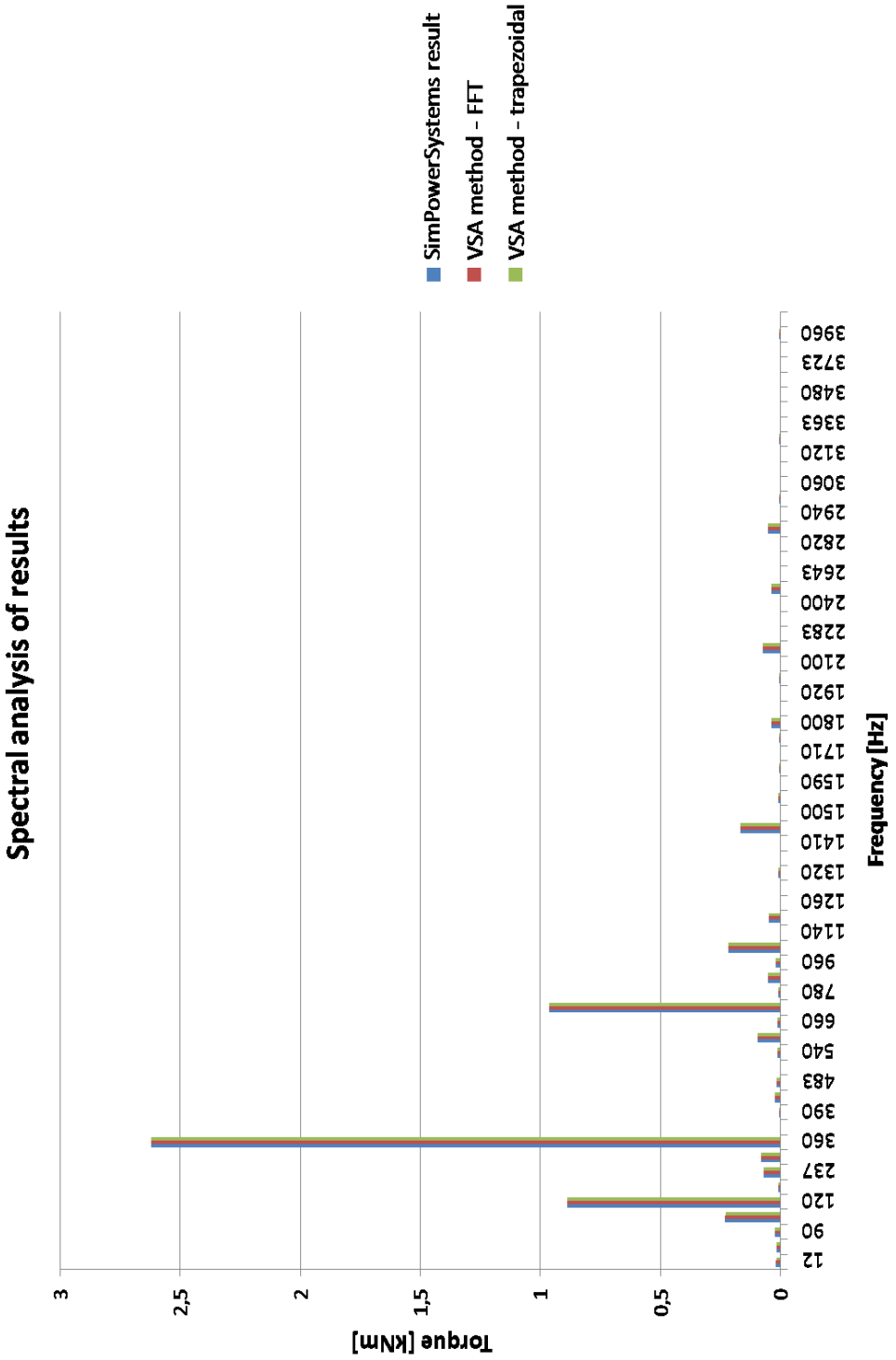

Fig. 4.7: Spectral analysis of results for simplified model

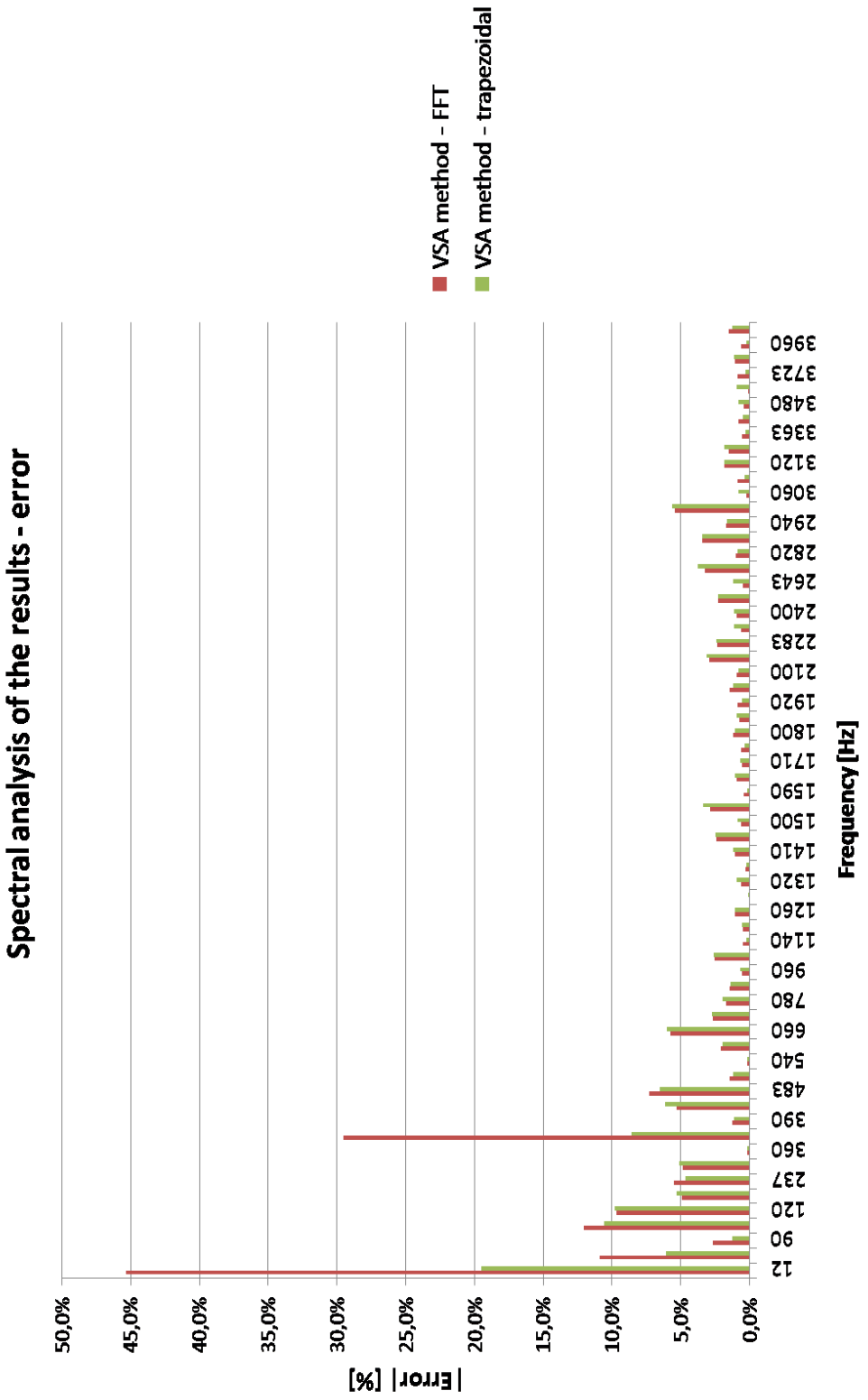

Fig. 4.8: Spectral analysis of results for simplified model - error

Fig. 4.8 shows the errors obtained for each implementation. Once more the error is bounded, but this time by the value 12.5%, apart from two spurious frequencies (12 Hz and 372 Hz) in which the error goes above the 12.5% boundary.

SimPowerSystems result	VSA method results			
	VSA method - FFT		VSA method - trapezoidal	
Torque [kNm]	Torque [kNm]	|Error| [%]	Torque [kNm]	|Error| [%]
52.535	52.648	0.2%	52.637	0.2%

Table 4.2: Constant components of computed torques and corresponding errors - simplified model

4.2. Torque computation for 19300 kW motor

For the first test bench at CESI a 19300 kW synchronous motor and the respective LCI system have been tested under full load (19300 kW) and nominal speed (3600 rpm) conditions. The results for the computed pulsating torque can be seen on Fig. 4.9.

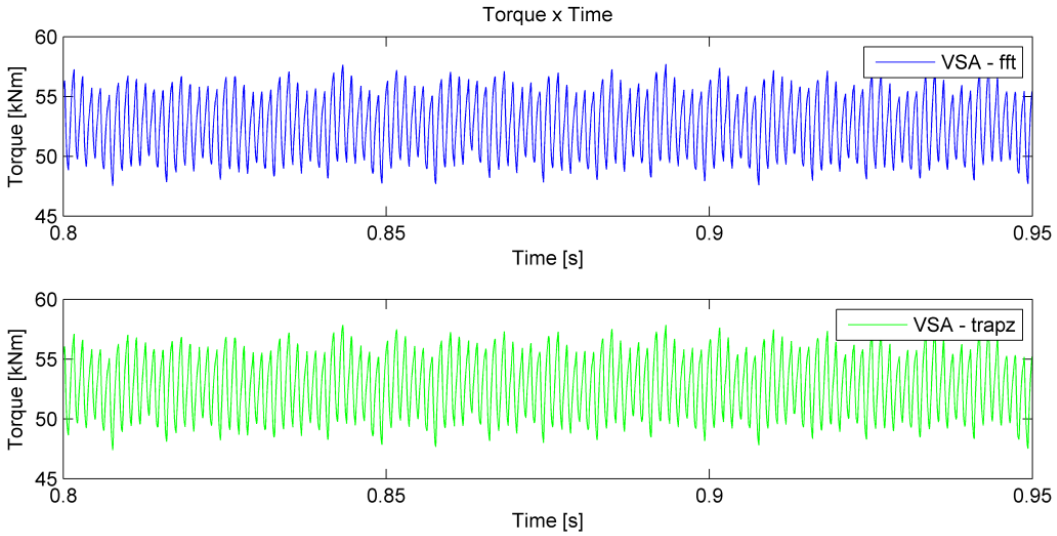

Fig. 4.9: Torque x Time results for 19300 kW motor

Remark: the figures of this section were obtained from the results of the data set collected on the moment "08 May 2013 - 12:03:09" of the test. Table 4.3 shows the key results of this data set and also of a second moment collected on "08 May 2013 - 16:45:47".

For clarity, Fig. 4.10 shows the results of the computation made with VSA method through the two different integral computation methods in a smaller time interval and overlapped.

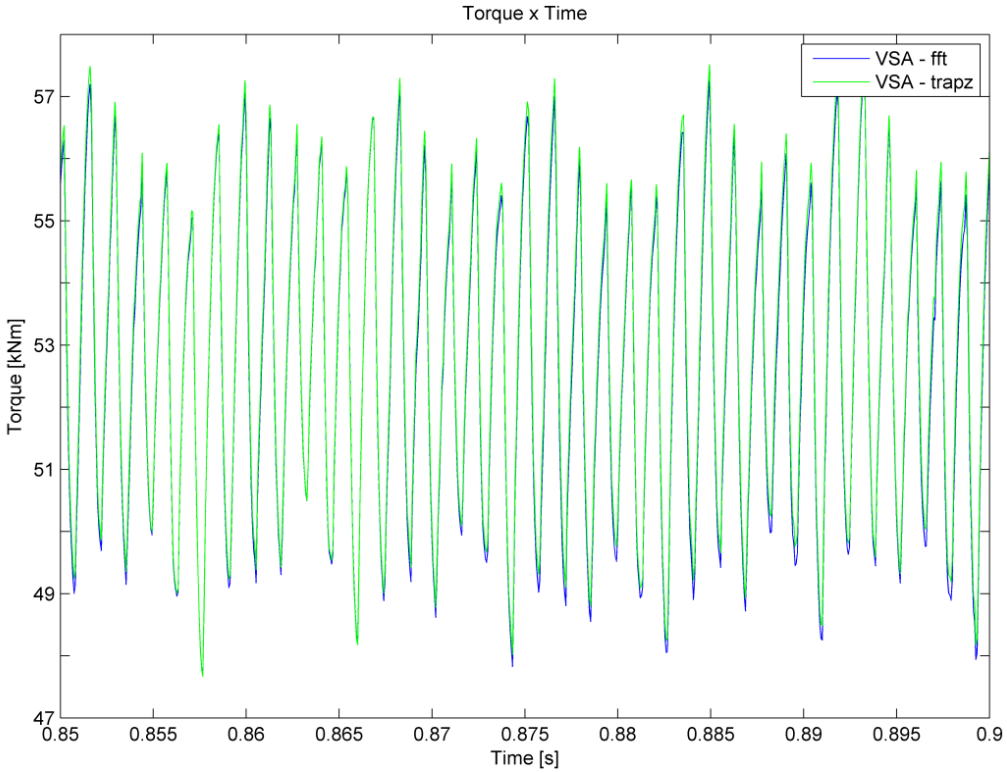

Fig. 4.10: Torque x Time results for 19300 kW motor - details

On Fig. 4.10 one can see the good correlation between the results computed through the different integral computation procedure. This fact is also evidenced by Fig. 4.11, Fig. 4.12 and Table 4.3.

On Fig. 4.11 and Fig. 4.12 it is also possible to notice that the pulsating components of the torque introduced by the current harmonics (as presented on section 1.3.2.4) are of notable amplitude when compared to the other pulsating components. For a two pole machine at 3600 rpm and 50 Hz line frequency, as the one under test, the expected frequencies on the pulsating torque are: 60 Hz, 100 Hz, 120 Hz, 240 Hz, 300 Hz, 360 Hz, 420 Hz, 600 Hz, 660 Hz, 720 Hz, 840 Hz, 960 Hz, 1020 Hz, 1080 Hz, 1320 Hz, 1440 Hz and other higher frequencies with smaller torque magnitude (the determination of the expected frequency components can be found on section 1.3.2.4).

Also on Fig. 4.11 and Fig. 4.12 it is important to highlight the pulsating torque components with frequency of 20 Hz and 40 Hz. These frequencies are not theoretically predicted, but their impact on the mechanical system can be dangerous due to the possible vicinity of the system natural frequency. Then, the existence of such components should be investigated with more care in future developments to understand if those components are originated by measurement errors, computational errors or real pulsating torque components.

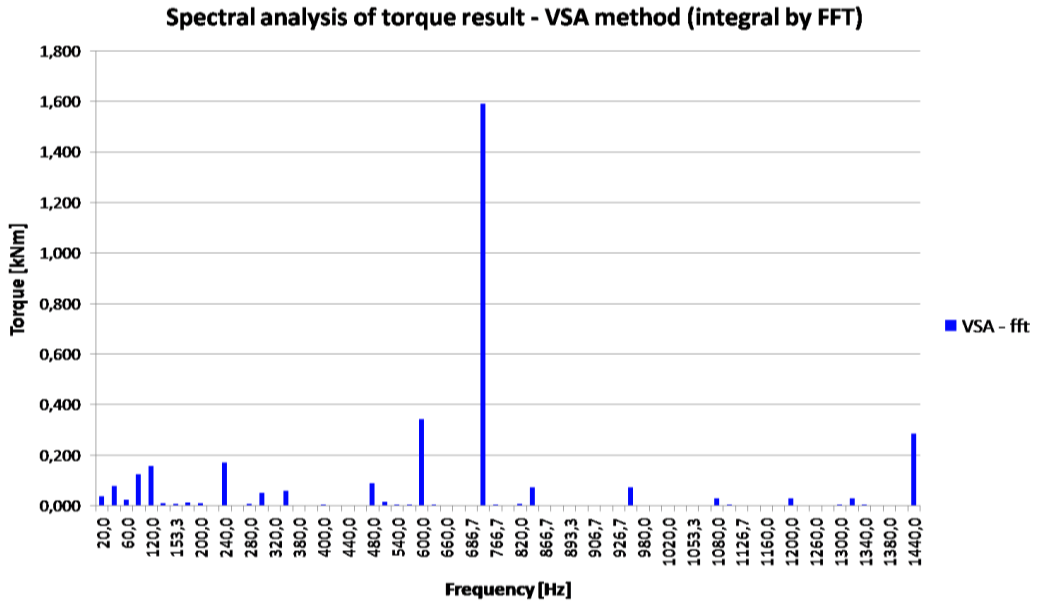

Fig. 4.11: Spectral analysis of torque results - VSA method (integral computed by FFT) - 19300 kW motor

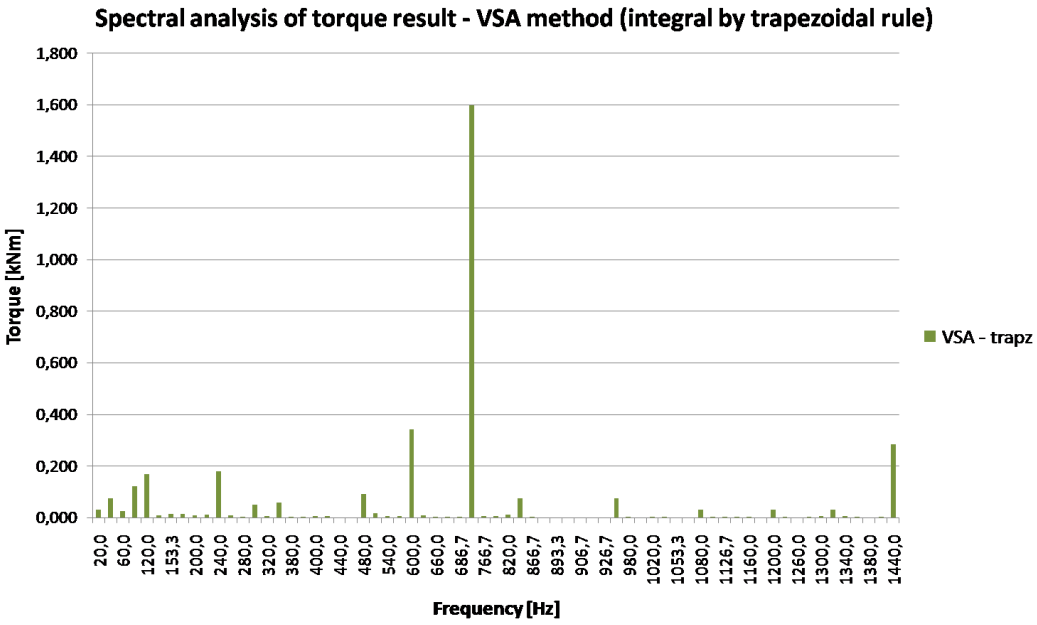

Fig. 4.12: Spectral analysis of torque results - VSA method (integral computed by trapezoidal rule) - 19300 kW motor

The expected components of the pulsating torque are also evidenced on Table 4.3. This table presents the results found for two measurement data set obtained in two different moments of the test and the value of the maximum expected amplitude for each component. The maximum expected amplitude was

computed by the ABB engineering team and it is part of the machine documentation.

	Maximum expected amplitude		Test 1 - 08 May 2013 12:03:09			Test 2 - 08 May 2013 16:45:47	
			VSA - fft	VSA - trapz		VSA - fft	VSA - trapz
Freq [Hz]	Torque [kNm]		Torque [kNm]			Torque [kNm]	
0	52.610*		52.515	52.685		52.655	52.776
60	0.161		0.026	0.025		0.031	0.034
100	NA		0.127	0.123		0.064	0.064
120	0.126		0.159	0.169		0.157	0.158
240	0.026		0.173	0.179		0.147	0.154
300	0.470		0.052	0.051		0.047	0.048
360	1.595		0.061	0.058		0.060	0.058
420	0.079		0.003	0.006		0.004	0.005
600	0.754		0.342	0.343		0.337	0.338
660	0.161		0.003	0.003		< 0.001	< 0.001
720	6.247		1.590	1.597		1.586	1.593
840	NA		0.073	0.074		0.076	0.078
960	0.026		0.073	0.074		0.069	0.071
1020	0.079		0.002	0.003		0.001	0.001
1080	0.295		0.031	0.030		0.029	0.029
1320	0.126		0.031	0.031		0.033	0.033
1440	1.221		0.285	0.285		0.279	0.279

Table 4.3: Pulsating torque components - 19300 kW motor

* The expected value for the 0 Hz frequency does not represent the maximum expected amplitude but the nominal expected value.

On Table 4.3 one can notice that a small variation can be found between the computed torque for the two data sets. This difference may be related to transient variations on the system (braking machines, motor or LCI) that could be present due to small changes on the operating conditions related to the tests that the motor must undergo during the test bench. At this point it is also important to highlight that for both data set the components corresponding to 120 Hz, 240 Hz and 960 Hz are bigger than the maximum expected ones. Once more an investigation on the origin of such magnitudes should be considered in future developments.

Regarding the average component of the torque, one can notice that the error between the expected value and the computed values is smaller than 0.5%.

For completeness, Table E.3 with the results of the spectral analysis up to 3 kHz can be found on Appendix E.

4.3. Torque computation for 20000 kW motor

For the second test bench at CESI a 20000 kW synchronous motor and the respective LCI system have been tested under different load conditions. The ones that will be considered for this thesis are the full load (20000 kW) and 75% load (15000 kW) conditions, both with nominal speed (3600 rpm). The results for the computed pulsating torque will be discussed on section 4.3.1 and section 4.3.2.

4.3.1. Full load (20000 kW) - 3600 rpm

The results for the full load test can be seen on Fig. 4.13 and Fig. 4.14

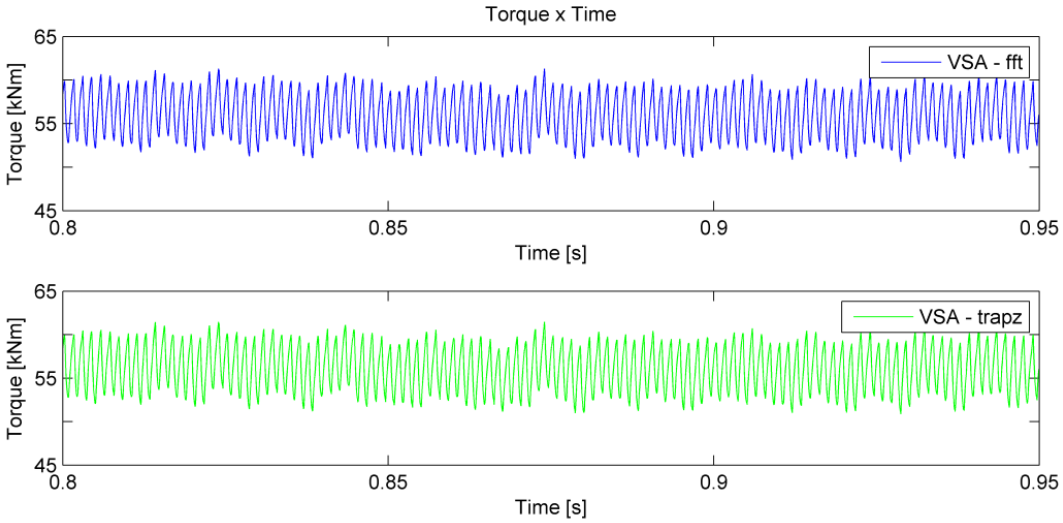

Fig. 4.13: Torque x Time results for 20000 kW motor - full load

Remark: the figures of this section were obtained from the results of the data set collected on the moment "18 June 2013 - 17:00:07" of the test. Table 4.4 shows the key results of this data set and also of two other moments collected on "18 June 2013 - 16:00:56" and "18 June 2013 - 17:30:12".

Once more, for clarity, Fig. 4.14 shows the results of the computed values for torque obtained through the VSA method in a smaller time interval and overlapped. In this figure it is possible to see the good match between the results computed through the different integral computation procedure. This fact is also evidenced by Fig. 4.15, Fig. 4.16 and Table 4.7.

On Fig. 4.15 and Fig. 4.16 it is possible to see, one more time, the expressive amplitude of the pulsating torque components related to the current harmonics with respect to the other pulsating components. Again two low frequency components at 33 Hz and 47 Hz should have their origin more deeply investigated in future developments.

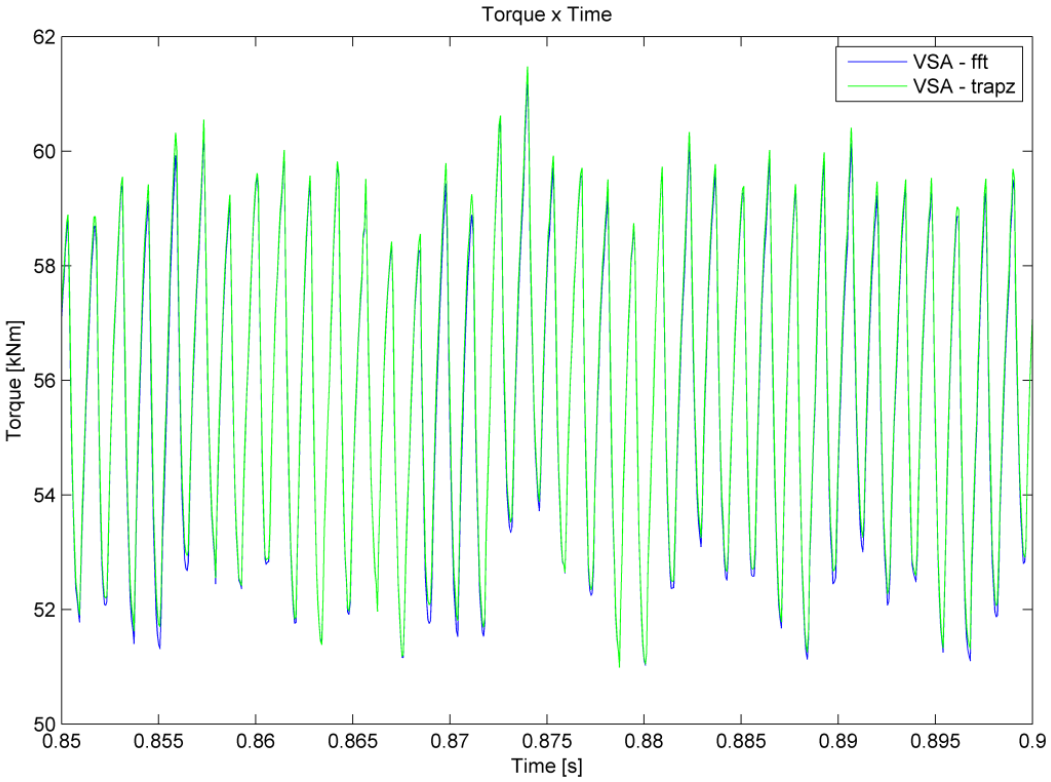

Fig. 4.14: Torque x Time results for 20000 kW motor - full load - details

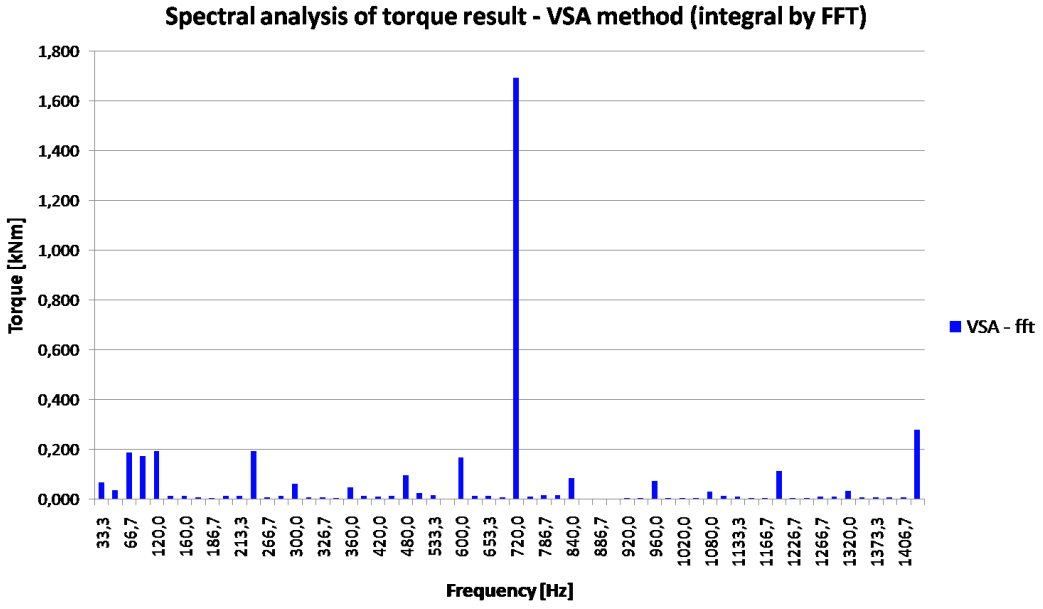

Fig. 4.15: Spectral analysis of torque results - VSA method (integral computed by FFT) - 20000 kW motor - full load

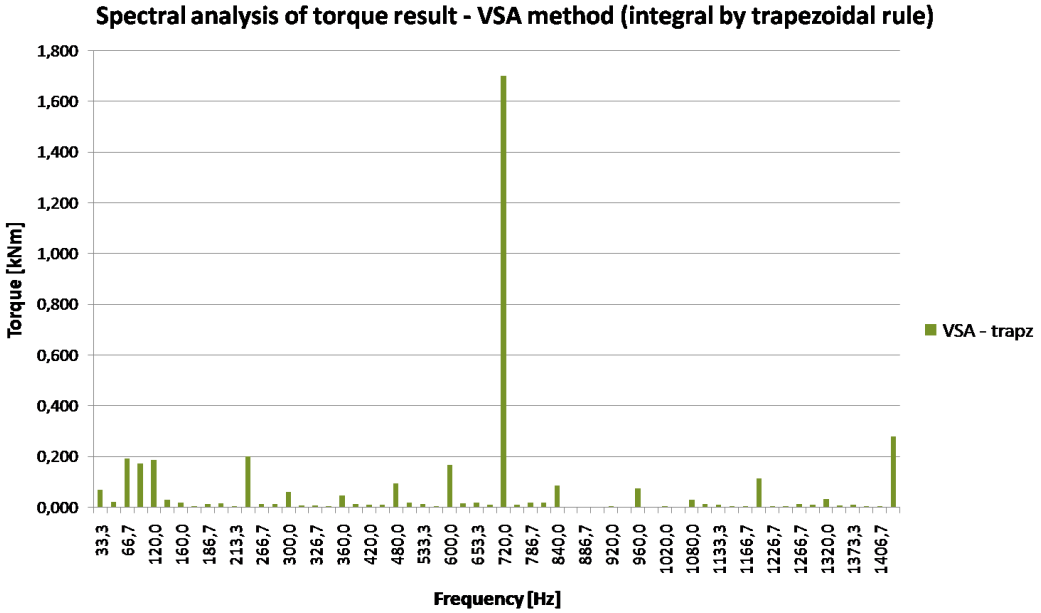

Fig. 4.16: Spectral analysis of torque results - VSA method (integral computed by trapezoidal rule) - 20000 kW motor - full load

	Test 1 - 18 June 2013 16:00:56		Test 2 - 18 June 2013 17:00:07		Test 3 - 18 June 2013 17:30:12	
	VSA - fft	VSA - trapz	VSA - fft	VSA - trapz	VSA - fft	VSA - trapz
Freq [Hz]	Torque [kNm]		Torque [kNm]		Torque [kNm]	
0	55.634	55.812	55.813	55.953	55.728	55.859
60	0.114	0.115	0.186	0.192	0.050	0.051
100	0.130	0.119	0.171	0.172	0.213	0.207
120	0.153	0.151	0.191	0.187	0.186	0.201
240	0.103	0.097	0.191	0.199	0.140	0.143
300	0.043	0.046	0.060	0.059	0.064	0.067
360	0.042	0.044	0.047	0.046	0.050	0.050
420	0.009	0.010	0.008	0.009	0.011	0.011
600	0.207	0.206	0.166	0.167	0.219	0.218
660	< 0.001	< 0.001	< 0.001	< 0.001	0.003	0.004
720	1.613	1.622	1.691	1.698	1.716	1.725
840	0.067	0.068	0.084	0.084	0.087	0.090
960	0.062	0.062	0.073	0.075	0.064	0.064
1020	< 0.001	< 0.001	0.004	0.005	0.006	0.006
1080	0.035	0.036	0.029	0.029	0.033	0.033
1320	0.030	0.031	0.031	0.030	0.029	0.028
1440	0.249	0.248	0.278	0.278	0.287	0.287

Table 4.4: Pulsating torque components - 20000 kW motor - full load

Table 4.4 compares the values found for three different data sets. Since the full load operation is not one of the operational points required by the client, the values for the expected maximum amplitude of the components are not available. However, the expected nominal value for the 0 Hz component is estimated to be 54.522 kNm and the error between the expected value and the computed values is smaller than 2.7%.

For completeness, Table E.4 with the results of the spectral analysis up to 3 kHz can be found on Appendix E.

4.3.2. 75% load (15000 kW) - 3600 rpm

The results for the 75% load test can be seen on Fig. 4.17 and compared, as done on the previous cases, on Fig. 4.18.

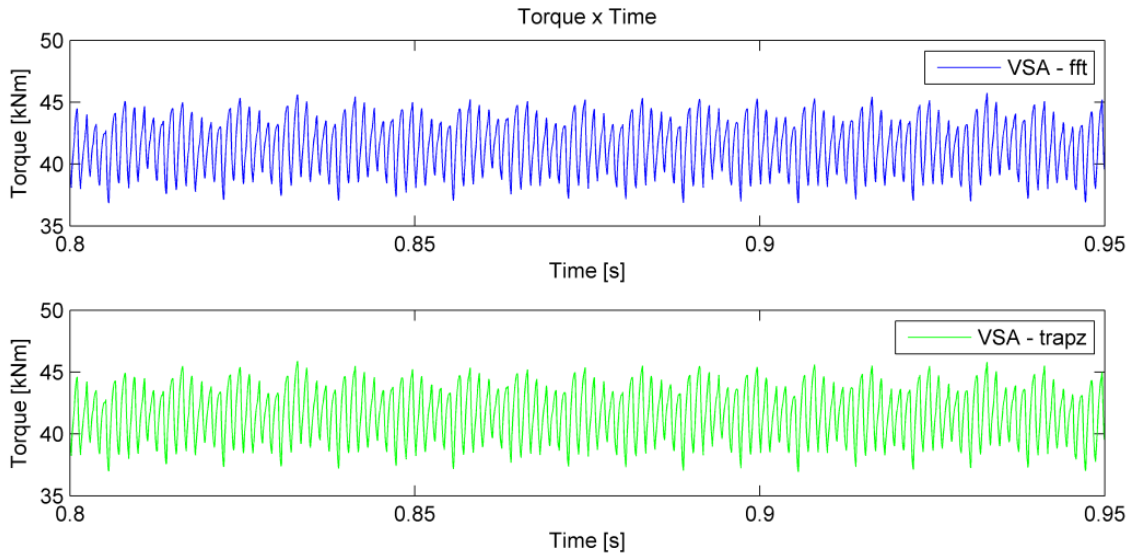

Fig. 4.17: Torque x Time results for 20000 kW motor - 75% load

On Fig. 4.19 and Fig. 4.20 the pulsating torque components related to the current harmonics and two low frequency components at 20 Hz and 40 Hz can be seen. As on the previous cases, the low frequency components should be more deeply investigated in future developments.

Similarly to the previous cases, the expected components of the pulsating torque are evidenced on Table 4.5. This table presents the results found for the torque computation and the value of the maximum expected amplitude for each component. Once more, an investigation should be considered in future developments to understand the reasons why the components corresponding to 240 Hz and 960 Hz are bigger than the maximum expected ones.

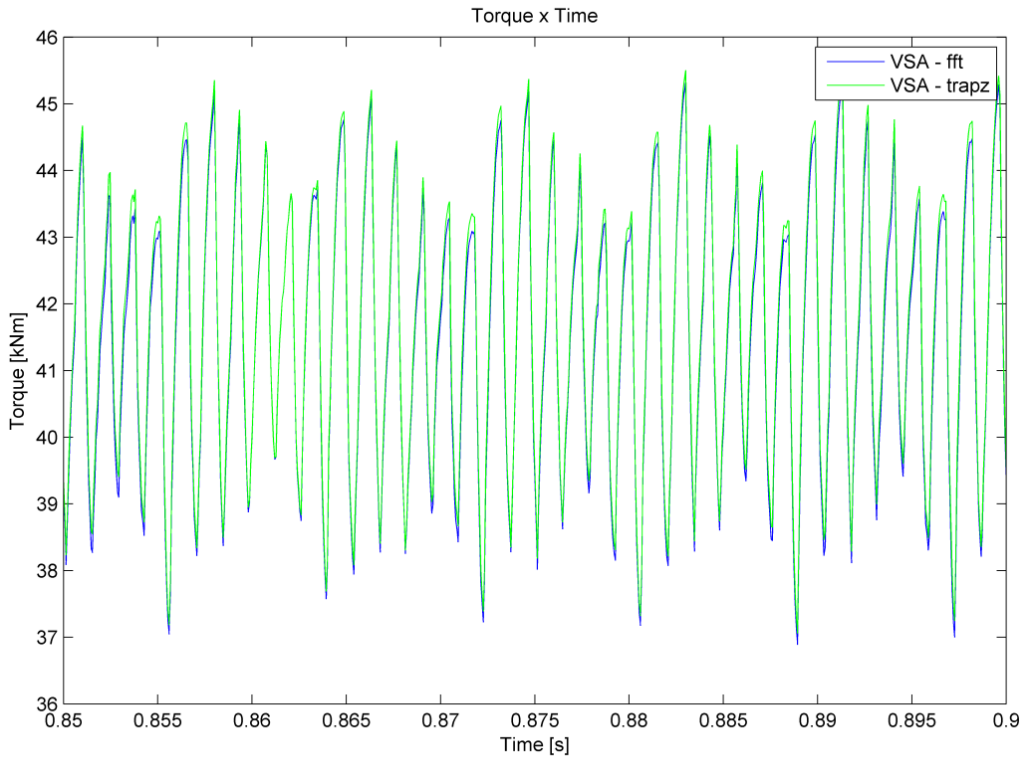

Fig. 4.18: Torque x Time results for 20000 kW motor - 75% load - details

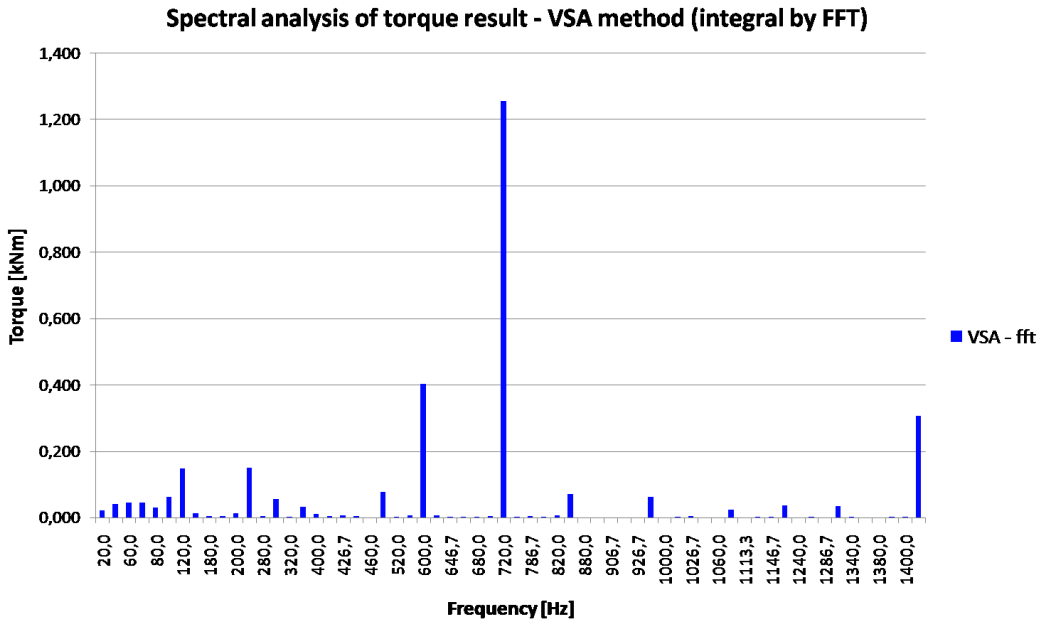

Fig. 4.19: Spectral analysis of torque results - VSA method (integral computed by FFT) - 20000 kW motor 75% load

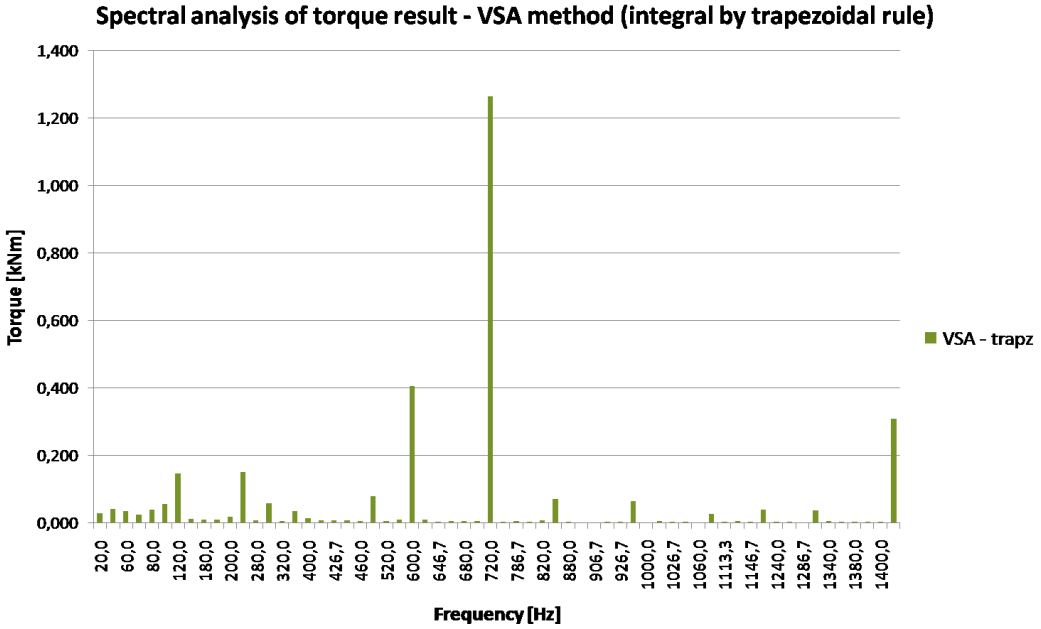

Fig. 4.20: Spectral analysis of torque results - VSA method (integral computed by trapezoidal rule) - 20000 kW motor - 75% load

	Maximum expected amplitudes		Test - 18 June 2013 - 18:00:17	
			VSA - fft	VSA - trapz
Freq [Hz]	Torque [kNm]		Torque [kNm]	
0	40.892*		41.416	41.572
60	0.190		0.045	0.033
100	NA		0.063	0.056
120	0.176		0.149	0.146
240	0.036		0.151	0.151
300	0.554		0.057	0.057
360	1.492		0.033	0.034
420	0.092		0.006	0.008
600	1.052		0.402	0.404
660	0.193		0.004	0.004
720	5.873		1.255	1.263
840	NA		0.071	0.071
960	0.036		0.063	0.064
1020	0.092		0.003	0.004
1080	0.288		0.025	0.025
1320	0.176		0.036	0.036
1440	1.292		0.307	0.308

Table 4.5: Pulsating torque components - 20000 kW motor - 75% load

* The expected value for the 0 Hz frequency does not represent the maximum expected amplitude but the nominal expected value.

Regarding the average component of the torque, one can notice that the error between the expected value and the computed values is smaller than 1.7%.

For completeness, Table E.5 with the results of the spectral analysis up to 3 kHz can be found on Appendix E.

5. Conclusions and future developments

The aim of this thesis was to compute the torque pulsations generated by current harmonics on synchronous machines fed by Adjustable Speed Drive. To achieve such objective the proposed solutions were based on the measurement of three-phase currents and three-phase voltages on the motor feeding system. With these measurements, two methods were applied: the Volt-Second Ampere method and the Modified Input Power method.

During the implementation of the Volt-Second Ampere method, a challenge was posed by the integral computation of the line-to-line voltages, that is present on the definition of such method. Two possible implementations were proposed: the first making use of a Fourier analysis and the second making use of both the moving average technique and the trapezoidal integration technique in order to overcome the problem of determining the initial condition of the integral to be computed.

The implementation of the methods was then validated and the results obtained with the Volt-Second Ampere method were more consistent than the ones found with the Modified Input Power method. The error computed for the Volt-Second Ampere method was bounded by a factor of 16.5% while the Modified Input method could not reach significant matching between the expected results and the results found with the method computation. For this reason, the analysis of the real data with the Modified Input Power method was not taken into consideration.

Continuing on the validation processes, none of the two integral methods utilized for the Volt-Second Ampere implementation demonstrated significantly better results than the other. The Fourier analysis method presented apparent better result in the whole range of frequencies, but presenting few spurious peaks in frequencies that were not expected. On the other hand, the trapezoidal method implementation demonstrated a slightly worst result in the whole frequency range, but with the presence of such spurious peaks significantly reduced.

At this point a difference between the two integral computation methods should be highlighted. For future developments it could be interesting to have the real time (with the motor in movement during the tests) torque computation, and for this implementation, the trapezoidal method with moving average would present an advantage since it would give the possibility of computing the torque for each new data point (or new small data set) while the Fourier method would require a bigger data set to be effective.

After the validation, the implemented methods were used, through the created graphical interface, to compute the pulsating torque with the real data sets obtained from the measurements of the tests on the motors. The use of the graphical interface significantly simplified the process specially when considering the test environment in which the tools should be as simple and fast as possible to provide the results.

The obtained results were confronted with the expected maximum values for the frequency components of the pulsating torque. In all the tests realized (19300 kW motor at full load, 20000 kW motor at full load and 20000 kW at 75% load) the presence of the pulsating torque components related to the current harmonics was verified and confirmed. The pulsating components of all the expected frequencies, apart from the 120 Hz, 240 Hz and 960 Hz, remained inside the maximum expected value and the average values for the torque, that were also compared to the expected ones, presented error always smaller than 2.7%.

Future developments should investigate the reasons for the components at 120 Hz, 240 Hz and 960 Hz be over the maximum expected value. Keeping the same reasoning, also the existence of low frequency non expected peaks at 20 Hz and 40 Hz should be investigated since the vicinity of the system natural frequency may bring dangerous consequences to the system.

Finally, as the tests developed during this thesis are performed on systems in which the availability is of extreme importance for the plant operation, a safer option for future developments could be to, at least once, apply different measurement methods for the pulsating torque, like the search coil method or an accurate mechanical method. Having this data at hand, one could compare the obtained results with the results obtained from the program created during this thesis and better understand the limitations of the proposed solution.

Appendix A: Park's transformation and circuit components

An important remark is that this development will be carried out taking as reference the book "Analysis of Electric Machinery and Drive Systems" [7].

It is convenient to treat resistive, inductive and capacitive circuit elements separately.

Resistive elements

For a 3-phase resistive circuit:

$$v_{abcs} = r_s\, i_{abcs} \tag{A.1}$$

From (A.1) we obtain:

$$v_{dq0s} = K_s\, r_s\, (K_s)^{-1}\, i_{dq0s} \tag{A.2}$$

Now it is necessary to specify the resistance matrix r_s. If we consider the realistic idea that all the stator phase windings of a synchronous machine are designed to have the same resistance, then all the nonzero elements of the diagonal matrix r_s are equal and:

$$K_s\, r_s\, (K_s)^{-1} = r_s \tag{A.3}$$

From here is easy to understand that the resistance matrix of the arbitrary reference variables is equal to the resistance matrix associated with the actual variables if each phase of the actual circuit has the same resistance. If the phase resistances are unbalanced the resistance resultant from the transformation is constant only if the reference frame is fixed where the unbalance physically exists.

Inductive elements

For a 3-phase inductive circuit:

$$v_{abcs} = \frac{d\lambda_{abcs}}{dt} \tag{A.4}$$

It is important to remark that the transformation is also valid for the flux linkages. This property saves a great amount of time comparing to the solution of expressing the voltage as a product of inductance and current and then making the transformation. Thus:

$$v_{dq0s} = K_s\, \frac{d\left[(K_s)^{-1}\, \lambda_{dq0s}\right]}{dt} \tag{A.5}$$

rewriting as:

$$\mathrm{v}_{dq0s} = K_s \frac{d[(K_s)^{-1}]}{\mathrm{dt}} \lambda_{dq0s} + K_s (K_s)^{-1} \frac{d\lambda_{dq0s}}{\mathrm{dt}} \tag{A.6}$$

applying the differentiation on (1.13):

$$\frac{\mathrm{d}[(\mathrm{K}_s)^{-1}]}{\mathrm{dt}} = \omega \begin{bmatrix} -\sin\theta & \cos\theta & 0 \\ -\sin\left(\theta - \frac{2\pi}{3}\right) & \cos\left(\theta - \frac{2\pi}{3}\right) & 0 \\ -\sin\left(\theta + \frac{2\pi}{3}\right) & \cos\left(\theta + \frac{2\pi}{3}\right) & 0 \end{bmatrix} \tag{A.7}$$

Then,

$$\mathrm{K}_s \frac{\mathrm{d}[(\mathrm{K}_s)^{-1}]}{\mathrm{dt}} = \omega \begin{bmatrix} 0 & -1 & 0 \\ 1 & 0 & 0 \\ 0 & 0 & 0 \end{bmatrix} \tag{A.8}$$

Now equation (A.6) can be expressed as:

$$\mathrm{v}_{dq0s} = \omega \lambda_{qds} + \frac{d\lambda_{dq0s}}{\mathrm{dt}} \tag{A.9}$$

where:

$$\left(\lambda_{qds}\right)^T = \left[-\lambda_{qs} \ \lambda_{ds} \ 0\right] \tag{A.10}$$

which is more commonly written as:

$$v_{ds} = -\omega \lambda_{qs} + \frac{d\lambda_{ds}}{\mathrm{dt}} \tag{A.11}$$

$$v_{qs} = \omega \lambda_{ds} + \frac{d\lambda_{qs}}{\mathrm{dt}} \tag{A.12}$$

$$v_{0s} = \frac{d\lambda_{0s}}{\mathrm{dt}} \tag{A.13}$$

The equations (A.11)-(A.13) are valid regardless if the system is magnetically linear or nonlinear and regardless of the form of the induction matrix if the system is magnetically linear.

Let us for a while consider linear magnetic systems, in which the flux linkage can be expressed as:

$$\lambda_{abcs} = \mathrm{L}_s \ i_{abcs} \tag{A.14}$$

or

$$\lambda_{dq0s} = \mathrm{K}_s \mathrm{L}_s (\mathrm{K}_s)^{-1} i_{dq0s} \tag{A.15}$$

As in the resistive circuit, it is necessary to define the inductance matrix. However, once the induction matrix has been specified one can just evaluate the equation (A.15) and then substitute the resulting $\lambda_{ds}\ \lambda_{qs}\ \lambda_{0s}$ into the equations (A.11) - (A-13).

As an example let us consider a induction matrix of the synchronous machines:

$$\mathrm{L}_s = \begin{bmatrix} \mathrm{L}_{ls} + \mathrm{L}_{ms} & -\frac{1}{2}\mathrm{L}_{ms} & -\frac{1}{2}\mathrm{L}_{ms} \\ -\frac{1}{2}\mathrm{L}_{ms} & \mathrm{L}_{ls} + \mathrm{L}_{ms} & -\frac{1}{2}\mathrm{L}_{ms} \\ -\frac{1}{2}\mathrm{L}_{ms} & -\frac{1}{2}\mathrm{L}_{ms} & \mathrm{L}_{ls} + \mathrm{L}_{ms} \end{bmatrix} \tag{A.16}$$

Where L_{ls} is a leakage inductance and L_{ms} is a magnetizing inductance. Then, we have:

$$\mathrm{K}_s\,\mathrm{L}_s(\mathrm{K}_s)^{-1} = \begin{bmatrix} \mathrm{L}_{ls} + \frac{3}{2}\mathrm{L}_{ms} & 0 & 0 \\ 0 & \mathrm{L}_{ls} + \frac{3}{2}\mathrm{L}_{ms} & 0 \\ 0 & 0 & \mathrm{L}_{ls} + \frac{3}{2}\mathrm{L}_{ms} \end{bmatrix} \tag{A.17}$$

For a linear 3-phase coupled system be considered magnetically symmetrical its inductance matrix should have the diagonal elements equal and all off-diagonal elements equal. Observe that the matrix (A.16) has this characteristic and note that the matrix (A.17) correspond to a magnetically uncoupled system. So we can understand that this transformation makes the initial magnetically symmetrical system become a magnetically uncoupled system for any reference frame. On the other hand it was shown that for salient pole synchronous machine just one reference frame will result in a magnetically uncoupled system.

Capacitive elements

For a 3-phase capacitive circuit:

$$\mathrm{i}_{abcs} = \frac{dq_{abcs}}{\mathrm{dt}} \tag{A.18}$$

In substitute variables:

$$\mathrm{i}_{dq0s} = K_s\ \frac{d\left[(K_s)^{-1}\,q_{dq0s}\right]}{\mathrm{dt}} \tag{A.19}$$

rewriting as:

$$\mathrm{i}_{dq0s} = K_s \frac{d[(K_s)^{-1}]}{\mathrm{dt}} q_{dq0s} + K_s (K_s)^{-1} \frac{dq_{dq0s}}{\mathrm{dt}} \tag{A.20}$$

substituting (1.23):

$$\mathrm{i}_{dq0s} = \omega q_{qds} + \frac{dq_{dq0s}}{\mathrm{dt}} \tag{A.21}$$

where:

$$(q_{qds})^T = [q_{qs} - q_{ds}\ 0] \tag{A.22}$$

which is more commonly written as:

$$i_{ds} = \omega q_{qs} + \frac{dq_{ds}}{\mathrm{dt}} \tag{A.23}$$

$$i_{qs} = -\omega q_{ds} + \frac{dq_{qs}}{\mathrm{dt}} \tag{A.24}$$

$$i_{0s} = \frac{dq_{0s}}{\mathrm{dt}} \tag{A.25}$$

The same considerations made for the inductive system can be made here. Equations (A.23)-(A.25) are valid regardless of the relationship between charge and voltage. Considering linear capacitive systems:

$$q_{abcs} = \mathrm{C}_s\ v_{abcs} \tag{A.26}$$

or, in arbitrary reference frame:

$$q_{dq0s} = \mathrm{K}_s\ \mathrm{C}_s (\mathrm{K}_s)^{-1}\ v_{dq0s} \tag{A.27}$$

And again the same considerations made for the inductive system holds. Once the capacitive matrix has been specified one can just evaluate the equation (A.27) and then substitute the resulting $q_{ds}\ q_{qs}\ q_{0s}$ into the equations (A.23) - (A.25).

Appendix B: Test requirements

Test requirements in international and oil and gas standards comparison table

IEC 61800-4	IEEE 1566	Typical oil & gas specification
Light load test	-	No load tests
Load characteristic test (Load envelope test)	Unit under load	Load tests
Load duty test (Intermittent load test)	-	110% nominal current test for at least 10 minutes
Allowable full load current versus speed test	-	-
Temperature rise tests	Verification of converter temperature rise	Motor winding temperature rise Converter temperature rises
Efficiency	Demonstration of the efficiency	Overall efficiency determination at full and half load curve
Line-side current distortion content	-	Harmonic distortion in the current on the line side
Power factor	-	Power factor determination at full and half load curve
Checking of auxiliary devices	-	-
Checking co-ordination of protective devices	Demonstration of the proper operation of all protective functions, both trip and alarm	Test of all protection, alarm and trip functions
Checking properties under unusual service conditions	-	Fault condition tests (earth fault, phase interruption…)
Shaft current/bearing insulation	-	Motor shaft voltage
Audible noise	-	Noise test
Torque pulsation	-	-
Motor vibration	Demonstration of vibration levels during startup, when operating under load in the speed range and when loads are suddenly applied or removed	Shaft vibration Vibration severity at bearing housing
EMC tests	-	Harmonic distortion in the current on the line side
Current limit and current loop test	-	Linearity between set point signal and output

Table B.1: IEC 61800-4, IEEE 1566 and typical oil & gas specification comparison [3]

Speed loop test	Demonstration of minimum and maximum speed adjustments Demonstration of acceleration and deceleration rates Demonstration of speed control from an external signal Demonstration of the accuracy of the monitoring panel speed indication meter by comparison with a frequency counter	Test the response times and the adjustability (ramp times) within the operational speed range
Automatic restart/re-acceleration	-	Test capability to restart VSDS and resynchronize converter onto a running motor after a voltage interruption
-	Demonstration of undervoltage disturbance ride-through and restart	Test capability to ride through voltage dips less than 20%
-	Demonstration of volts/hertz relationship from minimum to maximum speeds	-
-	Verification of all control parameters	-
-	Exciter supply voltage waveform shall be inspected to ensure compatibility with the machine exciter insulation voltage rating	-
-	-	Visual Inspection

Table B.2 (cont..): IEC 61800-4, IEEE 1566 and typical oil & gas specification comparison [3]

Appendix C: Sensors

Rogowski coil current transducer

Rogowski coils, also known as air-cored coils, are AC current transducers that have been used for the measurement of electric currents since 1884. Their principle of operation is simple. An 'air-cored' coil in a toroidal form is placed around the conductor that produces a magnetic field due to the current flow. This magnetic field induces a voltage in the coil that is proportional to the rate of change of current on the conductor. This voltage is integrated, producing an output proportional to the current [25].

Rogowski coils advantages

- linear response due to absence of magnetic hysteresis cause by the iron core.
- wide bandwidth.
- ease of use: solutions available to keep the conductor centered on the coil that sets the error to be < 3%.
- intrinsic galvanic insulation.
- good electromagnetic noise rejection.

Despite its simple structure that can be seen in Fig. C.1 and its apparent ease of use, the resulting measurements can be subjected to some errors that will briefly presented.

Conductor position in the Rogowski loop

Small variations on the winding density and coil cross section area may happen on the Rogowski coil and the transducer output may vary slightly depending on the position of the conductor inside the Rogowski coil. Another important aspect is the size of the conductor carrying the current with respect to area of the coil loop that also can cause errors.

To quantify these variations, tests were performed by Power Electronic Measurement (PEM) Ltd. in two different coil circumference, 300 mm and 700 mm, and two different conductor diameters 10 mm and 50 mm. The results are shown in Table C.1 and Table C.2. The Rogowski coils were calibrated with the conductor centralized on the loop (position 1 in Fig. C.2) and for this position has a accuracy of ±0.2%. The values listed on the tables are additional uncertainty related to the conductor position [26].

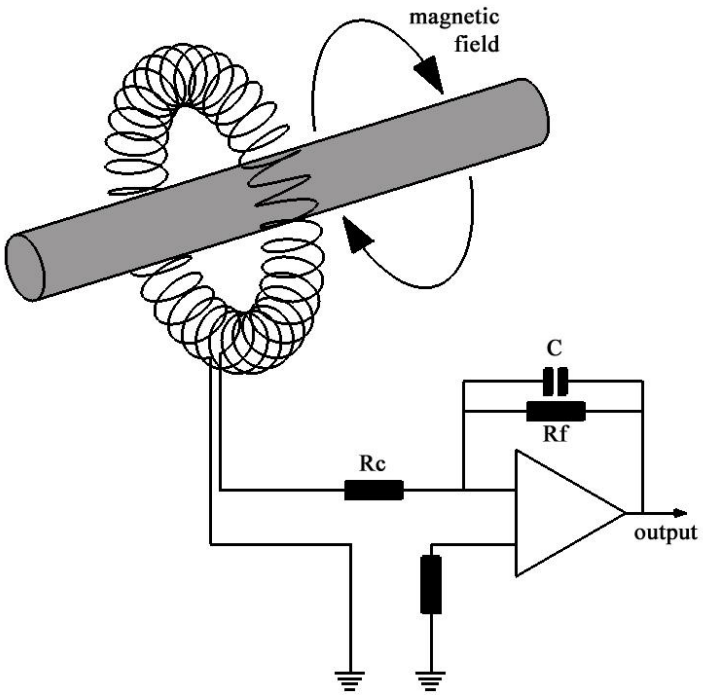

Fig. C.1: Rogowski coil current transducer (modified from [25])

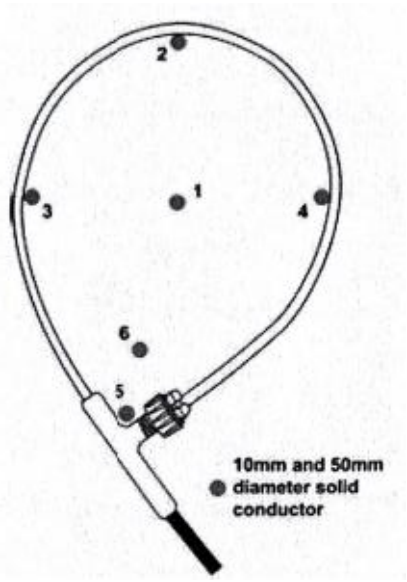

Fig. C.2: Conductor position in the Rogoswki coil [26]

Coil length [mm]	Touching the edge of the coil			Ferrule	3 cm from ferrule
	2	3	4	5	6
300	±1.0	±1.0	±1.0	-3.5	-3.5
700	±1.5	±2.0	±2.0	-3.5	-1.0
700 (x2)	±0.5	±0.5	±0.5	-1.5	-0.5

Table C.1: Position error % - 10 mm conductor [26]

Coil length [mm]	Touching the edge of the coil			Ferrule
	2	3	4	5
300	±0.5	±0.5	±0.5	-0.5
700	±1.0	±1.0	±1.0	-1.0
700 (x2)	±0.3	±0.3	±0.3	-0.3

Table C.2: Position error % - 50 mm conductor [26]

It can be noticed on the tables that the increasing of conductor size with respect to the Rogowski coil area, increases the accuracy on the measurement. Not only but also that wrapping the coil twice around the conductor has improved accuracy (configuration 700 mm (x2)). However, this configuration also halves the rated current and doubles the sensitivity (V/A) [26].

External currents interference

Errors can also arise from the interference of external conductors carrying current nearby the Rogoswski coil in use. If the external current is much greater than the current being measured, this error can be significant [26].

Results of tests performed by PEM are shown on Table C.3 and illustrates the typical % error for a 10 mm conductor and a 700 mm coil.

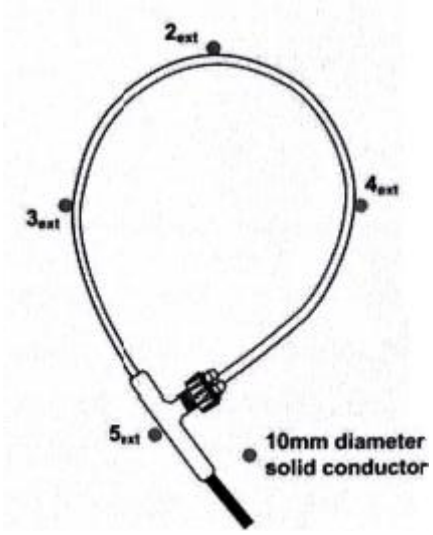

Fig. C.3: External conductor position - Rogoswki coil [26]

Coil length [mm]	Touching the edge of the coil			Ferrule
	2_{ext}	3_{ext}	4_{ext}	5_{ext}
700	±1.5	±2.0	±2.0	-3.5

Table C.3: % of external current measured by the Rogowski coil [26]

Temperature

Errors can also arise from temperature variations that can, mainly, cause expansion of the plastic former onto which the Rogowski coil is wound, causing reduction of the sensitivity and/or interfere on the passive components of the integrator, changing its time constant.

Usually, Rogoswki coils are made with very low coefficient of expansion materials and high stability passive components are utilized on the integrator. This values can be seen on Table C.4 [26].

	Drift %/°C
Coil expansion	-0.01
Integrator drift	±0.012

Table C.4: Thermal deviation [26]

Resistive-capacitive potential divider voltage transducer

A voltage divider has as aim to reduce the voltage V1 applied to its primary terminals by a prefixed ratio. It consists on the series of two impedances Z_1 and Z_2, as shown in Fig. C.4. If no load is connected on the output terminals, the secondary voltage V_2 is obtained as shown in equation (C.1).

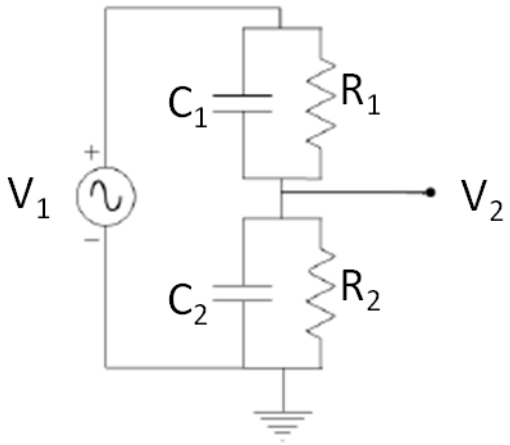

Fig. C.4: Resistive-capacitive potential divider voltage transducer

$$V_2 = \frac{Z_2}{Z_1 + Z_2} V_1 \qquad \text{(C.1)}$$

Under sinusoidal signal, the potential divider is said to be compensated when the ratio $\frac{Z_2}{Z_1+Z_2}$ is, at least theoretically, a real number independent of the signal frequency. This can be obtained by using either two impedances of the same kind (e.g. either two resistances or two capacitances) or series/parallel combinations of resistances and capacitances, properly chosen so that the two impedances Z_1 and Z_2 have the same time constant [27].

In real applications, the validity of equation (C.1) is affected, since the secondary terminals of the divider are always loaded by some load. But the higher the load with respect to the divider's output impedance, the lower the influence of the load itself on the measured signal [27].

The main advantage of voltage dividers are:

- reduced size
- reduced weight
- good linearity

The latest one gives a important property for the device, that is the possibility of usage of the same equipment in wide voltage ranges, thus allowing proper measurements under normal operating conditions and overvoltages [27].

Another advantage of the compensated potential divider is that it can guarantee very high bandwidth (from dc to tens of megahertz).

Finally, the main drawback is that voltage dividers do not guarantee insulation between high voltage and low voltage terminals. Then, the safety of the measurement or protection system should be ensured by either introducing additional devices (e.g. an isolation amplifier) or implementing alternative solutions, like the ones based on either grounding or surge arrestors [27].

Appendix D: System photos

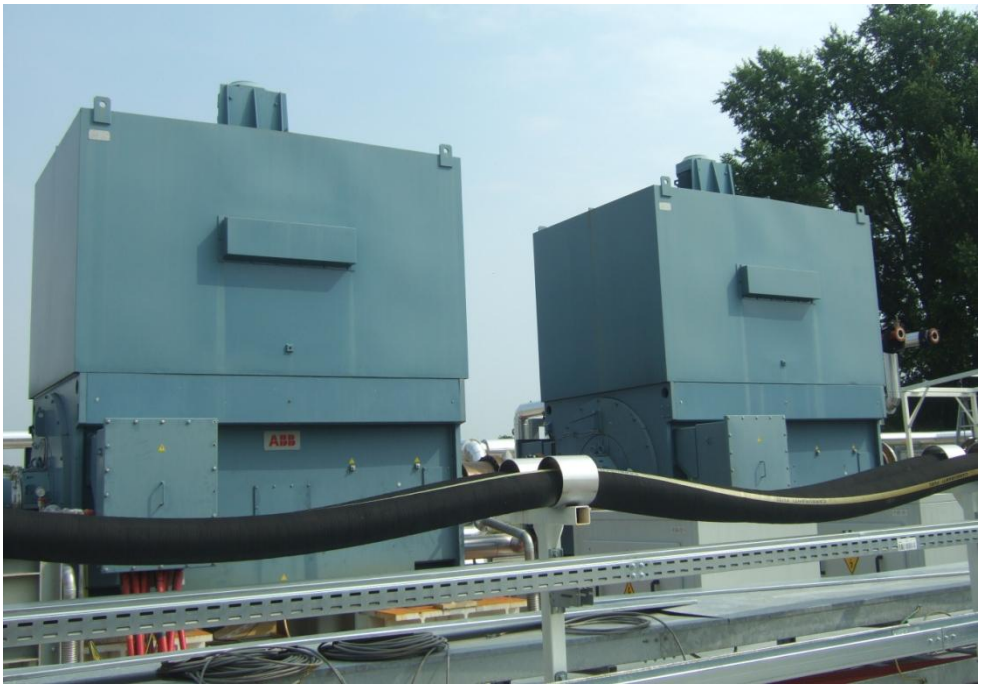

Fig. D.1: Braking machines

Fig. D.2: LCI

Fig. D.3: Motor under test, gearbox and load (from right to left)

Appendix E: Complete results

Results of validation with preset model (111.9 kW)

	SimPowerSystems result	VSA method results			
		VSA method - FFT		VSA method - trapezoidal	
Freq [Hz]	Torque [kNm]	Torque [kNm]	|Error| [%]	Torque [kNm]	|Error| [%]
0	6.00E-01	6.01E-01	0.1%	6.01E-01	0.0%
21	7.13E-04	7.16E-04	0.5%	7.34E-04	3.0%
33	6.86E-04	6.88E-04	0.3%	7.47E-04	8.8%
39	7.94E-04	7.98E-04	0.5%	9.16E-04	15.2%
51	9.68E-04	9.77E-04	0.9%	1.12E-03	15.9%
57	6.32E-04	7.30E-04	15.4%	7.35E-04	16.4%
63	1.31E-03	1.14E-03	12.6%	1.44E-03	9.9%
78	7.70E-04	7.70E-04	0.0%	8.42E-04	9.4%
90	1.18E-03	1.18E-03	0.1%	1.08E-03	8.9%
102	5.31E-04	5.33E-04	0.2%	5.46E-04	2.8%
120	2.32E-02	2.32E-02	0.0%	2.32E-02	0.1%
132	2.65E-04	2.66E-04	0.1%	2.63E-04	1.0%
150	1.65E-04	1.66E-04	0.7%	1.65E-04	0.2%
156	2.32E-04	2.32E-04	0.1%	2.25E-04	2.8%
180	3.74E-04	3.74E-04	0.0%	3.76E-04	0.6%
195	2.54E-04	2.54E-04	0.0%	2.55E-04	0.3%
210	1.17E-03	1.17E-03	0.0%	1.18E-03	1.6%
240	1.25E-03	1.24E-03	0.1%	1.25E-03	0.1%
255	1.01E-04	1.01E-04	0.4%	1.03E-04	2.5%
264	1.27E-04	1.27E-04	0.1%	1.25E-04	1.3%
300	3.03E-04	2.98E-04	1.5%	2.95E-04	2.8%
312	1.40E-04	1.40E-04	0.4%	1.44E-04	3.0%
330	1.64E-04	1.64E-04	0.2%	1.68E-04	2.0%
348	1.31E-04	1.30E-04	1.0%	1.30E-04	1.0%
360	2.08E-02	2.08E-02	0.1%	2.08E-02	0.0%
474	1.40E-04	1.41E-04	0.1%	1.40E-04	0.3%
480	3.55E-04	3.55E-04	0.1%	3.55E-04	0.1%
489	1.05E-04	1.05E-04	0.2%	1.05E-04	0.1%
540	1.73E-04	1.74E-04	0.2%	1.74E-04	0.2%
594	1.54E-04	1.54E-04	0.0%	1.54E-04	0.0%
600	5.61E-04	5.63E-04	0.4%	5.62E-04	0.0%

Table E.1: Results of validation with preset motor model

	SimPowerSystems result	VSA method results			
		VSA method - FFT		VSA method - trapezoidal	
Freq [Hz]	Torque [kNm]	Torque [kNm]	|Error| [%]	Torque [kNm]	|Error| [%]
720	8.04E-03	8.05E-03	0.1%	8.05E-03	0.0%
843	2.59E-04	2.59E-04	0.1%	2.59E-04	0.1%
957	1.68E-04	1.68E-04	0.1%	1.68E-04	0.0%
1080	1.90E-03	1.90E-03	0.1%	1.90E-03	0.0%
1200	2.59E-04	2.59E-04	0.2%	2.59E-04	0.1%
1440	1.39E-03	1.39E-03	0.0%	1.39E-03	0.1%
1800	3.58E-04	3.59E-04	0.2%	3.58E-04	0.0%
2037	1.55E-04	1.55E-04	0.0%	1.55E-04	0.0%
2160	6.27E-04	6.28E-04	0.1%	6.27E-04	0.0%
2520	3.24E-04	3.24E-04	0.1%	3.24E-04	0.0%
2880	4.60E-04	4.60E-04	0.0%	4.60E-04	0.0%
3600	1.16E-04	1.16E-04	0.3%	1.16E-04	0.0%
4320	1.92E-04	1.93E-04	0.2%	1.92E-04	0.0%

Table E.1 (cont.): Results of validation with preset motor model

Results of validation with simplified motor model (19300kW - single power supply system)

	SimPowerSystems result	VSA method results			
		VSA method - FFT		VSA method - trapezoidal	
Freq [Hz]	Torque [kNm]	Torque [kNm]	|Error| [%]	Torque [kNm]	|Error| [%]
0	52,535	52,649	0,2%	52,637	0,2%
12	0,015	0,021	45,3%	0,017	19,5%
33	0,022	0,019	10,9%	0,020	6,1%
90	0,026	0,025	2,7%	0,026	1,2%
111	0,208	0,233	12,1%	0,229	10,6%
120	0,811	0,890	9,7%	0,890	9,8%
210	0,012	0,013	5,0%	0,013	5,3%
237	0,069	0,073	5,5%	0,072	4,6%
243	0,086	0,082	4,9%	0,082	5,1%
360	2,617	2,621	0,2%	2,621	0,1%
372	0,001	0,002	29,5%	0,001	8,6%
390	0,009	0,008	1,3%	0,009	1,1%
477	0,025	0,027	5,3%	0,027	6,1%
483	0,020	0,018	7,3%	0,019	6,5%
510	0,006	0,006	1,4%	0,006	1,1%
540	0,015	0,015	0,2%	0,015	0,2%
600	0,096	0,098	2,1%	0,098	1,9%
660	0,014	0,015	5,8%	0,015	5,9%
720	0,990	0,964	2,7%	0,963	2,7%
780	0,011	0,011	1,8%	0,011	1,9%
843	0,057	0,056	1,5%	0,056	1,3%
960	0,023	0,023	0,6%	0,023	0,6%
1080	0,224	0,218	2,6%	0,218	2,6%
1140	0,004	0,004	0,5%	0,004	0,2%
1200	0,050	0,050	0,5%	0,050	0,5%
1260	0,002	0,002	1,1%	0,002	1,0%
1290	0,001	0,001	0,1%	0,001	0,1%
1320	0,013	0,013	0,7%	0,013	0,9%
1380	0,002	0,002	0,3%	0,002	0,2%
1410	0,002	0,002	1,1%	0,002	1,2%
1440	0,174	0,169	2,4%	0,170	2,4%
1500	0,002	0,002	0,6%	0,002	0,9%
1560	0,010	0,011	2,9%	0,011	3,3%

Table E.2: Results of validation with simplified motor model

	SimPowerSystems result	VSA method results			
		VSA method - FFT		VSA method - trapezoidal	
Freq [Hz]	Torque [kNm]	Torque [kNm]	|Error| [%]	Torque [kNm]	|Error| [%]
1590	0,002	0,002	0,4%	0,002	0,2%
1680	0,009	0,009	1,0%	0,009	1,0%
1710	0,001	0,001	0,6%	0,001	0,6%
1740	0,006	0,006	0,7%	0,006	0,3%
1800	0,039	0,040	1,2%	0,040	1,0%
1860	0,003	0,003	0,8%	0,003	0,9%
1920	0,003	0,003	0,9%	0,003	0,5%
2037	0,008	0,008	1,5%	0,008	1,2%
2100	0,003	0,003	0,9%	0,003	0,8%
2160	0,079	0,077	3,0%	0,077	3,1%
2283	0,006	0,005	2,4%	0,005	2,4%
2361	0,001	0,001	0,7%	0,001	1,1%
2400	0,005	0,005	1,0%	0,005	1,1%
2520	0,041	0,040	2,3%	0,040	2,3%
2643	0,003	0,003	0,5%	0,003	1,2%
2757	0,003	0,003	3,3%	0,003	3,8%
2820	0,003	0,003	1,0%	0,003	0,8%
2880	0,058	0,056	3,4%	0,056	3,4%
2940	0,005	0,005	1,7%	0,005	1,6%
3000	0,007	0,007	5,5%	0,007	5,6%
3060	0,002	0,002	0,2%	0,002	0,7%
3090	0,001	0,001	0,9%	0,001	0,3%
3120	0,004	0,004	1,8%	0,004	1,8%
3240	0,007	0,006	1,5%	0,006	1,8%
3363	0,004	0,004	0,6%	0,004	0,2%
3438	0,002	0,002	0,8%	0,002	0,4%
3480	0,003	0,004	0,4%	0,004	0,8%
3561	0,002	0,002	0,1%	0,002	0,9%
3723	0,003	0,003	0,9%	0,003	0,3%
3840	0,005	0,005	1,1%	0,005	1,1%
3960	0,009	0,009	0,6%	0,009	0,2%
4080	0,002	0,002	1,6%	0,002	1,2%
4083	0,002	0,002	4,9%	0,002	3,9%
4140	0,003	0,003	0,9%	0,003	0,3%

Table E.2 (cont.): Results of validation with simplified motor model

	SimPowerSystems result	VSA method results			
		VSA method - FFT		VSA method - trapezoidal	
Freq [Hz]	Torque [kNm]	Torque [kNm]	|Error| [%]	Torque [kNm]	|Error| [%]
4200	0,003	0,003	3,3%	0,003	4,0%
4260	0,003	0,003	0,3%	0,003	0,8%
4320	0,023	0,022	3,8%	0,022	4,1%
4440	0,005	0,005	1,6%	0,005	2,1%
4560	0,003	0,003	2,1%	0,003	1,5%
4638	0,001	0,001	1,4%	0,001	1,0%
4680	0,002	0,002	3,4%	0,002	3,4%
4740	0,002	0,002	0,7%	0,002	0,1%
4761	0,001	0,001	0,6%	0,001	1,3%
4800	0,001	0,001	0,2%	0,001	0,3%
4860	0,002	0,002	0,0%	0,002	0,7%
4920	0,001	0,001	0,1%	0,001	0,6%
5040	0,001	0,001	1,5%	0,001	0,7%
5100	0,002	0,002	0,3%	0,002	0,9%
5163	0,002	0,002	2,0%	0,002	1,4%
5283	0,003	0,003	0,2%	0,003	1,0%
5523	0,004	0,004	1,6%	0,004	0,8%
5637	0,002	0,002	3,0%	0,002	3,5%
5643	0,001	0,001	0,1%	0,001	0,1%
5763	0,008	0,008	3,4%	0,008	3,7%
5883	0,003	0,003	0,3%	0,003	0,4%
5940	0,001	0,001	1,0%	0,001	0,2%
6360	0,003	0,003	0,3%	0,003	0,3%
6480	0,002	0,002	0,2%	0,002	0,9%
7080	0,002	0,002	2,4%	0,002	2,2%
7260	0,001	0,001	0,0%	0,001	0,9%
7440	0,001	0,001	1,1%	0,001	0,2%
7560	0,001	0,001	0,2%	0,001	0,7%
7740	0,001	0,001	1,4%	0,001	0,3%
7920	0,001	0,001	2,0%	0,001	2,4%
8640	0,001	0,001	0,4%	0,001	0,1%
9237	0,002	0,002	3,8%	0,002	3,4%
10680	0,002	0,001	4,2%	0,001	3,6%

Table E.2 (cont.): Results of validation with simplified motor model

Results of torque computation - 19300 kW motor

Test 1 - 08 May 2013 - 12:03:09			Test 2 -08 May 2013 - 16:45:47		
Freq [Hz]	VSA - fft	VSA - trapz	Freq [Hz]	VSA - fft	VSA - trapz
	Torque [kNm]			Torque [kNm]	
0.0	52.515	52.685	0.0	52.655	52.776
20.0	0.039	0.031	40.0	0.085	0.088
40.0	0.080	0.074	60.0	0.031	0.034
60.0	0.026	0.025	80.0	0.032	0.031
100.0	0.127	0.123	100.0	0.064	0.064
120.0	0.159	0.169	120.0	0.157	0.158
140.0	0.013	0.010	146.7	0.007	0.010
153.3	0.008	0.015	160.0	0.005	0.005
180.0	0.013	0.014	180.0	0.002	0.007
200.0	0.011	0.008	200.0	0.021	0.024
213.3	0.003	0.011	240.0	0.147	0.154
240.0	0.173	0.179	266.7	0.004	0.007
260.0	0.004	0.008	273.3	0.006	0.003
280.0	0.007	0.003	300.0	0.047	0.048
300.0	0.052	0.051	320.0	0.004	0.002
320.0	0.004	0.005	333.3	0.001	0.004
360.0	0.061	0.058	360.0	0.060	0.058
380.0	0.004	0.002	380.0	0.001	0.004
386.7	0.004	0.003	400.0	0.010	0.006
400.0	0.005	0.007	420.0	0.004	0.005
420.0	0.003	0.006	440.0	0.005	0.005
440.0	0.002	0.002	480.0	0.092	0.093
446.7	0.003	0.001	500.0	0.004	0.009
480.0	0.089	0.091	506.7	0.006	0.009
500.0	0.017	0.017	540.0	0.004	0.004
540.0	0.006	0.006	560.0	0.007	0.010
560.0	0.006	0.007	600.0	0.337	0.338
600.0	0.342	0.343	640.0	0.005	0.006
620.0	0.007	0.009	680.0	0.004	0.005
660.0	0.003	0.003	686.7	0.003	0.005
673.3	0.003	0.004	700.0	0.005	0.006
686.7	0.003	0.004	720.0	1.586	1.593
720.0	1.590	1.597	760.0	0.006	0.007

Table E.3: Results of torque computation - 19300 kW motor

Test 1 - 08 May 2013 - 12:03:09				Test 2 -08 May 2013 - 16:45:47		
Freq [Hz]	VSA - fft	VSA - trapz		Freq [Hz]	VSA - fft	VSA - trapz
	Torque [kNm]				Torque [kNm]	
806.7	0.004	0.005		806.7	0.003	0.004
820.0	0.010	0.012		820.0	0.005	0.006
840.0	0.073	0.074		840.0	0.076	0.078
866.7	0.000	0.002		880.0	0.002	0.002
880.0	0.002	0.002		900.0	0.001	0.002
893.3	0.002	0.001		920.0	0.003	0.005
900.0	0.000	0.001		926.7	0.003	0.004
906.7	0.001	0.001		940.0	0.002	0.004
920.0	0.001	0.001		960.0	0.069	0.071
926.7	0.002	0.001		1000.0	0.002	0.001
960.0	0.073	0.074		1006.7	0.002	0.001
980.0	0.003	0.003		1020.0	0.001	0.001
1000.0	0.001	0.001		1046.7	0.003	0.003
1020.0	0.002	0.003		1080.0	0.029	0.029
1040.0	0.004	0.004		1100.0	0.003	0.002
1053.3	0.001	0.001		1113.3	0.001	0.002
1060.0	0.002	0.001		1140.0	0.003	0.004
1080.0	0.031	0.030		1160.0	0.004	0.004
1100.0	0.005	0.004		1200.0	0.057	0.057
1126.7	0.001	0.002		1220.0	0.002	0.004
1140.0	0.004	0.004		1240.0	0.002	0.003
1160.0	0.002	0.003		1260.0	0.003	0.003
1180.0	0.001	0.002		1273.3	0.002	0.003
1200.0	0.032	0.032		1300.0	0.002	0.002
1240.0	0.003	0.004		1320.0	0.033	0.033
1260.0	0.002	0.001		1340.0	0.002	0.002
1286.7	0.003	0.004		1366.7	0.002	0.003
1300.0	0.006	0.005		1380.0	0.002	0.002
1320.0	0.031	0.031		1400.0	0.004	0.005
1340.0	0.005	0.006		1420.0	0.003	0.003
1353.3	0.003	0.003		1440.0	0.279	0.279
1380.0	0.002	0.002		1466.7	0.001	0.000
1400.0	0.003	0.003		1500.0	0.005	0.004
1440.0	0.285	0.285		1526.7	0.001	0.002

Table E.3 (cont.): Results of torque computation - 19300 kW motor

Test 1 - 08 May 2013 - 12:03:09				Test 2 -08 May 2013 - 16:45:47		
Freq [Hz]	VSA - fft	VSA - trapz		Freq [Hz]	VSA - fft	VSA - trapz
	Torque [kNm]				Torque [kNm]	
1486.7	0.002	0.003		1560.0	0.026	0.027
1500.0	0.003	0.003		1600.0	0.003	0.003
1533.3	0.002	0.002		1620.0	0.002	0.001
1560.0	0.029	0.030		1646.7	0.002	0.002
1580.0	0.002	0.002		1660.0	0.000	0.001
1586.7	0.001	0.002		1680.0	0.012	0.011
1600.0	0.002	0.002		1693.3	0.004	0.004
1653.3	0.003	0.003		1706.7	0.002	0.002
1666.7	0.002	0.002		1720.0	0.001	0.001
1680.0	0.011	0.011		1740.0	0.002	0.002
1700.0	0.004	0.004		1760.0	0.002	0.003
1740.0	0.002	0.002		1800.0	0.027	0.027
1760.0	0.002	0.003		1820.0	0.002	0.002
1773.3	0.002	0.003		1826.7	0.002	0.002
1800.0	0.051	0.051		1840.0	0.002	0.002
1820.0	0.000	0.001		1860.0	0.002	0.002
1840.0	0.004	0.004		1886.7	0.001	0.002
1860.0	0.002	0.002		1920.0	0.010	0.010
1880.0	0.002	0.003		1940.0	0.002	0.002
1900.0	0.003	0.003		1953.3	0.002	0.003
1920.0	0.013	0.013		1986.7	0.002	0.002
1940.0	0.001	0.001		2013.3	0.001	0.001
1960.0	0.002	0.003		2020.0	0.001	0.001
1980.0	0.003	0.003		2040.0	0.023	0.023
1993.3	0.001	0.001		2073.3	0.001	0.001
2006.7	0.001	0.002		2100.0	0.003	0.003
2040.0	0.014	0.014		2113.3	0.001	0.001
2073.3	0.002	0.003		2120.0	0.001	0.002
2100.0	0.004	0.003		2160.0	0.132	0.130
2126.7	0.002	0.002		2180.0	0.002	0.002
2160.0	0.122	0.122		2193.3	0.002	0.002
2193.3	0.003	0.003		2220.0	0.003	0.003
2200.0	0.002	0.003		2240.0	0.002	0.002
2260.0	0.005	0.005		2260.0	0.002	0.003

Table E.3 (cont.): Results of torque computation - 19300 kW motor

Test 1 - 08 May 2013 - 12:03:09				Test 2 -08 May 2013 - 16:45:47		
Freq [Hz]	VSA - fft	VSA - trapz		Freq [Hz]	VSA - fft	VSA - trapz
	Torque [kNm]				Torque [kNm]	
2280.0	0.016	0.016		2280.0	0.021	0.021
2300.0	0.007	0.007		2300.0	0.007	0.006
2320.0	0.001	0.002		2320.0	0.001	0.001
2366.7	0.002	0.001		2360.0	0.002	0.002
2400.0	0.027	0.027		2380.0	0.001	0.001
2426.7	0.002	0.002		2400.0	0.025	0.026
2446.7	0.001	0.001		2433.3	0.002	0.002
2460.0	0.001	0.001		2446.7	0.002	0.002
2500.0	0.004	0.004		2460.0	0.001	0.002
2520.0	0.015	0.015		2480.0	0.001	0.002
2553.3	0.003	0.003		2500.0	0.005	0.005
2586.7	0.002	0.002		2520.0	0.015	0.015
2600.0	0.002	0.001		2546.7	0.001	0.001
2640.0	0.024	0.025		2566.7	0.001	0.001
2693.3	0.002	0.002		2593.3	0.002	0.002
2700.0	0.002	0.002		2606.7	0.002	0.002
2760.0	0.021	0.021		2640.0	0.024	0.024
2786.7	0.003	0.003		2660.0	0.002	0.002
2813.3	0.002	0.002		2680.0	0.001	0.002
2826.7	0.001	0.001		2700.0	0.002	0.002
2840.0	0.001	0.001		2713.3	0.002	0.002
2860.0	0.002	0.002		2740.0	0.001	0.001
2880.0	0.096	0.094		2760.0	0.022	0.022
2906.7	0.004	0.004		2780.0	0.003	0.003
2933.3	0.001	0.001		2793.3	0.002	0.002
2940.0	0.001	0.001		2840.0	0.002	0.003
2953.3	0.002	0.002		2860.0	0.002	0.003
3000.0	0.021	0.021		2880.0	0.096	0.094

Table E.3 (cont.): Results of torque computation - 19300 kW motor

Results of torque computation - 20000 kW motor - full load

Test 1 - 18 June 2013 - 17:00:07			Test 2 - 18 June 2013 - 17:00:07			Test 3 - 18 June 2013 - 17:30:12		
Freq [Hz]	VSA - fft	VSA - trapz	Freq [Hz]	VSA - fft	VSA - trapz	Freq [Hz]	VSA - fft	VSA - trapz
	Torque [kNm]			Torque [kNm]			Torque [kNm]	
0.0	55.634	55.812	0.0	55.813	55.953	0.0	55.728	55.859
37.0	0.065	0.081	33.3	0.067	0.069	20.0	0.071	0.068
66.6	0.114	0.115	46.7	0.036	0.020	40.0	0.027	0.031
103.7	0.130	0.119	66.7	0.186	0.192	60.0	0.050	0.051
118.5	0.153	0.151	100.0	0.171	0.172	100.0	0.213	0.207
155.5	0.015	0.020	120.0	0.191	0.187	120.0	0.186	0.201
185.1	0.006	0.020	153.3	0.012	0.028	146.7	0.001	0.016
199.9	0.023	0.021	160.0	0.012	0.017	160.0	0.004	0.006
244.3	0.103	0.097	173.3	0.006	0.004	166.7	0.003	0.009
259.1	0.013	0.016	186.7	0.002	0.012	180.0	0.003	0.009
296.2	0.046	0.046	200.0	0.012	0.015	200.0	0.013	0.016
303.6	0.043	0.046	213.3	0.011	0.004	240.0	0.140	0.143
318.4	0.006	0.008	240.0	0.191	0.199	273.3	0.005	0.008
333.2	0.007	0.005	266.7	0.007	0.011	300.0	0.064	0.067
362.8	0.042	0.044	280.0	0.010	0.013	326.7	0.003	0.004
399.8	0.021	0.018	300.0	0.060	0.059	360.0	0.050	0.050
422.0	0.009	0.010	320.0	0.007	0.005	380.0	0.005	0.007
451.6	0.006	0.009	326.7	0.007	0.006	400.0	0.014	0.015
481.2	0.091	0.094	340.0	0.003	0.004	420.0	0.011	0.011
503.5	0.016	0.015	360.0	0.047	0.046	440.0	0.004	0.003
518.3	0.007	0.008	400.0	0.012	0.012	480.0	0.083	0.081
533.1	0.011	0.008	420.0	0.008	0.009	500.0	0.028	0.028
555.3	0.001	0.004	426.7	0.011	0.008	520.0	0.004	0.006
577.5	0.002	0.002	480.0	0.095	0.093	540.0	0.005	0.005
599.7	0.207	0.206	500.0	0.022	0.018	573.3	0.002	0.007
621.9	0.011	0.013	533.3	0.014	0.013	600.0	0.219	0.218
644.1	0.006	0.008	566.7	0.000	0.004	620.0	0.015	0.018
673.7	0.008	0.008	600.0	0.166	0.167	640.0	0.003	0.003
681.1	0.007	0.009	620.0	0.011	0.014	660.0	0.003	0.004
718.2	1.613	1.622	653.3	0.012	0.016	680.0	0.009	0.013
762.6	0.006	0.008	680.0	0.007	0.008	700.0	0.005	0.006
784.8	0.007	0.009	720.0	1.691	1.698	720.0	1.716	1.725
821.8	0.012	0.015	753.3	0.008	0.010	740.0	0.007	0.008

Table E.4: Results of torque computation - 20000 kW motor - full load

Test 1 - 18 June 2013 - 17:00:07			Test 2 - 18 June 2013 - 17:00:07			Test 3 - 18 June 2013 - 17:30:12		
Freq [Hz]	VSA - fft	VSA - trapz	Freq [Hz]	VSA - fft	VSA - trapz	Freq [Hz]	VSA - fft	VSA - trapz
	Torque [kNm]			Torque [kNm]			Torque [kNm]	
844.0	0.067	0.068	786.7	0.014	0.017	760.0	0.008	0.012
866.2	0.001	0.001	820.0	0.013	0.017	780.0	0.005	0.006
903.3	0.002	0.003	840.0	0.084	0.084	800.0	0.004	0.006
918.1	0.001	0.002	880.0	0.002	0.002	820.0	0.018	0.020
932.9	0.002	0.002	886.7	0.001	0.002	840.0	0.087	0.090
962.5	0.062	0.062	900.0	0.002	0.001	880.0	0.002	0.003
984.7	0.001	0.002	920.0	0.003	0.004	900.0	0.001	0.002
999.5	0.004	0.003	933.3	0.002	0.002	920.0	0.002	0.002
1036.5	0.002	0.003	960.0	0.073	0.075	926.7	0.002	0.001
1051.3	0.000	0.003	1000.0	0.002	0.001	940.0	0.002	0.002
1080.9	0.035	0.036	1020.0	0.004	0.005	960.0	0.064	0.064
1103.2	0.008	0.009	1040.0	0.002	0.001	1000.0	0.003	0.004
1125.4	0.007	0.007	1080.0	0.029	0.029	1020.0	0.006	0.006
1132.8	0.007	0.007	1100.0	0.011	0.011	1046.7	0.002	0.002
1162.4	0.003	0.004	1133.3	0.010	0.010	1080.0	0.033	0.033
1199.4	0.064	0.065	1160.0	0.002	0.002	1100.0	0.011	0.012
1236.4	0.003	0.004	1166.7	0.002	0.003	1140.0	0.005	0.006
1273.4	0.005	0.005	1200.0	0.113	0.113	1160.0	0.002	0.001
1295.7	0.004	0.004	1226.7	0.003	0.004	1173.3	0.003	0.003
1317.9	0.030	0.031	1233.3	0.003	0.004	1180.0	0.003	0.002
1340.1	0.005	0.006	1266.7	0.010	0.011	1200.0	0.107	0.106
1369.7	0.004	0.004	1300.0	0.008	0.009	1220.0	0.002	0.003
1384.5	0.001	0.001	1320.0	0.031	0.030	1226.7	0.002	0.003
1399.3	0.002	0.003	1340.0	0.006	0.008	1246.7	0.003	0.003
1443.7	0.249	0.248	1373.3	0.006	0.008	1260.0	0.002	0.003
1473.3	0.003	0.004	1400.0	0.005	0.005	1266.7	0.003	0.003
1517.8	0.002	0.002	1406.7	0.005	0.005	1300.0	0.009	0.009
1532.6	0.003	0.003	1440.0	0.278	0.278	1320.0	0.029	0.028
1562.2	0.024	0.025	1460.0	0.003	0.004	1340.0	0.010	0.011
1599.2	0.001	0.002	1500.0	0.005	0.005	1366.7	0.001	0.002
1621.4	0.002	0.003	1540.0	0.004	0.004	1373.3	0.001	0.002
1651.0	0.002	0.002	1560.0	0.026	0.026	1380.0	0.001	0.001
1680.7	0.011	0.010	1593.3	0.002	0.003	1400.0	0.006	0.006
1717.7	0.001	0.001	1613.3	0.001	0.002	1420.0	0.003	0.003

Table E.4 (cont.): Results of torque computation - 20000 kW motor - full load

Test 1 - 18 June 2013 - 17:00:07			Test 2 - 18 June 2013 - 17:00:07			Test 3 - 18 June 2013 - 17:30:12		
Freq [Hz]	VSA - fft	VSA - trapz	Freq [Hz]	VSA - fft	VSA - trapz	Freq [Hz]	VSA - fft	VSA - trapz
	Torque [kNm]			Torque [kNm]			Torque [kNm]	
1739.9	0.001	0.001	1646.7	0.002	0.002	1440.0	0.287	0.287
1762.1	0.001	0.002	1680.0	0.011	0.012	1460.0	0.005	0.004
1799.1	0.022	0.023	1700.0	0.003	0.003	1473.3	0.001	0.002
1865.7	0.002	0.001	1713.3	0.002	0.002	1500.0	0.004	0.004
1873.1	0.001	0.002	1726.7	0.002	0.003	1540.0	0.002	0.003
1917.6	0.014	0.014	1753.3	0.001	0.002	1560.0	0.024	0.024
1954.6	0.002	0.002	1773.3	0.002	0.002	1593.3	0.002	0.003
1962.0	0.001	0.002	1800.0	0.018	0.018	1620.0	0.002	0.002
1976.8	0.003	0.003	1820.0	0.001	0.001	1626.7	0.002	0.002
1999.0	0.002	0.001	1840.0	0.001	0.002	1653.3	0.001	0.002
2043.4	0.023	0.022	1866.7	0.002	0.001	1680.0	0.012	0.012
2080.5	0.001	0.001	1873.3	0.001	0.002	1700.0	0.004	0.003
2102.7	0.002	0.002	1886.7	0.002	0.002	1746.7	0.002	0.002
2117.5	0.002	0.002	1920.0	0.017	0.017	1800.0	0.020	0.020
2161.9	0.146	0.144	1940.0	0.002	0.003	1820.0	0.002	0.001
2191.5	0.002	0.003	1980.0	0.001	0.002	1860.0	0.002	0.002
2221.1	0.003	0.004	1993.3	0.001	0.002	1880.0	0.001	0.001
2258.1	0.005	0.006	2013.3	0.001	0.001	1900.0	0.002	0.002
2280.4	0.022	0.022	2040.0	0.026	0.026	1920.0	0.015	0.014
2302.6	0.002	0.002	2073.3	0.002	0.002	1966.7	0.002	0.001
2332.2	0.004	0.003	2086.7	0.002	0.002	1980.0	0.002	0.002
2339.6	0.003	0.004	2106.7	0.001	0.002	2006.7	0.001	0.002
2361.8	0.002	0.002	2126.7	0.002	0.003	2013.3	0.001	0.002
2376.6	0.002	0.002	2160.0	0.151	0.150	2040.0	0.023	0.024
2398.8	0.045	0.045	2193.3	0.004	0.004	2060.0	0.002	0.003
2421.0	0.002	0.002	2226.7	0.005	0.007	2073.3	0.002	0.002
2435.8	0.002	0.002	2260.0	0.007	0.008	2100.0	0.002	0.002
2465.4	0.002	0.003	2280.0	0.025	0.025	2120.0	0.002	0.003
2495.1	0.003	0.004	2313.3	0.001	0.001	2140.0	0.001	0.001
2517.3	0.016	0.016	2333.3	0.005	0.005	2160.0	0.149	0.148
2546.9	0.001	0.001	2353.3	0.001	0.001	2180.0	0.002	0.002
2576.5	0.001	0.002	2366.7	0.002	0.001	2200.0	0.001	0.002
2583.9	0.002	0.002	2400.0	0.043	0.044	2220.0	0.002	0.002
2643.1	0.023	0.023	2433.3	0.002	0.002	2233.3	0.001	0.001

Table E.4 (cont.): Results of torque computation - 20000 kW motor - full load

Test 1 - 18 June 2013 - 17:00:07			Test 2 - 18 June 2013 - 17:00:07			Test 3 - 18 June 2013 - 17:30:12		
Freq [Hz]	VSA - fft	VSA - trapz	Freq [Hz]	VSA - fft	VSA - trapz	Freq [Hz]	VSA - fft	VSA - trapz
	Torque [kNm]			Torque [kNm]			Torque [kNm]	
2687.6	0.002	0.001	2453.3	0.003	0.003	2240.0	0.001	0.001
2702.4	0.000	0.001	2466.7	0.003	0.003	2260.0	0.008	0.008
2739.4	0.001	0.002	2520.0	0.018	0.018	2280.0	0.029	0.029
2761.6	0.021	0.021	2540.0	0.002	0.002	2340.0	0.002	0.003
2783.8	0.003	0.004	2566.7	0.002	0.002	2360.0	0.001	0.002
2806.0	0.002	0.003	2580.0	0.002	0.003	2373.3	0.001	0.001
2835.6	0.002	0.002	2600.0	0.001	0.002	2400.0	0.026	0.026
2850.4	0.002	0.003	2640.0	0.026	0.026	2433.3	0.002	0.001
2857.8	0.002	0.003	2660.0	0.003	0.003	2460.0	0.002	0.003
2880.1	0.098	0.097	2680.0	0.001	0.001	2500.0	0.005	0.005
2917.1	0.001	0.002	2693.3	0.002	0.002	2520.0	0.015	0.015
2931.9	0.002	0.003	2740.0	0.002	0.002	2546.7	0.003	0.003
2954.1	0.002	0.002	2760.0	0.020	0.020	2586.7	0.002	0.002
2976.3	0.002	0.002	2780.0	0.005	0.005	2613.3	0.001	0.001
2998.5	0.014	0.014	2806.7	0.004	0.005	2640.0	0.025	0.024
3028.1	0.002	0.002	2840.0	0.003	0.003	2666.7	0.001	0.001
			2853.3	0.002	0.003	2700.0	0.002	0.002
			2880.0	0.096	0.094	2720.0	0.001	0.002
			2900.0	0.008	0.008	2733.3	0.001	0.001
			2940.0	0.003	0.003	2760.0	0.023	0.023
			2946.7	0.003	0.003	2780.0	0.007	0.008
			2980.0	0.001	0.002	2806.7	0.001	0.001
			3000.0	0.012	0.012	2826.7	0.001	0.001
						2840.0	0.004	0.005
						2860.0	0.002	0.003
						2880.0	0.101	0.098
						2900.0	0.007	0.007
						2926.7	0.002	0.002
						2953.3	0.002	0.002
						2980.0	0.002	0.003
						3000.0	0.024	0.024

Table E.4 (cont.): Results of torque computation - 20000 kW motor - full load

Results of torque computation - 20000 kW motor - 75% load

Test - 18 June 2013 - 18:00:17		
Freq[Hz]	VSA - fft	VSA - trapz
	Torque [kNm]	
0.0	41.416	41.572
20.0	0.022	0.028
40.0	0.042	0.040
60.0	0.045	0.033
66.7	0.046	0.024
80.0	0.031	0.039
100.0	0.063	0.056
120.0	0.149	0.146
153.3	0.014	0.011
180.0	0.006	0.009
186.7	0.004	0.009
200.0	0.015	0.018
240.0	0.151	0.151
280.0	0.006	0.007
300.0	0.057	0.057
320.0	0.004	0.005
360.0	0.033	0.034
400.0	0.012	0.013
420.0	0.006	0.008
426.7	0.008	0.006
440.0	0.005	0.007
460.0	0.002	0.005
480.0	0.077	0.078
520.0	0.003	0.005
540.0	0.008	0.008
600.0	0.402	0.404
620.0	0.007	0.008
646.7	0.003	0.002
660.0	0.004	0.004
680.0	0.003	0.004
693.3	0.005	0.005
720.0	1.255	1.263
766.7	0.002	0.003

Test - 18 June 2013 - 18:00:17		
Freq[Hz]	VSA - fft	VSA - trapz
	Torque [kNm]	
786.7	0.006	0.004
806.7	0.003	0.003
820.0	0.007	0.006
840.0	0.071	0.071
880.0	0.001	0.002
886.7	0.001	0.001
906.7	0.001	0.001
920.0	0.002	0.003
926.7	0.002	0.002
960.0	0.063	0.064
1000.0	0.001	0.002
1020.0	0.003	0.004
1026.7	0.005	0.004
1040.0	0.002	0.002
1060.0	0.002	0.002
1080.0	0.025	0.025
1113.3	0.002	0.003
1140.0	0.003	0.004
1146.7	0.004	0.004
1200.0	0.037	0.038
1240.0	0.002	0.002
1260.0	0.002	0.002
1286.7	0.002	0.001
1320.0	0.036	0.036
1340.0	0.004	0.004
1360.0	0.002	0.002
1380.0	0.002	0.002
1386.7	0.003	0.002
1400.0	0.003	0.004
1440.0	0.307	0.308
1480.0	0.002	0.001
1486.7	0.002	0.002
1500.0	0.004	0.004

Table E.5: Results of torque computation - 20000 kW motor - 75% load

Test - 18 June 2013 - 18:00:17		
Freq[Hz]	VSA - fft	VSA - trapz
	Torque [kNm]	
1513.3	0.002	0.001
1560.0	0.034	0.033
1600.0	0.003	0.003
1626.7	0.002	0.002
1653.3	0.002	0.002
1680.0	0.019	0.019
1706.7	0.001	0.002
1740.0	0.003	0.003
1760.0	0.003	0.003
1800.0	0.056	0.056
1840.0	0.003	0.003
1853.3	0.001	0.001
1880.0	0.001	0.001
1900.0	0.001	0.002
1920.0	0.015	0.015
1953.3	0.001	0.001
1980.0	0.002	0.003
2000.0	0.003	0.003
2040.0	0.004	0.004
2100.0	0.005	0.005
2120.0	0.001	0.002
2160.0	0.043	0.043
2193.3	0.002	0.001
2206.7	0.002	0.001
2220.0	0.002	0.002
2246.7	0.002	0.001
2260.0	0.002	0.001

Test - 18 June 2013 - 18:00:17		
Freq[Hz]	VSA - fft	VSA - trapz
	Torque [kNm]	
2280.0	0.006	0.007
2300.0	0.007	0.006
2340.0	0.002	0.002
2400.0	0.029	0.029
2433.3	0.001	0.001
2460.0	0.003	0.003
2480.0	0.002	0.002
2506.7	0.003	0.003
2526.7	0.008	0.008
2546.7	0.002	0.002
2586.7	0.002	0.002
2613.3	0.002	0.002
2640.0	0.016	0.016
2646.7	0.016	0.016
2680.0	0.002	0.002
2706.7	0.003	0.003
2760.0	0.017	0.017
2800.0	0.001	0.001
2833.3	0.002	0.002
2853.3	0.001	0.001
2886.7	0.074	0.073
2906.7	0.005	0.005
2920.0	0.002	0.001
2933.3	0.002	0.002
2946.7	0.002	0.002
2966.7	0.002	0.002
3006.7	0.022	0.022

Table E.5 (cont.): Results of torque computation - 20000 kW motor - 75% load

References

[1] J.O. Ojo, V. Ostovic, T.A. Lipo, and J.C. White, "Measurement and Computation of Starting Torque Pulsations of Salient Pole Synchronous Motors," IEEE Transactions on Energy Conversion, vol. 5, no. 1, Mar. 1990, pp. 176 - 182.

[2] "MEGADRIVE-LCI Medium voltage AC Drives," ABB Switzerland Ltd., Doc No.: 3BHS261403 Rev.- , Aug. 2009.

[3] D. Buzzini, and M. Zago, "Testing Large ASDS," 2012 Petroleum and Chemical Industry Technical Conference, Paper No. PCIC-2012-48, Sep. 2012.

[4] R.H. Park, "Two-reaction Theory of Synchronous Machines - Generalized Method of Analysis - Part I," Transactions of the American Institute of Electrical Engineers, Jan. 1929, pp. 716 - 730.

[5] "ABB drives in chemical, oil and gas - Medium voltage drives for greater profitability and performance" ABB brochure, 2011, available at www.abb.com.

[6] G. Klempner, and I. Kerszenbaum, "Operation and Maintenance of Large Turbo Generators," John Wiley & Sons Inc, 2004, pp. 3 - 32.

[7] P.C. Krause, O. Wasynczuk, S.D. Sudhoff, "Analysis of Electric Machinery and Drive Systems," IEEE Press Power Engineering Series, John Wiley & Sons Inc. , Second Edition, 2002.

[8] P.M. Anderson, A.A. Fouad, "Power systems control and Stability," second edition, IEEE Press Power Engineering Series, John Wiley & Sons Inc., 2003, pp. 83 - 149.

[9] B.R. Prentice, "Fundamental concepts of synchronous machine reactances," Transactions of the American Institute of Electrical Engineers, Dec. 1937, pp. 1 - 21.

[10] C. Concordia, "Synchronous Machines - Theory and Applications," Wiley, 1951.

[11] IEC 61800-4 "Adjustable speed electrical power drive systems - General requirements - Rating specifications for A.C. power drive systems above 1000 V A.C and not exceeding 35 kV," Sep. 2002.

[12] IEEE 1566 "IEEE Standard for Performance of Adjustable Speed AC Drives Rated 375kW and Larger", Jun. 2006.

[13] IEEE 1225-2000 "IEEE Guide for Evaluation of Torque Pulsations During Starting of Synchronous Motors", Aug. 2000.

[14] J. Song-Manguelle, J.M. Nyobe-Yome, and G. Ekemb, "Pulsating Torques in PWM Multi-Megawatt Drives for Torsional Analysis of Large Shafts", IEEE Transactions on Industry Applications, Jan.-Feb. 2010, pp. 130 - 138.

[15] R. Lampl, and F. Healy, "Power Analysis of Converter Drives - Digital Transient Torque Measurement," Seventh International Conference on Power Electronics and Variable Speed Drives, (Conf. Publ. No. 456), Sep. 1998, pp. 579 - 585.

[16] E.M.H. Kamerbeek, "On the Theoretical and Experimental Determination of the Electromagnetic Torque in Electrical Machines", Philips Tech. Rev. Supplement, No. 4, 1970.

[17] T. Holt, "Measurement of Electromagnetic Air Gap Torque Produced by a Synchronous Motor During Starting," IEEE Transactions on Power Apparatus and Systems, Vol. PAS-100, No. 4, Apr. 1981, pp. 2059 - 2066.

[18] C.B. Mayer, and E.L. Owen, Discussion of "Measurement of Electromagnetic Air Gap Torque Produced by a Synchronous Motor During Starting, T. Holt" , IEEE Transactions on Power Apparatus and Systems, Vol. PAS-100, No. 4, Apr. 1981, pp. 2066 - 2067.

[19] M.T. Nguyen, M. Tu Xuan, and J.-J. Simond, "Digital transient torque or force measurement for rotating or linear A.C. machines (real time measurement)," EPE 1995.

[20] H.R. Gillard, "Measurements and Analysis of Synchronous Motor Starting Torque," MSc. Thesis, University of Toronto, 1993.

[21] F. Zappa, "Electronic Systems," Società Editrice Esculapio, Oct. 2012.

[22] V.J. Hodge, and J. Austin, "A Survey of Outlier Detection Methodologies," Kluwer Academic Publishers, 2004.

[23] R.D. Gibbons, and D.E. Coleman, "Statistical Methods for Detection and Quantification of Environmental Contamination," John Wiley & Sons, 2001.

[24] NIST/SEMATECH e-Handbook of Statistical Methods, http://www.itl.nist.gov/div898/handbook/, accessed on 30 of May of 2013.

[25] D.A. Ward and J. La T. Exon, "Using Rogowski coils for transient current measurements", Engineering Science and Education Journal, Jun. 1993, pp. 105 - 113.

[26] A. Cremasco, "Efficiency Evaluation of a High Power, Medium Voltage Synchronous Machine by Calorimetric Method According to IEC Standards", Università Degli Studi di Pavia, 2011/2012.

[27] N. Locci, C. Muscas, S. Sulis, "Experimental comparison of MV voltage transducers for power quality applications," Instrumentation and Measurement Technology Conference, 2009, pp. 92 - 97.

[28] J.J. Simond, A. Sapin, M. Tu Xuan, R. Wetter, P. Burmeister, "12-Pulse LCI Synchronous Drive for a 20 MW Compressor Modeling, Simulation and Measurements," Industry Applications Conference, 2005. Fourtieth IAS Annual Meeting. Conference Record of the 2005 (Volume: 4), Oct. 2005, pp. 2302 - 2308